DEVELOPMENT OF VBI MODELS WITH VEHICLE ACCELERATION FOR BRIDGE-VEHICLE DYNAMIC RESPONSE

Hossein Azimi

A Thesis

in the Department

of

Building, Civil, and Environmental Engineering

Presented in Partial Fulfillment of the Requirements

For the Degree of

Doctor of Philosophy (Civil Engineering) at

Concordia University

Montréal, Québec, Canada

November 2011

CONCORDIA UNIVERSITY
SCHOOL OF GRADUATE STUDIES

This is to certify that the thesis prepared

By: Hossein Azimi

Entitled: DEVELOPMENT OF VBI MODELS WITH VEHICLE ACCELERATION FOR BRIDGE-VEHICLE DYNAMIC RESPONSE

and submitted in partial fulfillment of the requirements for the degree of

Doctor of Philosophy (Civil Engineering)

complies with the regulations of the University and meets the accepted standards with respect to originality and quality.

Signed by the final examining committee:

Dr. Chevy Chen — Chair

Dr. Ashraf A. El Damatty — External Examiner

Dr. Subhash Rakheja — External to Program

Dr. Ashutosh Bagchi — Examiner

Dr. Lucia Tirca — Examiner

Dr. Khaled Galal & Dr. Oscar A. Pekau — Thesis Supervisor

Approved by

Chair of Department or Graduate Program Director

Dean of Faculty

ABSTRACT
DEVELOPMENT OF VBI MODELS WITH VEHICLE ACCELERATION FOR BRIDGE-VEHICLE DYNAMIC RESPONSE

Hossein Azimi, Ph.D.

Concordia University, 2011

There has been a growing interest to model and analyze the Vehicle-Bridge Interaction (VBI) of intricate vehicles on bridges. VBI analysis is used if the dynamic response of the vehicle in addition to that of the bridge is required. This is particularly sound in case of high-speed trains where the vehicle acceleration is a design criterion for passenger comfort and needs to be well predicted.

The main objective of this research is to establish efficient numerical procedures within the framework of finite element methods to solve the dynamic response of the VBI systems for vehicles moving with constant velocity or with acceleration. For vehicles with constant velocity, the dynamic condensation method is applied to reduce the vehicle DOFs to the VBI element. A new formulation is proposed for the mass, damping, and stiffness of the VBI element considering new formulation for the contact points.

For vehicles experiencing acceleration or deceleration, external forces resulting from vehicle horizontal acceleration are numerically formulated in a matrix form as the function of vertical contact forces. By defining a new variable called acceleration parameter, the contact force formula is reformulated. Consequently, a new formulation for the VBI element containing the effect of vehicle acceleration is developed.

The effect of shear deformation and consistent mass on the vehicle and bridge responses is investigated. The Timoshenko beam element is used to simulate the effect of

shear deformation with consistent mass including the effect of rotary mass. Results generally imply that all bridge responses are affected, particularly mid-span acceleration.

A comprehensive parametric study is conducted on the model variables and their effects on the dynamic response of the bridge and the vehicle. The studied parameters include vehicle and bridge damping, frequency parameter, system mass parameter, and a new parameter called vehicle mass parameter. The new VBI element for vehicles experiencing acceleration is studied for three types of vehicle models. Results demonstrate the capability of the developed VBI elements in capturing several dynamic effects when compared to the available models, particularly for high speed vehicles. The new VBI models showed better predictions for the vertical contact forces, vehicle vertical acceleration, and the bridge mid-span deflection.

ACKNOWLEDGEMENTS

I would like to express my sincere gratitude to my supervisors, Dr. Khaled Galal, and Dr. Oscar. A. Pekau for their guidance, encouragement and patience during my research. I believe that this research wouldn't have been completed without their continuous support. Their efforts in reviewing and correcting this thesis drafts are greatly appreciated.

The financial support provided by Canadian National Railway (CN) in the form of a fellowship is greatly appreciated. Encouraging awards from Concordia University are also acknowledged.

I would like to thank all my professors in Sharif University, Tehran, Iran. Their great help and support during my undergraduate and Masters studies really helped me to continue my studies here in Canada and to achieve what I aimed to. I would like also to thank my brother, Ali, and all my friends here in Montréal for their supports and helps during my study.

Finally, I dedicate this thesis to my wife, Zahra, and to my parents whose unconditional love is absolutely incredible. Their presence in my life encouraged me a lot to achieve my goals and to work hard on my research.

TABLE OF CONTENTS

LIST OF FIGURES…… x
LIST OF TABLES…… xv
LIST OF SYMBOLS…… xvi
NOMENCLATURE…… xix

CHAPTER 1
INTRODUCTION…… 1
1.1 BACKGROUND…… 1
1.2 MOTIVATION …… 2
1.3 OBJECTIVE AND SCOPE…… 3
1.4 OUTLINE OF THE THESIS …… 4

CHAPTER 2
LITERATURE REVIEW …… 6
2.1 INTRODUCTION …… 6
2.2 VEHICLE MODELING…… 7
2.2.1 Moving load models …… 7
2.2.2 Moving mass models …… 8
2.2.3 Moving sprung mass models …… 9
2.2.4 Moving system models …… 9
2.3 BRIDGE MODELING …… 11
2.3.1 Road roughness and rail irregularities …… 12
2.4 METHODS OF SOLUTION FOR VEHICLE-BRIDGE INTERACTION (VBI) …… 13
2.4.1 Iterative solution of contact forces …… 14
2.4.2 Modal superposition …… 16
2.4.3 Dynamic condensation …… 16
2.5 TREATMENT OF VEHICLE LONGITUDINAL ACCELERATION OR DECELERATION …… 19

CHAPTER 3
DEVELOPMENT OF 2-D NUMERICAL VEHICLE-BRIDGE INTERACTION ELEMENTS…… 22
3.1 INTRODUCTION…… 22
3.2 NUMERICAL VBI ELEMENT FOR VEHICLES WITH CONSTANT VELOCITY …… 23
3.2.1 Basic equations…… 23
3.2.2 Effect of road irregularities in the new formulation…… 25
3.2.3 Bridge element nodal displacement, velocity, and accelerations…… 27
3.2.4 VBI element structural matrices…… 28

3.2.5 Working procedure of the VBI analysis using new modified element……. 29
3.3 NUMERICAL VBI ELEMENT FOR VEHICLES EXPERIENCING ACCELERATION OR DECELERATION…….……..….. 30
3.3.1 Formulation of acceleration forces based on vertical contact forces…… 30
(a) Sample Vehicle of 4-DOFs……. 31
3.3.2 Generalized procedure for formulation of acceleration forces……..... 35
3.3.3 Numerical formulation of the vehicle equations of motion including the effect of acceleration…….. 36
3.3.4 Numerical formulation of vertical contact forces……...…. 37
3.3.5 Structural matrices of VBI element for vehicles experiencing acceleration or deceleration……..... 40
3.3.6 Working procedure of time-history analysis for VBI systems including acceleration…….. 44
3.3.7 More vehicle examples ……..…. 45
(a) Effect of tire in the modeling (a car model with 6 DOFs)…..…. 46
(b) Half-car planar vehicle model of 8 DOFs……... 48
(c) Train model of 10 DOFs……. 49
3.4 NUMERICAL VERIFICATIONS……..…… 52
3.4.1 Moving sprung mass model…….……..... 52
3.4.2 Suspended rigid beam model ……..… 52
3.4.3 Half-Car planar model including the effect of tires……..……..….. 53
3.5 LIMITATIONS AND ASSUMPTIONS …...…….…… 54
3.6 SUMMARY……...…….. 54

CHAPTER 4

EFFECT OF SHEAR DEFORMATION AND CONSISTENT MASS ON VBI ANALYSIS……... 65
4.1 GENERAL……..……. 65
4.2 BRIDGE AND VEHICLE MODELING…….……... 67
4.3 EFFECT OF SHEAR DEFORMATION ON BRIDGE NATURAL FREQUENCIES ……..……. 69
4.4 EFFECT OF SHEAR DEFORMATION ON TWO NUMERICAL MODELS …… 71
4.5 EFFECT OF SHEAR DEFORMATION ON SAMPLE RAILWAY BRIDGES AND VEHICLES……..…. 71
4.5.1 Bridge and vehicle models and methodology…….. 71
4.5.2 Bridge mid-span deflection…….. 73
4.5.3 Bridge mid-span acceleration…….. 75
4.5.4 Vehicle vertical acceleration…… 76
4.6 EFFECT OF CONSISTENT MASS CONSIDERING FLEXURAL EFFECTS ONLY…….…… 76
4.7 EFFECT OF CONSISTENT MASS CONSIDERING FLEXURAL AND SHEAR EFFECTS……..……. 79

4.7.1 Mass Matrices…. 79
4.7.2 Bridge and vehicle models and methodology…….. 80
4.7.3 Bridge Model of 6 m Span……... 81
4.7.4 Bridge Model of 20 m Span…… 84
4.8 SUMMARY……...…….. 85

CHAPTER 5
EVALUATION AND INVESTIGATION OF THE SIGNIFICANSE OF NEW VBI ELEMENTS…….. 99
5.1 GENERAL……..… 99
5.2 EVALUATION OF THE NEW VBI ELEMENT FOR VEHICLES WITH CONSTANT VELOCITY…… 100
5.2.1 Parameters to be investigated and bridge and vehicle models……. 100
5.2.2 Effect of bridge and vehicle damping…….. 102
5.2.3 Effect of Frequency parameter, γ ……...……...…. 103
5.2.4 Effect of System mass parameter, κ ……..……. 104
5.2.5 Effect of a new parameter called vehicle mass parameter, η …….. 105
5.3 Effect of the new VBI element for vehicles experiencing acceleration or Deceleration…….. 106
5.3.1 A Symmetrical Vehicle Model…… 107
(a) Vehicle responses and discussions……...…….. 107
(b) Bridge responses……. 110
5.3.2 An unsymmetrical Truck Model…….. 111
(a) Bridge and truck models……..... 111
(b) Discussion on bridge and vehicle responses……... 113
5.3.3 A Sample Train Model……...……. 114
(a) Contact forces……. 114
(b) Midspan deflection……...….. 115
(c) Vehicle horizontal acceleration…….. 117
(d) Other important parameters…… 117
5.4 Summary. …… 118

CHAPTER 6
CONCLUSIONS AND RECOMMENDATIONS …….. 150
6.1 SUMMARY……. 150
6.2 CONTRIBUTIONS AND APPLICATIONS ……..…. 151
6.3 CONCLUSIONS ……. 154
6.4 RECOMMENDATIONS FOR FUTURE RESEARCH ……. 156

REFERENCES ……... 158

APPENDIX A

VEHICLE-BRIDGE INTERACTION ELEMENT DEVELOPED BY YANG AND WU (2001)……...……... 166
A.1 Vehicle equations and contact forces……...…… 166
A.2 Solution of contact forces…….…….... 169
A.3 VBI element considering vertical contact forces only…….…..... 170
A.4 VBI Element considering vertical and horizontal contact forces……..….. 172
A.5 Bridge equation of motion……...…… 173

APPENDIX B

REQUIRED VEHICLE MATRICES FOR DEVELOPED VBI ELEMENTS …... 175
B.1 Sprung mass model (Yang and Wu 2001)……..……. 175
B.2 Suspended rigid beam or 4 DOF car model (Yang and Wu 2001)……..…… 175
B.3 Car model including the effect of tires with 6 DOFs…….….. 176
B.4 Half-Car planar vehicle model with 8 DOFs……..…….…… 177
B.5 Train model with 10 DOFs……..…… 179

APPENDIX C

FRICTION MODELS AND COEFFICIENT OF FRICTION …… 181

LIST OF FIGURES

Figure 2.1	Sprung mass model …….	20
Figure 2.2	A 2D model of one car of a train (Wu and Yang, 2003) ……	20
Figure 2.3	A 3D model of one car of a train (Majka and Hartnett, 2008) ……...	20
Figure 2.4	Train-Bridge model: (a) a general model, (b) simplified sprung mass	21
Figure 2.5	A Vehicle-Bridge Interaction (VBI) element (Yang et al., 2004) …..	21
Figure 3.1	Two-dimensional VBI element...…….	58
Figure 3.2	A car model of 4-DOF ……	58
Figure 3.3	Free body diagrams of 4-DOF car model of: (a) the car body, (b) wheels ……	58
Figure 3.4	Two-dimensional VBI element for vehicles with acceleration ……..	59
Figure 3.5	A car model of 6-DOF having the effect of tires ……	59
Figure 3.6	Free body diagrams of 6-DOF car model for (a) wheels (b) tire ……	59
Figure 3.7	A Half-car planar Vehicle model of 8-DOF having the effect of tires	60
Figure 3.8	Free body diagrams of the half-car planar model for (a) passenger or driver (b) vehicle body (c) wheels (d) tires …….	60
Figure 3.9	Four-wheel model of one car of a train ……...	61
Figure 3.10	Free body diagram of the car body, a bogie, and a wheel ……..	61
Figure 3.11	Numerical verification, moving sprung mass model ……..	62
Figure 3.12	Displacement at the beam mid-span, numerical verification using moving sprung mass model ……	62
Figure 3.13	Numerical verification, suspended rigid beam model ……	63
Figure 3.14	Displacement at mid-span of the beam, numerical verification using suspended rigid beam model ……..	63
Figure 3.15	Displacement at mid-span of the bridge for half-car planar model …	64
Figure 3.16	Driver bouncing for half-car planar model …….	64
Figure 4.1	Required designations for Timoshenko shear coefficient ……...	88
Figure 4.2	Effect of shear deformations on sprung mass model ……..	88
Figure 4.3	Effect of shear deformations on suspended rigid beam model ……...	88

Figure 4.4 Maximum mid-span deflection for bridge models including or excluding the effect of shear deformations, bridge spans of (a) 6m, (b) 12m, (c) 20m …… 89

Figure 4.5 The percentage of difference for mid-span deflection response regarding models including shear deformation effects with respect to models including flexural effects only for various bridge spans … 89

Figure 4.6 Maximum bridge mid-span acceleration for bridge models including or excluding the effect of shear deformations, bridge spans of (a) 6 m, (b) 12 m, (c) 20 m …….. 90

Figure 4.7 Maximum vehicle vertical acceleration for bridge models including or excluding the effect of shear deformations, bridge spans of (a) 6m, (b) 12m, (c) 20m ……. 91

Figure 4.8 Effect of the consistent mass on the maximum vehicle vertical acceleration for the bridge model of 6 m …… 91

Figure 4.9 Effect of the consistent mass on the maximum midspan deflection for the bridge model of 6 m …… 92

Figure 4.10 Effect of the consistent mass on the maximum midspan vertical acceleration for the bridge model of 6 m …… 92

Figure 4.11 Midspan acceleration in the 6 m bridge for four speed parameters (a) 0.05, (b) 0.3, (c) 0.6, (d) 1.0 ……. 93

Figure 4.12 Midspan deflection in the 6 m bridge for four speed parameters (a) 0.05, (b) 0.3, (c) 0.6, (d) 1.0 …… 94

Figure 4.13 Vehicle vertical acceleration in the 6 m bridge for four speed parameters (a) 0.05, (b) 0.3, (c) 0.6, (d) 1.0 …… 95

Figure 4.14 Midspan acceleration in the 20 m bridge for four speed parameters (a) 0.05, (b) 0.3, (c) 0.6, (d) 1.0 …….. 96

Figure 4.15 Midspan deflection in the 20 m bridge for four speed parameters (a) 0.05, (b) 0.3, (c) 0.6, (d) 1.0 …… 97

Figure 4.16 Vehicle vertical acceleration in the 20 m bridge for four speed parameters (a) 0.05, (b) 0.3, (c) 0.6, (d) 1.0 …… 98

Figure 5.1 The comparison of the effect of the bridge damping ζ_B on DAF with Yang and Wu (2001) model ……... 123

Figure 5.2 The comparison of the effect of the bridge damping ζ_B on DAF with Majka and Hartnett (2008) model ……... 123

Figure 5.3 The comparison of the effect of the bridge damping ζ_B on the bridge mid-span acceleration with Yang and Wu (2001) model …… 124

Figure 5.4	The comparison of the effect of the bridge damping ζ_B on the bridge mid-span acceleration with Majka and Hartnett (2008) model	124
Figure 5.5	The comparison of the effect of the bridge damping ζ_B on the vehicle vertical acceleration with Yang and Wu (2001) model ……..	125
Figure 5.6	The comparison of the effect of the bridge damping ζ_B on the vehicle vertical acceleration with Majka and Hartnett (2008) model	125
Figure 5.7	The comparison of the effect of the vehicle damping ζ_V on DAF with Yang and Wu (2001) model ……...	126
Figure 5.8	The comparison of the effect of the vehicle damping ζ_V on DAF with Majka and Hartnett (2008) model ……..	126
Figure 5.9	The comparison of the effect of the vehicle damping ζ_V on the bridge mid-span acceleration with Yang and Wu (2001) model ……	127
Figure 5.10	The comparison of the effect of the vehicle damping ζ_V on the bridge mid-span acceleration with Majka and Hartnett (2008) model	127
Figure 5.11	The comparison of the effect of the vehicle damping ζ_V on the vehicle vertical acceleration with Yang and Wu (2001) model ……..	128
Figure 5.12	The comparison of the effect of the vehicle damping ζ_V on the vehicle vertical acceleration with Majka and Hartnett (2008) model	128
Figure 5.13	The comparison of the effect of the frequency parameter γ on DAF with Yang and Wu (2001) model ……...	129
Figure 5.14	The comparison of the effect of the frequency parameter γ on DAF with Majka and Hartnett (2008) model ……..	129
Figure 5.15	The comparison of the effect of the frequency parameter γ on the bridge mid-span acceleration with Yang and Wu (2001) model ……	130
Figure 5.16	The comparison of the effect of the frequency parameter γ on the bridge mid-span acceleration with Majka and Hartnett (2008) model	130
Figure 5.17	The comparison of the effect of the frequency parameter γ on the vehicle vertical acceleration with Yang and Wu (2001) model ……..	131
Figure 5.18	The comparison of the effect of the frequency parameter γ on the vehicle vertical acceleration with Majka and Hartnett (2008) model	131
Figure 5.19	The comparison of the effect of the system mass parameter κ on DAF with Majka and Hartnett (2008) model ……..	132
Figure 5.20	The comparison of the effect of the system mass parameter κ on the bridge mid-span acceleration with Majka and Hartnett (2008) model	132
Figure 5.21	The comparison of the effect of the system mass parameter κ on the vehicle vertical acceleration with Majka and Hartnett (2008) model	133

Figure 5.22 The comparison of the effect of the vehicle mass parameter η on DAF with Yang and Wu (2001) model …….. 133
Figure 5.23 The comparison of the effect of the vehicle mass parameter η on the bridge mid-span acceleration with Yang and Wu (2001) model …… 134
Figure 5.24 The comparison of the effect of the vehicle mass parameter η on the vehicle vertical acceleration with Yang and Wu (2001) model …….. 134
Figure 5.25 Ratio of vertical contact forces over static contact forces in the front wheel of the rigid beam model ……... 135
Figure 5.26 Ratio of vertical contact forces over static contact forces in the rear wheel of the rigid beam model ……... 135
Figure 5.27 Ratio of horizontal acceleration over initial acceleration of the rigid beam model ……. 136
Figure 5.28 Simplified illustration of the vehicle model dynamics ……... 136
Figure 5.29 Vehicle vertical acceleration of the rigid beam model ……... 137
Figure 5.30 Bridge midspan deflection of the rigid beam model ……... 137
Figure 5.31 Bridge mid-span vertical acceleration of the rigid beam model ……. 138
Figure 5.32 Hinge support horizontal reaction of the rigid beam model ……... 138
Figure 5.33 Truck model vertical acceleration for μ=0.1 ……..……... 139
Figure 5.34 Truck model vertical acceleration for μ=0.7 ……..……... 139
Figure 5.35 Ratio of horizontal deceleration over initial deceleration for the truck model ……. 140
Figure 5.36 Bridge midspan deflection of the truck model for μ=0.1 ……..…… 141
Figure 5.37 Bridge midspan deflection of the truck model for μ=0.7 ……..…… 141
Figure 5.38 Vehicle midspan acceleration of the truck model for μ=0.1 …..…... 142
Figure 5.39 Vehicle midspan acceleration of the truck model for μ=0.7 …..…... 142
Figure 5.40 Ratio of vertical contact forces over static contact forces of the train model, for initial vehicle speed of 50 m/s …….. 143
Figure 5.41 Ratio of vertical contact forces over static contact forces of the train model, for initial vehicle speed of 100 m/s …… 144
Figure 5.42 Midspan deflection of the train model, for initial vehicle speed of 50 m/s ……... 145

Figure 5.43 Ratio of the summation of vertical contact forces under each bogie over corresponding total static contact forces of the train model, for initial vehicle speed of 50 m/s …… 145

Figure 5.44 Vehicle pitching of various parts of the train model, for initial vehicle speed of 50 m/s ……... 146

Figure 5.45 Vehicle bouncing of various parts of the train model, for initial vehicle speed of 50 m/s …….. 146

Figure 5.46 Ratio of vehicle horizontal acceleration over initial acceleration of the train model for initial vehicle speeds of (a) 50 m/s, (b) 100 m/s, and (c) 200 m/s ……... 147

Figure 5.47 Vertical acceleration of the car body of the train model, for initial vehicle speed of 50 m/s ……... 148

Figure 5.48 Bridge midspan acceleration of the train model for initial vehicle speeds of (a) 50 m/s, and (b) 100 m/s ……. 149

Figure 5.49 Hinge support vertical reaction of the train model, for initial vehicle speed of 50 m/s ……... 149

Figure C.1 Free-body diagram of a wheel …….…….... 185

Figure C.2 Simplified friction models, (a) smooth non-linear friction law, (b) regularized approach (Pfeiffer and Glocker, 1996)…..…….... 185

LIST OF TABLES

Table 3.1	Properties of the half-car planar vehicle model and the bridge (Esmailzadeh and Jalili 2003) …….……	57
Table 3.2	Bridge properties for the half-car planar model (Emailzadeh and Jalili 2003) ……..	57
Table 4.1	Modal frequencies for a simply-supported beam obtained from computer code compared to linear FEM …….	87
Table 4.2	Structural properties of the designed plate-girder open-deck railway bridges …….	87
Table 5.1	Properties of the unsymmetrical truck model …….	122
Table 5.2	Properties of the train model ……...	122

LIST OF SYMBOLS

A	cross-sectional area of beam
a	vehicle longitudinal acceleration
a_0 to a_7	coefficient as defined in Eq. A.10
$[C]$	damping matrix of structure
$[C_b]$	bridge damping matrix, free of any vehicle actions
$[c_b]$	damping matrix of bridge element
$[c_c]$	contact matrix as defined in Eq. A.17
$\left[c^*_{cij}\right]$	damping matrix of VBI element
$[c_{uu}]$	a partitioned damping matrix of the vehicle
$[c_{ww}]$	a partitioned damping matrix of the vehicle
$[c_{uw}]$	a partitioned damping matrix of the vehicle
$[c_{wu}]$	a partitioned damping matrix of the vehicle
$\left[\bar{c}_c\right]$	transformed contact damping matrix by the constraint matrix $\left[\Gamma\right]$
$\left[\hat{c}_c\right]$	transformed contact damping matrix defined in Eq. 3.44
$\{D\}$	bridge displacement vector
$\{d_b\}$	beam element displacement vector
d_c	displacement of an individual contact point
$\{d_c\}$	displacement vector of contact points
$\{d_w\}$	displacement vector of wheels
E	modulus of elasticity
$\{F\}$	vector of internal horizontal forces F
$\{f_a\}$	vector of acceleration forces
$\{f_{ua}\}$	vector of acceleration forces on the DOFs of upper-part
$\{f_{wa}\}$	vector of acceleration forces on the DOFs of wheels
$\{F_b\}$	external loads of bridge
$\{f_b\}$	external nodal forces of bridge element
$\{f_{bci}\}$	vector of consistent nodal forces for ith contact point
$\{f_{bi}\}$	vector of external nodal forces for ith element of bridge
$\{f_c\}$	vector of contact forces
F_w	internal horizontal forces
G	shear modulus
g	acceleration of gravity
h_i	vertical spacing of vehicle discrete masses
I	unit matrix
$[K_b]$	bridge stiffness matrix, free of any vehicle actions
$[k_b]$	stiffness matrix of bridge element
$[\hat{k}]$	stiffness matrix of condensed system
$[k_c]$	contact matrix as defined in Eq. A.18
$\left[k^*_{cij}\right]$	stiffness matrix of VBI element
$[k_{uu}]$	a partitioned stiffness matrix of the vehicle

$[k_{ww}]$	a partitioned stiffness matrix of the vehicle
$[k_{uw}]$	a partitioned stiffness matrix of the vehicle
$[k_{wu}]$	a partitioned stiffness matrix of the vehicle
$\left[\bar{k}_c\right]$	transformed contact stiffness matrix by the constraint matrix $\left[\Gamma\right]$
$\left[\hat{k}_c\right]$	transformed contact stiffness matrix defined in Eq. 3.44
L	length of beam element
$[l]$	transformation matrix
M_t	total mass of the vehicle
$[M_b]$	mass matrix of bridge structure
$[m_b]$	mass matrix of bridge element
$[m_c]$	contact matrix as defined in Eq. A.16
$\left[m^*_{cij}\right]$	mass matrix of VBI element
$[m_{uu}]$	a partitioned mass matrix of the vehicle
$[m_{ww}]$	a partitioned mass matrix of the vehicle
$[m_{uw}]$	a partitioned mass matrix of the vehicle
$[m_{wu}]$	a partitioned mass matrix of the vehicle
$\left[\bar{m}_c\right]$	transformed contact mass matrix by the constraint matrix $\left[\Gamma\right]$
$\left[\hat{m}_c\right]$	transformed contact mass matrix defined in Eq. 3.44
$\{N_c\}$	interpolation vector for displacement of contact point
$\{N^v_c\}$	interpolation vector only for vertical DOFs
$\{N^{vr}_c\}$	interpolation vector for vertical and rotational DOFs
$\{N^h_c\}$	interpolation vector only for horizontal DOFs
$\{N^h_c\}$	interpolation vector only for horizontal DOFs
$\{p_c\}$	load vector as defined in Eq. A.19
$\{p^*_{ci}\}$	equivalent loads as defined in Eq. 3.17a
$\left\{\hat{p}_c\right\}$	transformed load vector defined in Eq. 3.44
$\{P^*_c\}$	equivalent contact forces of structure
$\{q_c\}$	load vector as defined in Eq. A.20
$\{q^*_{ci}\}$	equivalent loads as defined in Eq. 3.17b
$\left\{\hat{q}_c\right\}$	transformed load vector defined in Eq. 3.44
r	radius of gyration
r_{ci}	irregularity profile at the contact point of i^{th} wheel
$\{r\}$	vector of irregularity profile at contact points
$\left\{r^*\right\}$	equivalent irregularity profile as defined in Eq. 3.18
S	speed parameter, defined in Eq. 4.8
SP	spring-damper forces
T_E	torque applied by the engine exerted on the wheel axle
t	time, or time at the beginning of time step
$t+\Delta t$	time at the end of the time step
V_i	total vertical force acting at i^{th} contact point of bridge
V_i'	dynamic vertical contact forces

$\{V\}$	vector of total vertical contact forces
v	vehicle speed
X	beam global coordinate
x	beam local coordinate
$\bar{x}$	ratio of the local wheel location x over the beam element length L.
$[z]$	acceleration parameter, defined in Eq. 3.42
γ	frequency parameter
$[\Gamma]$	constraint matrix
$\{\Delta d_u\}$	upper-part vehicle displacement increments
Δt	time increment
η	vehicle mass parameter
κ	system mass parameter
μ_i	coefficient of friction for i^{th} wheel
$[\mu]$	diagonal matrix of coefficient of frictions of all wheels
ξ	damping coefficient
ρ	mass per unit length
$[\Phi]$	geometry matrix
$[\Phi_w]$	a partitioned geometry matrix due to DOFs of wheels
$[\Phi_u]$	a partitioned geometry matrix due to DOFs of upper-parts
$[\psi_{uu}]$	equivalent matrix for upper part of car body, Eq. A.12
$[\psi_{wu}]$	matrix as defined in Eq. A.21
$[\Omega]$	dimensionless matrix of equilibrium
Ω	vehicle driving frequency, defined in Eq. 4.6
ω	bridge fundamental frequency

NOMENCLATURE

AASHTO	American Association of State Highway and Transportation Officials
AREMA	American Railway Engineering and Maintenance-of-Way Association
DAF	Dynamic Amplification Factor
DOF	Degree Of Freedom
VBI	Vehicle-Bridge Interaction
LRFD	Load and Resistance Factor Design
FE	Finite Element
FL	Flexure stiffness, Lumped mass
FSL	Flexural plus Shear stiffness, Lumped mass
FSCR	Flexural plus Shear stiffness, Consistent-Rotary mass
2-D	two dimensional
3-D	three dimensional

CHAPTER 1

INTRODUCTION

1.1 BACKGROUND

The dynamic interaction between moving vehicles and a bridge lies within the vast area of structural dynamics. This is a coupled, time-dependant dynamic problem. The vehicle and the bridge are the two subsystems interacting with each other through contact forces. If the vehicle speed is constant and there is no obstruction ahead, contact forces will be only vertical forces. However, if the vehicle experiences acceleration or deceleration, horizontal contact forces will be present in addition to vertical contact forces. The two subsystems are commonly considered as two elastic systems oscillating and interacting with each other. Therefore, the main dominant parameter is the natural frequencies of the vehicle and the bridge and also the vehicle driving frequency. The driving frequency is important since it governs the rate of forces acting on the two subsystems.

In the design of conventional highway or railway bridges, the dynamic effects are considered with the well known Dynamic Amplification Factor (DAF) or impact factor. There are many parameters that affect the dynamic behaviour of the bridge in addition to its span or natural frequency. Some of these parameters include vehicle speed, weight, and dynamic characteristics, the state of the structure, roadway or track roughness, expansion joints, the type of bridge supports, and influence of secondary elements.

Numerical methods have been used widely to analyze bridge dynamics since they can incorporate complex models of bridges and vehicles. However, there is still a need for the development of better, more comprehensive numerical models that addresses the limitations of the existing models.

1.2 MOTIVATION

There has been much research on the analysis of bridges traversed by running vehicles. Appropriate simulation of the interaction of vehicles and bridges is vital in bridge engineering applications. Majority of the available research work is limited to a few vehicle models or bridge models. Such studies require the extraction of long equations for each vehicle or bridge model individually in every analysis. Therefore, a generalized model that represents the vehicle and bridge interaction will ease the analysis procedure.

Majority of research in this area focused on the dynamic response of the bridge and not the vehicle. In this case, where only the response of the bridge is required, the moving vehicles are usually simplified and approximated by a number of moving loads. However, the vehicle response can also be of importance depending on the application under consideration. In the design of high-speed railways, the vehicle's vertical acceleration is a design criterion concerning the passenger comfort and should be calculated appropriately. Moreover, a comprehensive study on the dynamic response of a given bridge would necessitate accounting for various sources of dynamic effects (e.g. effect of road roughness or rail irregularities). In such cases, a Vehicle-Bridge Interaction

(VBI) is required. The VBI analysis deals with those types of analysis where the response of both the vehicles and the bridge is simulated.

One of the most efficient methods of the vehicle-bridge interaction analysis is to adopt the dynamic condensation method and to *condense* the effect of running vehicles into the bridge equations. One of these methods involves the application of VBI elements referring to bridge beam elements (or other types of elements such as shell elements) that are in direct contact with one or more wheels of the running vehicles. Other bridge elements are treated as regular beam elements. In spite of the available models in this area, there is still a need to develop upgraded models that addresses shortcomings of available models; in particular, for the case of vehicles with acceleration or deceleration.

1.3 OBJECTIVE AND SCOPE

The main objective of this thesis is to establish efficient procedures within the framework of Finite Element Method (FEM) for solving the dynamic response of the VBI problems for various vehicle operating conditions. The formulation of these models will be kept as general as possible, so that they can be applied to most practical applications, while identifying the effect of various parameters on the response of vehicles and the bridge.

In order to achieve the thesis objective, the scope of the research is to:

1. Develop a modified VBI element for vehicles moving with constant velocity where the longitudinal acceleration is zero.
2. Develop a VBI element for vehicles moving with acceleration or deceleration. In this case, horizontal longitudinal forces exist which necessitates new formulation.

3. Verify the validity of the developed VBI elements numerically by using other models and results available in literature.
4. Investigate the significances of the developed VBI elements and identify the response parameters that could be particularly captured.
5. Study the effect of important parameters and model variables on the VBI analysis response, and also indicate the sensitivity of the bridge/vehicle important responses. The emphasis will be on assessing the key responses that would influence the design of bridge structures or bridge components (e.g. track structure of railway bridges). The studied key responses are: bridge mid-span deflection, bridge mid-span acceleration, and vehicle's vertical acceleration. The parameters and variables included in modeling are shear deformation, consistent mass, bridge and vehicle damping ratios, frequency parameter, system mass parameter, and a newly proposed parameter called vehicle mass parameter.

1.4 OUTLINE OF THE THESIS

The thesis is organized in six chapters as follows:

- Chapter two presents a review of previous work in the analysis of vehicle-bridge interaction, and the modeling of the vehicle and bridge.
- Chapter three includes the development of two VBI elements; one for vehicles moving with constant velocity, and another for vehicles with acceleration. This chapter also includes verification models to validate the developed VBI elements and the coded MATLAB program.

- Chapter four investigates the effect of shear deformation and consistent mass of the bridge modeling on the response of the vehicle and the bridge.
- Chapter five compares the results of new VBI elements with available models in literature. It also includes a parametric study of important model variables in the VBI analysis.
- Chapter six presents the important outcomes and conclusions of this thesis and recommendations for future work.

CHAPTER 2

LITERATURE REVIEW

2.1 INTRODUCTION

Research efforts in the area of studying the dynamic response of bridges subjected to moving vehicles experienced two distinguished phases. The application of digital computers can be considered as the separation limit of these two phases. Before the application of computers, methods were analytical, simplified or approximate in order to analyze simple and fundamental problems. As the simplified analysis of the early research efforts is not applicable in the analysis of complex VBI problems, this literature review will be focusing mostly on the relatively recent research. If required, an exhaustive literature review on the vehicle-bridge dynamics can be consulted in Yang et al. (2004).

The availability of digital computers assisted researchers to consider more realistic vehicle and bridge models in the analysis. Early studies conducted by Timoshenko and Young (1955) and later by Biggs (1964) focused only on the moving load analysis of the bridge. More studies on the moving load analysis were performed by Frýba (1972). The dynamics of railway bridges were later studied comprehensively by Garg and Dukkipati (1984) and Frýba (1996). Nowadays, researchers can model and analyze the vehicle-bridge interaction phenomenon with almost no limitation in the bridge or vehicle models. However, the majority of the research is focused on the bridge response not the vehicle response.

2.2 VEHICLE MODELING

Various types of vehicle modeling can be selected depending on the application required. Vehicle modeling has a significant effect on the amount of the analysis time and effort involved, and should be chosen carefully.

2.2.1 Moving Load Models

The simplest model that can be considered for the dynamic interaction of vehicles and bridges is the moving load (or moving force) model. Wheel loads or axle loads are simplified by constant vertical forces traversing the bridge with the velocity equal to the vehicle speed. Hence, the interaction between vehicle and the bridge is ignored and the inertia effect of the vehicle is neglected. This is an acceptable method in cases where the ratio of the vehicle mass to the bridge mass is small and only the response of the bridge is of interest (Yang et al. 2004). Moreover, this method can be used if some sources of dynamic effects (such as road irregularities, rail joints, bumpers, wheel flat, etc.) are not required to be considered in the analysis. In addition, this model could be interesting in cases where a closed form solution is required or in the rough assessment of the dynamic effects of the bridge as used by Frýba (2001) and Brady et al. (2006).

Although the moving load method is approximate, it is the most applied in the analysis and design of bridges due to its simplicity. Sample of research work in this area includes: Frýba 1972, Wu and Dai (1987), Weaver et al. (1990), Galdos et al. (1993), Gbadeyan and Oni (1995), Wang (1997), Zheng et al. (1998), Rao (2000), Chen and Li (2000), and Dugush and Eisenberger (2002). Another reason of vast application of simplified methods is that the key governing parameters can be identified using closed-

from solutions; hence, rational simple formulas can be developed for application in design codes (Humar and Kashif, 1993).

2.2.2 Moving Mass Models

This is the next simplest model after the moving load model used for cases where the ratio of the vehicle mass to the bridge mass is not small and the inertia effect of the vehicle may have considerable effect on the bridge response. Considerable research has been conducted on the development of numerical and analytical solutions for moving mass problems. Fourier series expansion was used by Stanišić and Hardin (1969) to obtain the response of a simple beam under an arbitrary number of moving masses. Ting et al. (1974) and Sadiku and Leipholz (1987) applied Green's function to study the moving mass problem. A closed form solution was first derived by Stanišić (1985) for the analysis of a single mass passing a simple beam. The same closed-form moving mass model was applied by Akin and Mofid (1989) in an analytical-numerical approach for the moving mass problem of beams with various boundary conditions.

Although the moving mass model can include the inertia effect of the moving vehicle, it neglects the effect of relative displacement (vehicle bouncing) between the vehicle and the bridge. This may have significant effect on the bridge response where the road roughness or rail irregularities to be included in the analysis and also for high-speed vehicles. In addition, the moving mass model can not be used if the response of the vehicle is also of importance since the vibration of the moving mass is commonly assumed as the contact point of the bridge surface in a no-jump algorithm.

2.2.3 Moving Sprung Mass Models

The simplest model considering the effect of suspension system is the so-called moving sprung mass model. In this model, the moving mass model is supported by a spring and dashpot as shown in Fig. 2.1. This model can be used as a generic model to study the interaction between a vehicle and the bridge. The problem of sprung mass traversing a simple beam was solved by Biggs (1964) using a semi-analytical approach. Frýba (1972) studied different types of vehicle modeling including, moving load, moving mass, and moving sprung mass model. The researcher studied the main parameters and the effect and sensitivity of various variables in the bridge response, followed by developing analytical and numerical solutions. This book was revised in the second edition (Frýba 1999). Other studies were also carried out for the analysis of an elastic continuum traversed by multiple moving oscillations by Pesterev et al. (2001) and Pesterev et al. (2003) using a series expansion technique.

2.2.4 Moving System Models

More elaborate models compared to sprung models that consist of many DOFs are usually called moving system models (Majka and Hartnett, 2008). The various parts of the vehicle are modeled as discrete masses connected to each other by a suspension system. The suspension system is commonly modeled having stiffness and damping properties. The stiffness properties of tires and suspension system have been modeled by springs with linear properties; and damping properties of tires, suspension system, and air cushions have been modeled by linear dashpots (Genin et al., 1975; Blejwas et al., 1979; Genin and Chung, 1979; Humar and Kashif, 1993; Green and Cebon, 1994; Xia et al.,

2003; Majka and Hartnett, 2008). However, nonlinear models for forces in suspension system were also utilized by Hwang and Nowak (1991) for trucks with numerous DOFs.

Due to significant dynamic interaction between railway bridges and trains, various models have been applied to model the train. A simple model that is capable of including the pitching effect of the car body was adopted by Yang et al. (1999). This model was a 4-DOF model, three vertical and one rotational (or pitching) DOF. The car body was modeled as a rigid beam supported by two suspension systems (linear spring and dashpot), each connected to one wheel. Models including various mechanical parts of a train such as wheelset, bogie, and the car body with linear suspension properties have been used extensively (Zhang et al. 2001; Xia et al. 2001; Xia et al., 2003; Kwark et al., 2004; Lee et al. 2006; Majka and Hartnett 2008). In North America, bogie is called *wheel truck* or simply *truck*. However, in order to clearly differentiate between a truck vehicle and the truck (or bogie), the term *bogie* will be used in the current thesis.

Detailed train models are used primarily for the analysis of the vehicle-bridge interaction of high-speed trains. A sample of 2D train model used by Wu and Yang (2003) is shown in Fig. 2.2. This is a 10-DOF model composed of the vehicle body, front and rear bogies, and four wheels. All are assumed to be rigid bodies connected by linear springs and dashpots as shown. Vertical and rotational (or pitching) DOFs are considered for the vehicle body (or the car body) and bogies, and only vertical DOFs are adopted for wheels. A sample 3D vehicle model is shown in Fig. 2.3 applied by Majka and Hartnett (2008). Similar parts are considered for the vehicle model with additional DOFs. For the car body and the two bogies, a total of 5 DOFs were assumed. Two translational DOFs for vertical and lateral displacements and three rotational DOFs for pitching, rolling

(about x-axis), and yawing (about z-axis) motions were considered. For wheels, only 3 DOFs were considered including the vertical, lateral and rolling motions. Therefore, a total of 27 DOFs were used to model one car of a moving train.

2.3 BRIDGE MODELING

Various types of bridge modeling have been adopted in the study of the vehicle-bridge dynamics. The selection of the model depends on the analysis procedure and intended goals. Some of the most important models are summarized below.

Early studies on the VBI analysis utilized the continuum models represented by Euler-Bernoulli beam equation. These models were used mostly for the simple span bridges with limited cross sectional variety. The advantage of these models, in addition to its simplicity, is the ability to obtain a closed-form solution. This model is still attractive for researchers who intend to study the VBI theoretically with closed-form equations (Biondi et al., 2005). Euler-Bernoulli beam has some simplifications which may not be acceptable in some cases; therefore, other models such as the Timoshenko beam element can be used which includes shear deformations and rotary inertia.

The continuum beam models are sufficient only for simple structures. For more complex bridges, combined continuum-discrete models were developed. This approach was applied to model three-span uniform cross-section continuous bridge with internal hinge (Veletsos and Huang, 1970), double-I-girder bridges (Chu et al., 1979), and truss bridge with rigid, semi-rigid or pinned joints (Garg and Dukkipati, 1984).

Advancements in the computational technology have provided the required tools to model any complex structures using the discrete methods. These methods also provide

good programming ability for writing computer programs in step-by-step calculations. Among these methods, Finite Element Method (FEM) has attracted the greatest interest to model various types of bridges in the majority of recent works.

As an example of the bridge modeling using FEM, Majka and Hartnett (2008) introduced a three-dimensional, two-node finite beam element for a railway bridge. Euler-Bernoulli formulation was applied to result in an element capable of capturing the axial, bi-directional bending and torsional displacement. Six DOFs on each node make a 12-DOF element sufficient to simulate different types of motions.

2.3.1 Road Roughness and Rail Irregularities

One of the essential parameters in the dynamic response of the bridge and also the vehicle is the road roughness (for highway bridges) or rail irregularities (for railway bridges). Surface profile can have different conditions depending on the initial construction, weather conditions, and maintenance. The surface roughness or rail irregularities are 3D in nature, but they are frequently modeled in 2D. For track structure of railway bridges, each rail can have its own irregularities independently from the other rail.

The roughness of the pavement of highway bridges is a random parameter in nature. It was modeled primarily by Power Spectral Density (PSD) functions. Random functions are generated depending on the road condition (poor to excellent) and provide a profile along the bridge (Hwang and Nowak, 1991; Marcondes et al., 1991; Pan and Li, 2002; Yang and Lin, 1995). Another source of dynamic effect in highway bridges is the thermal expansion joints, effect of which may be included in the analysis.

Most of the sources of dynamic effects in railway bridges have been summarized by Frýba (1996). They can be categorized into two main groups, periodic and random irregularities. Periodic irregularities can be described by Fourier series. These irregularities can generate resonance vibrations because of their periodic nature; however, this rarely occurs in regular railway bridges. Some of the sources of periodic irregularities are rail joints, wheel flats, isolated irregularities, undulated rail surface, and presence of cross-beams and ties. The second group of dynamic sources is random irregularities which are mostly due to track roughness and imperfection. Similar to road pavement, random rail irregularities are commonly described by PSD functions. Detailed numerical models are available to model various sources of dynamic effects such as wheel flat (Uzzal, 2008; Zhu et al., 2009; Zhu et al., 2010).

2.4 METHODS OF SOLUTION FOR VEHICLE-BRIDGE INTERACTION (VBI)

VBI analysis is called to those vehicle-bridge interaction analyses where the responses of both the bridge and the vehicle are calculated (Yang et al., 2004). For very basic and simple cases, where the moving load or moving mass models are considered together with basic beam models, closed-form solutions are available in literature (Frýba, 1972; Stanišić, 1985). These solutions are approximate due to the simplifications in the applied loading, and they can be used only if the bridge dynamics are of interest and the vehicle velocity is low. However, VBI analysis should be performed when the vehicle response is also required or more sophisticated dynamic analyses need to be done.

Considering vehicle and bridge models, two sets of equations of motion are written, one for the vehicle and another one for the bridge. Each equation of motion is a second-order differential equation. These two sets of equations are coupled through the interaction between the two subsystems (i.e. the vehicle and the bridge). The interaction is exerted by contact forces which are the forces induced at the contact points between the wheels and the bridge surface. Since the contact points move with respect to time, the equations of motions are two sets of coupled time-dependent second-order differential equations needed to be solved simultaneously.

All the analysis methods proposed for the VBI analysis are step-by-step dynamic methods. At each time step, it is required to solve a set of second order differential equations of motion. Methods that have been more frequently adopted in solving second-order differential equations in VBI problems include the direct integration methods such as, Newmark-β method (Inbanathan and Wieland, 1987; Yang and Lin, 1995), Wilson's θ method (Sridharan and Mallik, 1979), and fourth-order Runge–Kutta method (Chu et al., 1986). In addition to the direct integration schemes, the Fourier transformation method has also been used (Green and Cebon, 1994; Chang and Lee, 1994).

The most important and frequently used methods for the VBI analysis can be classified into three main categories: Iterative Solution of Contact Forces, Modal Superposition, and Dynamic Condensation.

2.4.1 Iterative Solution of Contact Forces

This method can be categorized as the simplest yet the most direct approach of the treatment for the VBI problem. Two sets of equation of motions (one for the vehicle and

another one for the bridge) are coupled through the contact forces. The main idea is to calculate contact forces at each time step that satisfy both sets of equations of motion. Depending on the analysis approach, various procedures can be adopted (Hwang and Nowak, 1991; Green and Cebon, 1997; Yang and Fonder, 1996). For instance, one way of analysis is to assume initial values for the displacement of contact points at each time step which is usually the values calculated from the previous time step. Then, contact forces are calculated using the vehicle equation of motion. Using these contact forces, bridge equation of motion is solved and new values for contact points are obtained. The procedure is repeated until a convergence criterion is satisfied.

Yang and Fonder (1996) introduced a more versatile iterative solution method. They divided the interaction forces exerted by running vehicle on the bridge element into two main categories: movement-dependent and movement-independent forces. Using the vehicle kinematic property at the beginning of the time step, these forces can be calculated. Then, the trial value for the motion of the bridge is calculated to be compared with the last available guess, after which, the convergence criterion is verified. If the convergence is not achieved, an improved trial value for the initial guess is introduced which can be based on two techniques: relaxation, or Aitken acceleration (Dahlquist and Bjorck, 2008).

Despite the simplicity of these iterative methods, the convergence rate is likely to be low particularly for a series of vehicles where many contact points are involved. In addition, the convergence criterion is questionable and the selection of a suitable value may require several separate complete analyses. The VBI analysis of trains consisting of many cars and locomotives can be very time-consuming using simple iterative methods.

2.4.2 Modal Superposition

The modal superposition technique was used by many researchers as of 1960 to analyze the dynamic interaction of vehicle and bridges (Frýba, 1967; Frýba, 1972; Richardson and Wormley, 1974; Ting and Genin, 1980; Genin et al., 1982) and still is being used (Xia et al. 2001 and 2003) depending on the analysis approach. After the construction of the bridge model, the mode shapes and modal frequencies are calculated. Then, only some lowest dominant bridge modes are considered to analyze the bridge equation of motion at each time step. Hence, the computational effort will be substantially reduced. Xia et al. (2001) formulated a 3D-vehicle equation of motion solved at each time step using Newmark-β integration algorithm with $\beta=0.25$.

Despite the advantages of this method, it is not versatile to add other additional effects to the model, such as wheel impact and rail irregularities (in case of railway bridges) or road roughness (in case of highway bridges). In addition, due to the interaction between vehicles and the bridge considering the inertial effects of the moving vehicle, bridge modal characteristics are being modified since they do not remain constant especially for heavy vehicles such as freight trains. The change in the modal properties was studied by Li et al. (2003).

2.4.3 Dynamic Condensation

In general, in the dynamic condensation methods, a portion of the structure's DOFs, known as 'master', are kept and the remaining DOFs, known as 'slave', are eliminated by relating them to the retained DOFs. In other words, these methods primarily reduce the order of the system by condensing the *slave* DOFs to the *master*

DOFs. Hence, less computational effort will be required to solve the equations of motion including only the master DOFs. Dynamic condensation method on the element level is viewed as one of the most efficient approaches in solving the VBI equations (Yang et al, 2004).

If only the response of the bridge is desired, all vehicle DOFs can be condensed to those of the bridge. Garg and Dukkipati (1984) adopted the Guyan (1965) condensation scheme to eliminate all vehicle DOFs. Although the vehicle response can be calculated from equations of *slave* DOFs, they are not accurate enough due to the approximations inherent in relating the vehicle (slave) DOFs to the bridge (master) DOFs.

Another method was used by Yang and Lin (1995) to condense all vehicle DOFs on the element level in a finite element formulation. They introduced the concept of VBI element. Using the finite element scheme, a bridge model can be constructed by a number of beam elements (say, for example, Euller-Bernouli beam elements). In addition, the body of each railroad car was assumed to be a rigid bar and was idealized as two lumped masses at the two ends of the rigid bar. As shown in Fig. 2.4, the train is then simplified by a series of sprung mass models. Some of the beam elements are in direct contact with the sprung masses. These are called interaction elements or more specifically vehicle-bridge interaction (VBI) elements with the same DOFs as the original beam elements but different mass, stiffness, and damping properties. A VBI element with the element length of l is shown in Fig. 2.5. Using an iterative dynamic condensation method, eigenvalues (ω^2) of the VBI elements were calculated. Then, the associated mass matrix is also obtained followed by the modified stiffness matrix. To calculate the damping coefficient of the VBI element, Rayleigh method was adopted. Since the VBI elements have the

same number of DOFs of other original beam elements, the overall bridge matrices are easily assembled using the conventional assembling methods.

Later, Yang and Yau (1997) introduced a more advanced VBI element. They used the same vehicle idealization as used by Yang and Lin (1995); i.e. sprung mass units were applied to model the entire train. Two sets of equations were written, one for the sprung mass units and another one for the beam elements. The vehicle equations of motion were then solved by the Newmark-β integration scheme at each time step. Using the formulation obtained by Newmark-β and the concept of condensation, the vehicle (slave) DOFs were condensed to the associated beam (master) DOFs of the VBI elements. Then, the overall bridge matrices are assembled using a conventional element-assembly process. The modified bridge equation of motion is solved using an iterative procedure based on Newton-Raphson algorithm until a convergence criterion is satisfied. Using the VBI elements, various dynamic properties of the bridge and vehicles can be considered in the formulation, including the rail irregularities, ballast stiffness, wheel flat, damping of the beam, and stiffness and damping of the vehicles.

A more versatile method was proposed by Yang and Wu (2001) based on the concept of VBI elements. This method does not have the vehicle idealization as sprung masses and applies the real vehicle models with any complexity. At each time step, Newmark-β method is used to solve the vehicle equation of motion which is written separately for in-contact and not-in-contact DOFs. In-contact DOFs are due to the wheels DOFs which are in direct contact with the bridge, and the rest of the vehicle DOFs are considered as not-in-contact. With the no-jump assumption, the contact point displacements are related to the wheel DOFs by a constraint relationship. Then, the

vertical contact forces are formulated based on the contact points. These forces are substituted to the beam equation of motion as external forces. Their equivalent nodal forces are then calculated applying suitable interpolation functions. The bridge's overall matrices are assembled and the bridge equation of motion is solved by Newmark-β with no iterations. Due to the versatility and computational advantages of this method, it has been widely acknowledged and used by researchers. The details of the formulation are presented in Appendix A.

2.5 TREATMENT OF VEHICLE LONGITUDINAL ACCELERATION OR DECELERATION

Few studies have investigated the effect of vehicle horizontal acceleration on the response of the vehicle and its interaction with the bridge. Yang and Wu (2001) simply modeled horizontal contact forces using friction coefficients multiplied by vertical contact forces. They used the same vertical contact forces calculated based on the formulation developed for vehicles with constant velocity. Ju and Lin (2007) presented a finite element model of vehicle-bridge interaction considering braking and acceleration. Their method needs iteration in each time increment and they assumed constant horizontal acceleration for their formulation.

It is more common to construct the vehicle models used in VBI analysis with no embedded horizontal DOFs (Yang and Wu, 2001; Law and Zhu, 2005). However, few studies applied horizontal DOFs with linear spring-dashpot units (Ju and Lin, 2007). In current thesis, the VBI elements are developed for vehicle models with no horizontal DOFs.

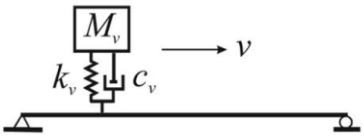

Fig. 2.1 Sprung mass model

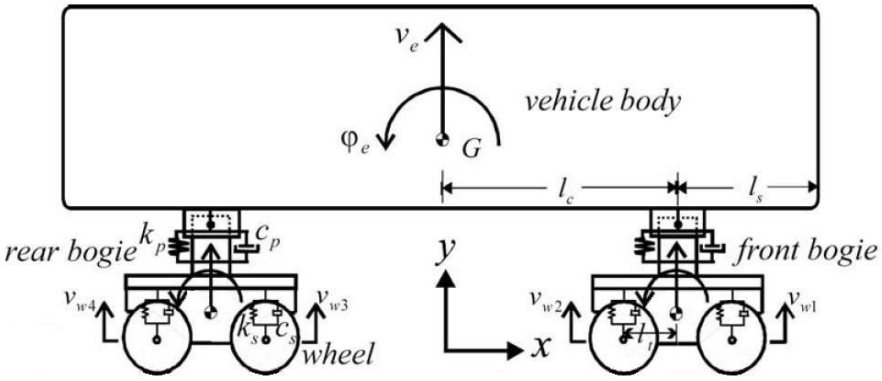

Fig. 2.2 A 2D model of one car of a train (Wu and Yang, 2003)

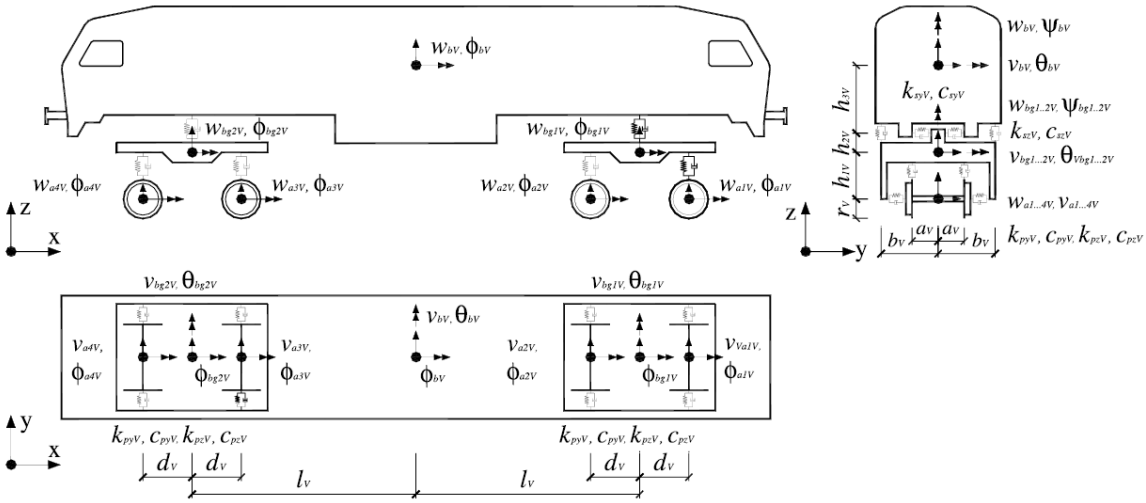

Fig. 2.3 A 3D model of one car of a train (Majka and Hartnett, 2008)

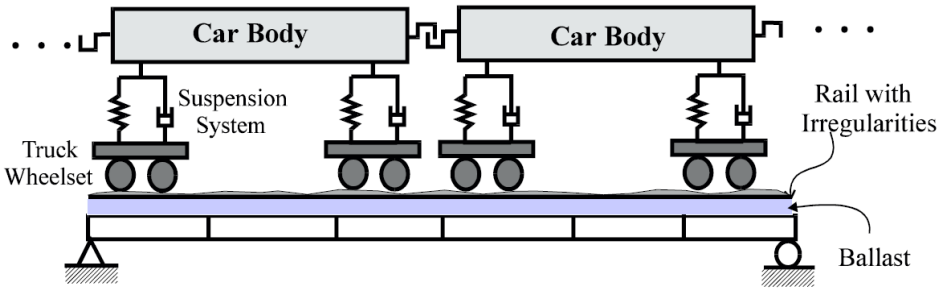

(a)

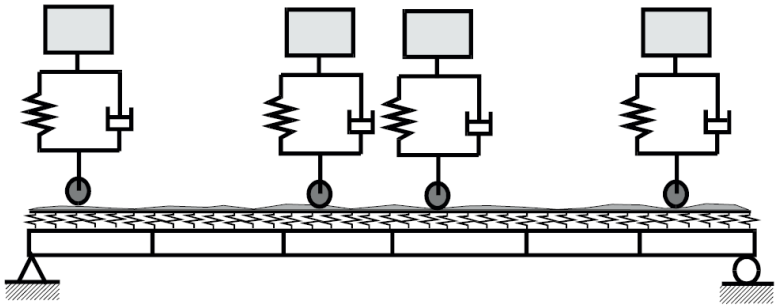

(b)

Fig. 2.4 Train-Bridge model: (a) a general model, (b) simplified sprung mass model (Yang et al., 2004)

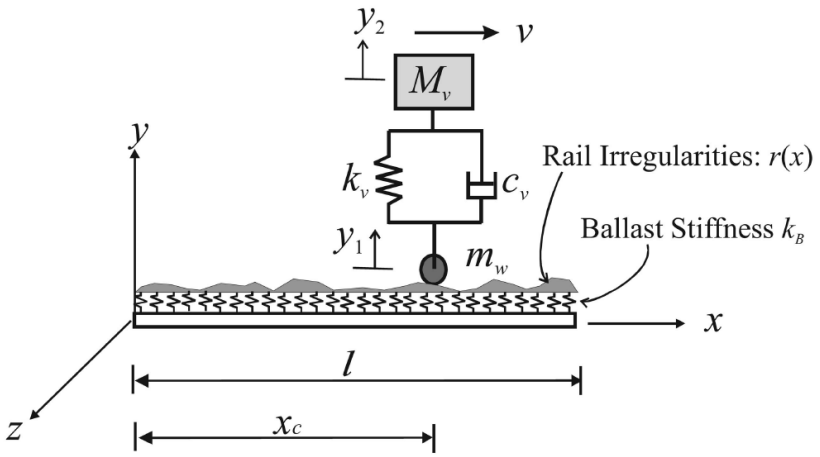

Fig. 2.5 A Vehicle-Bridge Interaction (VBI) element (Yang et al., 2004)

CHAPTER 3

DEVELOPMENT OF 2-D NUMERICAL VEHICLE-BRIDGE INTERACTION ELEMENTS

3.1 INTRODUCTION

There has been a growing interest to model and analyze Vehicle–Bridge Interaction (VBI) of intricate vehicles on bridges. The objective of such an analysis is to realistically investigate the dynamic effects of moving vehicles particularly in case of high-speed trains, where the vehicle acceleration is a design criterion and should be well predicted. One method of analysis is to eliminate the wheel degrees of freedom (DOF) that are in direct contact with the bridge surface resulting in a VBI element, which is a modified conventional beam element that is acted upon directly by wheels of a running vehicle. The bridge may have other elements that have no imposed wheels, which are treated as regular beam elements. In this study, the analysis type used for the VBI problem is the time history analysis with suitable time increments.

In this chapter, numerical VBI elements are developed for two cases of vehicles: vehicles with constant velocity, and vehicles experiencing acceleration or deceleration. Vehicles are modeled as a combination of solid parts (e.g. vehicle body, wheels, tires, etc.) connected by a linear suspension system. The vehicle models excluding horizontal DOFs are used for developing the VBI elements. This type of vehicle modeling is more common and was used by majority of researchers (Yang and Wu 2001; Xia et al. 2003; Majka and Hartnett 2008); however models with horizontal DOFs were also used by few researchers (e.g. Ju and Lin 2007). Moreover, the bridge is modeled by beam elements

which can be Euler-Bernoulli or other types of beam elements. The VBI element developed for vehicles with constant velocity is used in the development of the VBI element for vehicles with acceleration.

In the development of the VBI element for vehicles with constant velocity, the available formulation obtained by Yang and Wu (2001) is used to formulate the contact forces. The contact forces are the mutual forces between the wheel and the bridge surface. For vehicles with acceleration, the procedure is first developed for a basic vehicle model and then it is generalized for a general vehicle. More vehicle examples are presented to demonstrate how the procedure works.

3.2 NUMERICAL VBI ELEMENT FOR VEHICLES WITH CONSTANT VELOCITY

3.2.1 Basic Equations

In the two-dimensional (2-D) analysis of a vehicle with constant speed, there is no horizontal acceleration in the vehicle, implying that no horizontal contact forces are present and only the vertical contact forces are transferring vehicle loads to the bridge. The equation of motion for a beam element traversed by the *i*th wheel at the end of the time increment ($t + \Delta t$) can be shown as:

$$[m_{bi}]\{\ddot{d}_{bi}\}_{t+\Delta t} + [c_{bi}]\{\dot{d}_{bi}\}_{t+\Delta t} + [k_{bi}]\{d_{bi}\}_{t+\Delta t} = \{f_{bi}\}_{t+\Delta t} - \{f_{bci}\}_{t+\Delta t} \quad (3.1)$$

where $[m_{bi}]$, $[c_{bi}]$, and $[k_{bi}]$ are the mass, damping and stiffness matrices of the beam element. $\{d_{bi}\}$ is the nodal displacement vector of this element and $\{f_{bi}\}$ is the vector of

the nodal external forces. $\{f_{bci}\}$ is the vector of the equivalent nodal forces resulting from the $V_{i,t+\Delta t}$ contact force.

Vertical contact forces $V_{i,t+\Delta t}$ are entries of the corresponding vector $\{f_c\}_{t+\Delta t}$ which can be formulated as (Yang and Wu 2001):

$$\{f_c\}_{t+\Delta t} = [m_c]\{\ddot{d}_w\}_{t+\Delta t} + [c_c]\{\dot{d}_w\}_{t+\Delta t} + [k_c]\{d_w\}_{t+\Delta t} + \{p_c\}_{t+\Delta t} + \{q_c\}_t \tag{3.2}$$

where $[m_c]$, $[c_c]$, and $[k_c]$ are called the contact matrices and they are all known, and follow Eqs. A.16 to A.18. $\{d_w\}$ is the displacement vector of the wheels which is unknown. $\{p_c\}_{t+\Delta t}$ is the effect of external forces on the vehicle DOFs at the end of the time increment and is known given in Eq. A.19. Finally, $\{q_c\}_t$ represents the effect of the vehicle displacement vector and its derivatives at the beginning of the time increment which is known in a step-by-step analysis given in Eq. A.20.

To relate the contact force V to the corresponding element nodal forces $\{f_b\}$, an interpolation function $\{N_c\}$ is used:

$$\{f_b\} = \{N_c\}V \tag{3.3}$$

The interpolation functions are chosen depending on the method of modeling and the dynamic degrees of freedom (DOFs) considered for the bridge elements. For the case that a lumped mass model is used, an interpolation function $\{N_c^v\}$ incorporating only vertical DOFs is sufficient; i.e. all the entries in $\{N_c^v\}$ are set to zero except those regarding vertical DOFs. This ensures that there would only be vertical resultant nodal forces. Nevertheless, for a model based on consistent mass, an interpolation function $\{N_c^{vr}\}$ is needed which includes the effect of the rotational DOFs in addition to the

vertical DOFs. In this study the lumped mass model is used. Hermitian cubic polynomials can be used as the interpolation functions. $\{N_c^v\}$ or $\{N_c^{vr}\}$ are calculated based on the location of the wheel on the element, *x*, which is a function of time. For a two dimensional 6-DOF Euler-Bernoulli beam element composed of vertical, horizontal, and rotational DOFs at each node, the corresponding interpolation functions are as follows:

$$\{N_c^v\} = \langle 1 - 3\bar{x}^2 + 2\bar{x}^3, 0, 0, 3\bar{x}^2 - 2\bar{x}^3, 0, 0 \rangle^T \tag{3.4a}$$

$$\{N_c^{vr}\} = \langle 1 - 3\bar{x}^2 + 2\bar{x}^3, 0, x(1 - 2\bar{x} + \bar{x}^2), 3\bar{x}^2 - 2\bar{x}^3, 0, x(\bar{x}^2 - \bar{x}) \rangle^T \tag{3.4b}$$

where $\bar{x}$ is the local coordinate of the contact point on the element, i.e. $\bar{x} = x/L$ where L is the element length (see Fig. 1).

3.2.2 Effect of Road Irregularities in the New Formulation

The wheel displacement vector $\{d_w\}$ can be related to the contact displacement $\{d_c\}$ of the bridge by the following constraint equation (Wu et al. 2001),

$$\{d_w\} = [\Gamma]\{d_c\} + \{r\} \tag{3.5}$$

where $[\Gamma]$ is a constant transformation matrix and $\{r\}$ represents the effect of the road irregularities. $\{r\}$ usually is defined based on the power spectral density functions which by themselves are functions of the location of the vehicle on the bridge *X* with respect to an origin, such as the beginning of the bridge.

Before starting the differentiations, it is required to distinguish between the local coordinate *x* and the global coordinate *X*, and their effect on the differentiation. For any beam element of the bridge, the relationship between *x* and *X* using a constant can be written as $X = x +$ Cons. Using the chain rule, one can show that the derivative of any

function of X (such as $\{r\}$) with respect to X is equal to the derivative of that function with respect to x. Since $X = x + \text{Cons.}$, $\frac{dX}{dx} = \frac{dx}{dX} = 1$, where $\frac{d}{dx}$ is the derivative operator with respect to the variable specified in the denominator. By the chain rule, $\frac{d(\{r\})}{dX} = \frac{d(\{r\})}{dx}\frac{dx}{dX}$, where $\frac{dx}{dX} = 1$. Hence, $\frac{d(\{r\})}{dX} = \frac{d(\{r\})}{dx}$. This means that if $\frac{d(\{r\})}{dx}$ is required, it can be calculated from $\frac{d(\{r\})}{dX}$, which is easier to be calculated.

The first derivative of the wheel displacement vector $\{d_w\}$ with respect to the local coordinate x is obtained as:

$$\{\dot{d}_w\} = [\Gamma]\{\dot{d}_c\} + \frac{dx}{dt}\{r\}_{,x} = [\Gamma]\{\dot{d}_c\} + v\{r\}_{,x} \tag{3.6}$$

where v is the velocity of the vehicle and the comma denotes the differentiation with respect to the coordinates specified. By taking another derivative,

$$\{\ddot{d}_w\} = [\Gamma]\{\ddot{d}_c\} + a\{r\}_{,x} + v^2\{r\}_{,x} \tag{3.7}$$

where a is the vehicle acceleration which is zero for the case of the constant vehicle speed. Substituting Eqs. 3.5, 3.6, and 3.7 in Eq. 3.2 and also defining new transformed contact matrices $[\bar{m}_c]$, $[\bar{k}_c]$, and $[\bar{c}_c]$ instead of $[\Gamma][m_c]$, $[\Gamma][k_c]$, and $[\Gamma][c_c]$ respectively, a new formulation for the contact force is obtained,

$$\{f_c\}_{t+\Delta t} = [\bar{m}_c]\{\ddot{d}_c\}_{t+\Delta t} + [\bar{c}_c]\{\dot{d}_c\}_{t+\Delta t} + [\bar{k}_c]\{d_c\}_{t+\Delta t} + \{p_c\}_{t+\Delta t} + \{q_c\}_t + \{r_c\}_{t+\Delta t} \tag{3.8}$$

where $\{r_c\}_{t+\Delta t}$ is defined as a new parameter representing the effect of the road irregularities in the contact force which is:

$$\{r_c\}_{t+\Delta t} = v^2[m_c]\{r\}_{,xx} + v[c_c]\{r\}_{,x} + [k_c]\{r\} \tag{3.9}$$

3.2.3 Bridge Element Nodal Displacement, Velocity, and Acceleration

The next step is to relate the displacement of the contact point to that of the nodal ones. This is usually done in the finite element analysis by applying interpolation (or shape) functions.

For a 6-DOF beam element shown in Fig. 3.1, in order to obtain contact displacement d_c from nodal displacement vector $\{d_b\}$, an interpolation function $\{N_c^{vr}\}$ represented in Eq. 3.4b should be used which includes the effect of the rotational DOFs in addition to the vertical DOFs:

$$d_c = \langle N_c^{vr} \rangle \{d_b\} \tag{3.10}$$

Velocity of the contact point can be determined using the chain rule by taking the first derivative of Eq. 3.10 with respect to time:

$$\dot{d}_c = \frac{d\langle N_c^{vr} \rangle}{dt}\{d_b\} + \langle N_c^{vr} \rangle \{\dot{d}_b\} \tag{3.11}$$

According to Eq. 3.4b, $\{N_c^{vr}\}$ is a function of x, which is the location of the wheel and by itself is a function of time. Therefore:

$$\frac{d\langle N_c^{vr} \rangle}{dt} = \frac{d\langle N_c^{vr} \rangle}{dx} \times \frac{dx}{dt} = \langle N_c^{vr} \rangle_{,x} \times v \tag{3.12}$$

where the comma denotes the differentiation with respect to the coordinates specified, and v is the velocity of the vehicle. Hence, the first derivative of the displacement of the contact point is:

$$\dot{d}_c = v\langle N_c^{vr} \rangle_{,x} \{d_b\} + \langle N_c^{vr} \rangle \{\dot{d}_b\} \tag{3.13}$$

Similarly, the acceleration of the contact point is obtained as:

$$\ddot{d}_c = \left\langle N_c^{vr} \right\rangle \{\ddot{d}_b\} + 2v\left\langle N_c^{vr} \right\rangle_{,x} \{\dot{d}_b\} + \left(v^2 \left\langle N_c^{vr} \right\rangle_{,xx} + a\left\langle N_c^{vr} \right\rangle_{,x}\right)\{d_b\} \tag{3.14}$$

where a is the acceleration of the vehicle. However, for the case of the constant velocity, the acceleration is zero.

3.2.4 VBI Element Structural Matrices

Using Eq. 3.8, 3.10, 3.13, and 3.14, the equation of motion for the bridge element (Eq. 3.1), traversed by ith wheel, can be reformulated as:

$$\begin{aligned} &[m_{bi}]\{\ddot{d}_{bi}\}_{t+\Delta t} + [c_{bi}]\{\dot{d}_{bi}\}_{t+\Delta t} + [k_{bi}]\{d_{bi}\}_{t+\Delta t} \\ &= \{f_{bi}\}_{t+\Delta t} - \sum_{j=1}^{n}\left([m_{cij}^*]\{\ddot{d}_{bj}\} + [c_{cij}^*]\{\dot{d}_{bj}\} + [k_{cij}^*]\{d_{bj}\}\right) - \{p_{ci}^*\}_{t+\Delta t} - \{q_{ci}^*\}_t - \{r_{ci}^*\}_{t+\Delta t} \end{aligned} \tag{3.15}$$

where n is the total number of wheels and the matrices with an asterisk are calculated using contact matrices and interpolation vectors as:

$$[m_{cij}^*] = \{N_{ci}^v\}\overline{m}_{cij}\left\langle N_{cj}^{vr} \right\rangle \tag{3.16a}$$

$$[c_{cij}^*] = \{N_{ci}^v\}\left(2v \times \overline{m}_{cij}\left\langle N_{cj}^{vr} \right\rangle_{,x} + \overline{c}_{cij}\left\langle N_{cj}^{vr} \right\rangle\right) \tag{3.16b}$$

$$[k_{cij}^*] = \{N_{ci}^v\}\left(v^2 \times \overline{m}_{cij}\left\langle N_{cj}^{vr} \right\rangle_{,xx} + v \times \overline{c}_{cij}\left\langle N_{cj}^{vr} \right\rangle_{,x} + \overline{k}_{cij}\left\langle N_{cj}^{vr} \right\rangle\right) \tag{3.16c}$$

and the equivalent nodal loads are:

$$\{p_{ci}^*\}_{t+\Delta t} = \{N_{ci}^v\}p_{ci,t+\Delta t} \tag{3.17a}$$

$$\{q_{ci}^*\}_t = \{N_{ci}^v\}q_{ci,t} \tag{3.17b}$$

similarly, the equivalent vector of road irregularities is:

$$\{r_{ci}^*\}_{t+\Delta t} = \{N_{ci}^v\}r_{ci,t+\Delta t} \tag{3.18}$$

In the latter three formulas, parameters with *i* or *j* are the entries of the corresponding vectors or matrices, e.g. $\overline{m}_{cij}$, $\overline{k}_{cij}$, and $\overline{c}_{cij}$ are entries of the *i*th row and *j*th column of the transformed contact matrices $[\overline{m}_c]$, $[\overline{k}_c]$, and $[\overline{c}_c]$, respectively. Eqs. 3.15 to 3.18 comprise the formulations for the proposed VBI element including modified mass, damping, and stiffness matrices. Using these equations, the new modifications can be easily consulted compared with the VBI element proposed by Yang and Wu (2001) presented in Appendix A in Eqs. A.28 to A.30. The new element incorporates explicitly the effect of the moving vehicle with the asterisk matrices and vectors. The overall bridge structural matrices (mass, damping, and stiffness) can be assembled using Eqs. 3.15 to 3.18, and are updated in each time increment. The detailed procedure can be found in Appendix A.

3.2.5 Working Procedure of the VBI Analysis Using the Modified Element

The step-by-step time-history numerical procedure to analyze a bridge traversed by a moving vehicle with constant velocity is as follows:

(a) Construct the structural matrices (i.e. mass, damping, and stiffness) for the bridge free of any vehicle. Rayleigh method is used to calculate the damping matrix. In addition, determine the structural matrices for the vehicle model.

(b) Define t_{end} and x_{end} and also Δt. The parameter x_{end} is needed to determine whether the vehicle is still on the bridge or not. This parameter can be specified for any wheel and its value is vehicle length plus bridge length.

(c) Consider initial conditions for the bridge elements and vehicle DOFs. Let $t = 0$.

(d) Perform the new time increment $t_{new} = t + \Delta t$. Stop the analysis if $t_{new} > t_{end}$ or the position of the first wheel is greater than x_{end}.

(e) Compute interpolation functions $\{N_c^v\}$ and $\{N_c^{vr}\}$ based on wheel positions using Eq. 3.4.

(f) Determine corresponding asterisk matrices $[m_c^*]$, $[c_c^*]$, and $[k_c^*]$ using Eq. 3.16, and also asterisk vectors $\{p_c^*\}_{t+\Delta t}$, $\{q_c^*\}_t$, and $\{r_c^*\}_{t+\Delta t}$ by Eqs. 3.17 and 3.18.

(g) Update the global bridge structural matrices using asterisk values calculated in the previous step.

(h) Solve the bridge equation of motion by Newmark-β method and find the bridge displacement vector for time $t + \Delta t$.

(i) Find $\{d_w\}$, $\{\dot{d}_w\}$, and $\{\ddot{d}_w\}$ for time $t + \Delta t$ using Eqs. 3.5, 3.6, and 3.7.

(j) Calculate the displacement vector for the upper part of the vehicle, which are not in direct contact with the bridge, at time $t + \Delta t$.

(k) Go to Step "d" for the new time increment.

3.3 NUMERICAL VBI ELEMENT FOR VEHICLES EXPERIENCING ACCELERATION OR DECELERATION

3.3.1 Formulation of Acceleration Forces Based on Vertical Contact Forces

The term 'acceleration forces' is used here to distinguish those forces generated by longitudinal (or horizontal) vehicle acceleration or deceleration in the considered DOFs of the vehicle model. These forces are treated as external forces and can be added to the

regular vector of external forces. A procedure is presented here to formulate such forces based on vertical contact forces. This will result in a concise formulation to be used in the numerical analysis of VBI systems. Before introducing the generalized formulation, it would be beneficial to review an example and then use it for a general vehicle.

(a) Sample Vehicle of 4 DOFs

Consider a basic model of a car comprised of two wheels, and one car body. The suspension system consists of linear spring-dampers (k_v and c_v) illustrated in Fig. 3.2 with shown dynamic DOFs r_1 to r_4, the car body mass m_c, the rotary inertia I_c, and the mass of wheels m_{w1} and m_{w2}. The vehicle velocity is denoted as v and the vehicle acceleration as a.

The free body diagrams of dynamic forces for the car body and one wheel are shown in Fig. 3.3 where SP_w are the spring-damper forces, F_w are the internal horizontal forces, V_i are the total vertical contact forces, V_i' are the dynamic vertical contact forces, and μ is the kinetic friction coefficient in case of braking with sliding, or static friction in case of traction. T_E is the torque applied by the engine exerted on the wheel axle, which is not required to be calculated since only horizontal and vertical equations of motion will be considered for wheels.

In the formulation of VBI element, it is assumed that the vehicle has reached its static equilibrium at rest before starting the movement. Therefore, vehicle self-weight and associated static deflections are not considered in the dynamic analysis of the vehicle. The vertical contact force V_i' is used excluding the effect of the vehicle self-weight. However, for the bridge analysis and also for calculation of the horizontal contact forces

generated by friction, the total vertical contact force denoted as V_i has to be used. The effect of the vehicle self-weight is treated as external loads applying on the contact points which are constant throughout the analysis. Equilibrium for wheels implies that:

$$\mu_i V_i - m_{wi} a + F_{wi} = 0 \qquad i = 1, 2 \tag{3.19a}$$

$$V_i' + SP_{wi} - m_{wi} \ddot{r}_m = 0 \qquad i = 1, 2 \tag{3.19b}$$

and for the car body,

$$F_{w1} + F_{w2} - m_c a = 0 \tag{3.20a}$$

$$SP_{w1} + SP_{w2} + m_c \ddot{r}_1 = 0 \tag{3.20b}$$

$$I_c \ddot{r}_2 + SP_{w2} d_2 - SP_{w1} d_1 = -(F_{w1} + F_{w2}) h_1 \tag{3.20c}$$

where a is the vehicle acceleration. Knowing that Eqs. 3.19a, 3.20b, and 3.20c are those for the assumed DOFs, they comprise the equations of motion for the vehicle. Comparing these three equations with the case of constant velocity, only one new term is present which is $-(F_{w1} + F_{w2}) h_1$ in Eq. 3.20c representing an extra rotational pitching moment on the car body. Therefore, the effect of vehicle horizontal acceleration only on the vehicle DOFs can be represented by new rotary moments.

One can define a vector of acceleration forces $\{f_a\}$ as a vector whose entries are regarding each DOF specified in Fig. 3.2. For this type of vehicle modeling with no horizontal DOFs, all entries are set to zero except those regarding pitching DOF,

$$\{f_a\} = \langle 0, -(F_{w1} + F_{w2}) h_1, 0, 0 \rangle^T \tag{3.21}$$

Then, the vector of acceleration forces $\{f_a\}$ can be decomposed into two parts as:

$$\{f_a\} = [\Phi]\{F\} \tag{3.22}$$

where $[\Phi]$ is named as geometry matrix and is obtained as:

$$[\Phi]=\begin{bmatrix} 0 & 0 \\ -h_1 & -h_1 \\ 0 & 0 \\ 0 & 0 \end{bmatrix} \tag{3.23}$$

and $\{F\}$ is the vector of internal horizontal forces F,

$$\{F\}=\langle F_{w1}, F_{w2}\rangle^T \tag{3.24}$$

To determine internal horizontal force vector $\{F\}$, Eq. 3.19a can be used where F is based on vertical contact forces V and vehicle acceleration a. Since there is no horizontal dynamic DOF, all parts of the vehicle move equally in the horizontal direction (longitudinal direction) with the same velocity and acceleration. Hence, the vehicle horizontal acceleration a can be calculated based on the horizontal contact forces and total vehicle masses as:

$$a=\frac{\sum_{i=1}^{n}\mu_i V_i}{M_t} \tag{3.25}$$

where M_t is the total mass of the vehicle and n is the number of wheels. Assuming that μ_i is known (see Appendix C), horizontal internal forces F are determined only as a function of vertical contact forces according to Eq. 3.19a. Using Eq. 3.19a together with Eq. 3.25, vector $\{F\}$ can be formulated as:

$$\{F\}=[\Omega][\mu]\{V\} \tag{3.26}$$

where $[\Omega]$ is defined as dimensionless matrix of equilibrium,

$$[\Omega]=\begin{bmatrix} 1-\frac{m_{w1}}{M_t} & -\frac{m_{w1}}{M_t} \\ -\frac{m_{w2}}{M_t} & 1-\frac{m_{w2}}{M_t} \end{bmatrix} \tag{3.27}$$

and $\{V\}$ is the vector of vertical contact forces and also $[\mu]$ is the matrix of the corresponding friction coefficients that is as follows for the sample vehicle model,

$$[\mu]=\begin{bmatrix}\mu_1 & 0\\ 0 & \mu_2\end{bmatrix} \tag{3.28}$$

Finally, applying Eq. 3.22 with Eq. 3.26, the vector of acceleration forces $\{f_a\}$ is obtained as a function of vertical contact forces $\{V\}$,

$$\{f_a\}=[\Phi][\Omega][\mu]\{V\} \tag{3.29}$$

where the matrices $[\Phi]$, $[\Omega]$, and $[\mu]$ are calculated for any vehicle model and are known throughout the analysis.

It would be constructive for later sections to mention that, one can separate the acceleration forces into those forces due to wheel DOFs $\{f_{wa}\}$ and the ones for car body DOFs $\{f_{ua}\}$. As a result, $\{f_a\}$ can be shown as:

$$\{f_a\}=\begin{Bmatrix}\{f_{ua}\}\\ \{f_{wa}\}\end{Bmatrix} \tag{3.30}$$

For each of $\{f_{wa}\}$ and $\{f_{ua}\}$, corresponding geometry matrices $[\Phi_w]$ and $[\Phi_u]$ could be determined, and the rest of components $[\Omega]$, $[\mu]$, and $\{V\}$ remain the same as above. For this example, the geometry matrix $[\Phi_w]$ due to wheel DOFs is a 2×2 zero matrix and $[\Phi_u]$ for upper DOFs are obtained as:

$$[\Phi_u]=\begin{bmatrix}0 & 0\\ -h_1 & -h_1\end{bmatrix} \tag{3.31}$$

3.3.2 Generalized Procedure for Formulation of Acceleration Forces

With a close look at the above procedures for obtaining the required matrices to formulate the vector of acceleration forces, we can summarize and generalize the procedure for the vehicle models excluding horizontal spring-dampers as follows.

1. Using the equation of motion of the vehicle about all pitching DOFs, determine the vector of acceleration forces $\{f_a\}$ as a function of internal horizontal contact forces.
2. Considering number of wheels (i.e. axles for a 2-D model) for the vehicle model, divide $\{f_a\}$ into $\{f_{wa}\}$ and $\{f_{ua}\}$ due to wheel DOFs and upper DOFs, respectively.
3. Determine corresponding geometry matrices $[\Phi_w]$ and $[\Phi_u]$.
4. Starting from wheels, using the equilibrium equation for horizontal forces, determine internal horizontal forces $\{F\}$ based on horizontal contact forces μV. Upper internal horizontal forces could be determined by those formulas obtained for lower internal horizontal forces.
5. Derive the dimensionless matrix of equilibrium $[\Omega]$ by arranging the equations obtained from previous step.
6. Determine $[\mu]$ which is an $n \times n$ diagonal matrix composed of the friction coefficient of all n wheels of the vehicle model.
7. Finally, the vector of acceleration forces is formulated by Eq. 3.29 for each $\{f_{wa}\}$ and $\{f_{ua}\}$ as:

$$\{f_{wa}\} = [\Phi_w][\Omega][\mu]\{V\} \tag{3.32a}$$

$$\{f_{ua}\} = [\Phi_u][\Omega][\mu]\{V\} \tag{3.32b}$$

Note: For a 2-D analysis, $\{f_{wa}\}$ and $[\Phi_w]$ will be zero matrices, but they are kept in order to have a generalized and consistent formulation.

3.3.3 Numerical Formulation of the Vehicle Equations of Motion Including the Effect of Acceleration

As stated in Section 3.3.1, the effect of the horizontal acceleration can be treated as external forces; therefore one can apply the equation of motions for a vehicle with constant velocity presented by other researchers (Yang and Wu, 2001) and add a new term similar to external forces representing the effect of acceleration (for comparison see Appendix A, Eq. A.4). Therefore, the equation of motion for a general vehicle including the effect of acceleration could be written as:

$$\begin{bmatrix}[m_{uu}] & [m_{uw}]\\ [m_{wu}] & [m_{ww}]\end{bmatrix}\begin{Bmatrix}\{\ddot{d}_u\}\\ \{\ddot{d}_w\}\end{Bmatrix}_{t+\Delta t}+\begin{bmatrix}[c_{uu}] & [c_{uw}]\\ [c_{wu}] & [c_{ww}]\end{bmatrix}\begin{Bmatrix}\{\dot{d}_u\}\\ \{\dot{d}_w\}\end{Bmatrix}_{t+\Delta t}$$
$$+\begin{bmatrix}[k_{uu}] & [k_{uw}]\\ [k_{wu}] & [k_{ww}]\end{bmatrix}\begin{Bmatrix}\{d_u\}\\ \{d_w\}\end{Bmatrix}_{t+\Delta t}=\begin{Bmatrix}\{f_{ue}\}\\ \{f_{we}\}\end{Bmatrix}_{t+\Delta t}+\begin{bmatrix}[l_u]\\ [l_w]\end{bmatrix}\{f_c\}_{t+\Delta t}+\begin{Bmatrix}\{f_{ua}\}\\ \{f_{wa}\}\end{Bmatrix}_{t+\Delta t} \tag{3.33}$$

Eq. 3.33 represents the equation of motion for two sets of vehicle DOFs, the upper part or non-contact part $\{d_u\}$ and wheel DOFs $\{d_w\}$. Each matrices of mass, damping, and stiffness are divided into four sub-matrices. External forces are those on upper part DOFs $\{f_{ue}\}$ and wheel DOFs $\{f_{we}\}$. Contact forces are also represented with the vector $\{f_c\}_{t+\Delta t}$. Matrices $[l_u]$ and $[l_w]$ transform the contact forces from contact points to the vehicle DOFs. Apparently, $[l_u]$ is a zero matrix, since the contact forces are only acting on wheels and $[l_w]$ is a unit matrix for 2-D models. Last term in Eq. 3.33 including $\{f_{ua}\}$ and $\{f_{wa}\}$ are those representing the effect of horizontal acceleration. For convenience,

let define $\{f_a\}_{t+\Delta t}$ as the forces induced by acceleration formulated using Eq. 3.29 and 3.30,

$$\{f_a\}_{t+\Delta t} = \begin{Bmatrix} \{f_{ua}\} \\ \{f_{wa}\} \end{Bmatrix}_{t+\Delta t} \tag{3.34}$$

Similar to external forces, the first part, $\{f_{ua}\}_{t+\Delta t}$, is regarding the upper part or non-contact DOFs and the other vector $\{f_{ua}\}_{t+\Delta t}$ is due to the wheel or contact part DOFs. Using Eq. 3.29 aforementioned force vectors are obtained,

$$\{f_{ua}\}_{t+\Delta t} = [\Phi_u][\Omega][\mu]\{f_c\}_{t+\Delta t} \tag{3.35a}$$

$$\{f_{wa}\}_{t+\Delta t} = [\Phi_w][\Omega][\mu]\{f_c\}_{t+\Delta t} \tag{3.35b}$$

where matrices $[\Phi_u]$ and $[\Phi_w]$ are the decomposed form of the matrix $[\Phi]$ due to upper DOFs and wheel DOFs respectively. The corresponding matrices $[\Phi]$, $[\Omega]$, and $[\mu]$ are determined using the procedures and formulas presented in the preceding section.

3.3.4 Numerical Formulation of Vertical Contact Forces

The effect of acceleration forces is the same as external forces in the vehicle equation of motion Eq. 3.34. The effect of external loads is included in a parameter denoted as $\{p_c\}_{t+\Delta t}$ in Eq. A.19:

$$[p_c]_{t+\Delta t} = [l_w]^{-1}\left([\Psi_{wu}][\Psi_{uu}]^{-1}\{f_{ue}\}_{t+\Delta t} - \{f_{we}\}_{t+\Delta t}\right) \tag{3.36}$$

where $[\Psi_{uu}]$ and $[\Psi_{wu}]$ are constant matrices determined based on properties of the vehicle and factors of Newmark-β method defined in Eqs. A.12 and A.21. To avoid repetition and retain brevity, extra required information can be consulted from Yang and

Wu (2001) given in Appendix A. According to Eq. 3.36, only vector $\{p_c\}_{t+\Delta t}$ including the effect of external load has to be adjusted. Hence, to apply the effects of the forces induced by vehicle acceleration, $\{f_{ua}\}_{t+\Delta t}$ and $\{f_{wa}\}_{t+\Delta t}$ are added to external forces $\{f_{ue}\}_{t+\Delta t}$ and $\{f_{we}\}_{t+\Delta t}$ respectively. Consequently, the new vector $\{\bar{p}_c\}_{t+\Delta t}$ is obtained as:

$$\{\bar{p}_c\}_{t+\Delta t} = [l_w]^{-1}\left([\Psi_{wu}][\Psi_{uu}]^{-1}\left(\{f_{ue}\}_{t+\Delta t} + \{f_{ua}\}_{t+\Delta t}\right) - \left(\{f_{we}\}_{t+\Delta t} + \{f_{wa}\}_{t+\Delta t}\right)\right) \tag{3.37}$$

Hence, the new formulation for the vector of external forces $\{\bar{p}_c\}_{t+\Delta t}$ is determined as:

$$\{\bar{p}_c\}_{t+\Delta t} = \{p_c\}_{t+\Delta t} + [l_w]^{-1}\left([\Psi_{wu}][\Psi_{uu}]^{-1}\{f_{ua}\}_{t+\Delta t} - \{f_{wa}\}_{t+\Delta t}\right) \tag{3.38}$$

where $\{p_c\}_{t+\Delta t}$ is calculated by Eq. 3.36.

Using Eqs. 3.29 and 3.30 to substitute $\{f_{ua}\}_{t+\Delta t}$ and $\{f_{wa}\}_{t+\Delta t}$ in Eq. 3.37, one can obtain:

$$\{\bar{p}_c\}_{t+\Delta t} = \{p_c\}_{t+\Delta t} + [l_w]^{-1}\left([\Psi_{wu}][\Psi_{uu}]^{-1}[\Phi_u] - [\Phi_w]\right)[\Omega][\mu]\{f_c\}_{t+\Delta t} \tag{3.39}$$

Using $\{\bar{p}_c\}_{t+\Delta t}$, the contact force formula given in Ea. A.15 by Yang and Wu (2001) will be modified as follows for vehicles experiencing acceleration,

$$\{f_c\}_{t+\Delta t} = [m_c]\{\ddot{d}_c\}_{t+\Delta t} + [c_c]\{\dot{d}_c\}_{t+\Delta t} + [k_c]\{d_c\}_{t+\Delta t} + \{\bar{p}_c\}_{t+\Delta t} + \{q_c\}_t \tag{3.40}$$

where $\{d_c\}_{t+\Delta t}$ is the vector of contact point displacement, and $[m_c]$, $[c_c]$, and $[k_c]$ are called contact matrices given in Eqs. A.16 to A.18. By applying Eq. 3.39 into Eq. 3.40 we have:

$$\begin{aligned}&\left(I - [l_w]^{-1}\left([\Psi_{wu}][\Psi_{uu}]^{-1}[\Phi_u] - [\Phi_w]\right)[\Omega][\mu]\right)\{f_c\}_{t+\Delta t} \\ &\quad = [m_c]\{\ddot{d}_c\}_{t+\Delta t} + [c_c]\{\dot{d}_c\}_{t+\Delta t} + [k_c]\{d_c\}_{t+\Delta t} + \{p_c\}_{t+\Delta t} + \{q_c\}_t\end{aligned} \tag{3.41}$$

where *I* is the unit matrix. For simplicity, let an acceleration parameter $[z]$ be defined as:

$$[z] = \left(I - [l_w]^{-1}\left([\Psi_{wu}][\Psi_{uu}]^{-1}[\Phi_u] - [\Phi_w]\right)[\Omega][\mu]\right)^{-1} \tag{3.42}$$

All terms in Eq. 3.42 are time-independent. Finally, the contact forces $\{f_c\}_{t+\Delta t_t}$ are obtained as

$$\{f_c\}_{t+\Delta t} = [\hat{m}_c]\{\ddot{d}_c\}_{t+\Delta t} + [\hat{c}_c]\{\dot{d}_c\}_{t+\Delta t} + [\hat{k}_c]\{d_c\}_{t+\Delta t} + \{\hat{p}_c\}_{t+\Delta t} + \{\hat{q}_c\}_t \tag{3.43}$$

where matrices with hat-sign are transformed form of the corresponding matrices which are multiplied by the acceleration parameter $[z]$, namely:

$$[\hat{m}_c] = [z][m_c] \tag{3.44a}$$

$$[\hat{c}_c] = [z][c_c] \tag{3.44b}$$

$$[\hat{k}_c] = [z][k_c] \tag{3.44c}$$

$$\{\hat{p}_c\}_{t+\Delta t} = [z]\{p_c\}_{t+\Delta t} \tag{3.44d}$$

$$\{\hat{q}_c\}_t = [z]\{q_c\}_t \tag{3.44e}$$

Subsequently, *i*th entry of the $\{f_c\}_{t+\Delta t}$ as the contact force between *i*th wheel and the bridge $V_{i,t+\Delta t}$ is determined as:

$$V_{i,t+\Delta t} = \hat{p}_{ci,t+\Delta t} + \hat{q}_{ci,t} + \sum_{j=1}^{n}\left(\hat{m}_{cij}\ddot{d}_{cj,t+\Delta t} + \hat{c}_{cij}\dot{d}_{cj,t+\Delta t} + \hat{k}_{cij}d_{cj,t+\Delta t}\right) \tag{3.45}$$

where m_{crj}, c_{crj}, and k_{crj} are respectively the entry in the *i*th row and *j*th column of the contact matrices $[m_c]$, $[c_c]$, and $[k_c]$. Similarly, the $\hat{p}_{cj,t+\Delta t}$ and $\hat{q}_{cj,t}$ are the entries located in the *j*th row of the corresponding vectors, i.e. $\{\hat{p}_c\}_{t+\Delta t}$ and $\{\hat{q}_c\}_t$.

3.3.5 Structural Matrices of VBI Element for Vehicles Experiencing Acceleration or Deceleration

For vehicles with constant velocity, there are only vertical contact forces transferring vehicle loads to the bridge element. On the other hand, if a vehicle is experiencing acceleration or deceleration, in addition to the vertical contact forces, horizontal contact forces will be present at the contact points. However, in the finite element formulation, having structural matrices (i.e. mass, damping, and stiffness) of the bridge, it is required to find the nodal forces induced by those contact forces shown in Fig. 3.4 to be able to solve bridge equation of motion.

Those *consistent* nodal forces f_{bcj}, j=1 to 6, can be determined from contact forces by using interpolation functions $\{N_c^v\}$ and $\{N_c^h\}$ as follows (Yang and Wu, 2001),

$$\{f_{bc}\} = \{N_c^v\}V + \{N_c^h\}H \tag{3.46}$$

The interpolation vector $\{N_c^v\}$ can be calculated by Hermitian cubic polynomials, while $\{N_c^h\}$ is usually considered as a linear function. All the entries in $\{N_c^v\}$ are set to zero except those regarding vertical DOFs. This ensures that there would only be vertical resultant nodal forces. Similarly, all entries of the vector $\{N_c^h\}$ are set to zero except those due to horizontal DOFs in order to relate horizontal contact force H to horizontal nodal forces f_{bc2} and f_{bc5}. For a two dimensional 6-DOF Euler-Bernoulli beam element, the corresponding interpolation functions are as follows,

$$\{N_c^v\} = \langle 1-3\bar{x}^2+2\bar{x}^3 \,,\, 0 \,,\, 0 \,,\, 3\bar{x}^2-2\bar{x}^3 \,,\, 0 \,,\, 0 \rangle^T \tag{3.47a}$$

$$\{N_c^h\} = \langle 0 \,,\, 1-\bar{x} \,,\, 0 \,,\, 0 \,,\, \bar{x} \,,\, 0 \rangle^T \tag{3.47b}$$

where $\bar{x}$ is the local coordinate of the contact point on the element, i.e. $\bar{x} = x/L$ where L is the element length (see Fig. 3.4). Hence, these interpolation functions are calculated based on the location of the wheel on the element which is a function of time because of the moving vehicle.

By applying the new formula for vertical contact forces (Eq. 3.45) in the method developed for the VBI element for vehicles with constant velocity in Sections 3.2.3 and 3.2.4, the new formulation for VBI element considering the effect of acceleration is obtained.

After relating the contact forces to consistent nodal forces in Eq. 3.46, it is required to relate the displacement of the contact point to those of the nodal ones. This is usually done in finite element analysis by applying the interpolation functions. For a 6-DOF beam element shown in Fig. 3.4, in order to obtain contact displacement d_c from nodal displacement vector $\{d_b\}$, an interpolation function $\{N_c^{vr}\}$ is used which includes the effect of the rotational DOFs in addition to the vertical DOFs,

$$d_c = \langle N_c^{vr} \rangle \{d_b\} \tag{3.48}$$

The interpolation function $\{N_c^{vr}\}$ is determined using Hermitian cubic polynomials as

$$\{N_c^{vr}\} = \langle 1 - 3\bar{x}^2 + 2\bar{x}^3 \text{ , } 0 \text{ , } L(\bar{x} - 2\bar{x}^2 + \bar{x}^3), 3\bar{x}^2 - 2\bar{x}^3 \text{ , } 0 \text{ , } L(\bar{x}^3 - \bar{x}^2) \rangle^T \tag{3.49}$$

By taking derivative of Eq. 3.48 with respect to time and using the chain rule, the velocity of the contact point can be obtained,

$$\dot{d}_c = \frac{d\langle N_c^{vr} \rangle}{dt} \{d_b\} + \langle N_c^{vr} \rangle \{\dot{d}_b\} \tag{3.50}$$

According to Eq. 3.49, $\{N_c^{vr}\}$ is a function of *x*, the location of the wheel, which by itself is a function of time; therefore:

$$\frac{d\langle N_c^{vr}\rangle}{dt} = \frac{d\langle N_c^{vr}\rangle}{dx} \times \frac{dx}{dt} = \langle N_c^{vr}\rangle_{,x} \times v \tag{3.51}$$

where the comma denotes the differentiation with respect to the coordinates specified, and *v* is the vehicle velocity. Hence, the first derivative of the displacement of the contact point is:

$$\dot{d}_c = v\langle N_c^{vr}\rangle_{,x}\{d_b\} + \langle N_c^{vr}\rangle\{\dot{d}_b\} \tag{3.52}$$

Similarly, the second derivative of the contact point is obtained as,

$$\ddot{d}_c = \langle N_c^{vr}\rangle\{\ddot{d}_b\} + 2v\langle N_c^{vr}\rangle_{,x}\{\dot{d}_b\} + \left(v^2\langle N_c^{vr}\rangle_{,xx} + a\langle N_c^{vr}\rangle_{,x}\right)\{d_b\} \tag{3.53}$$

The differentiation functions of the interpolation vector $\{N_c^{vr}\}$ with respect to local wheel's location *x* are:

$$\langle N_c^{vr}\rangle_{,x} = \frac{1}{L}\left\langle 6\bar{x}^2 - 6\bar{x},\ 0,\ L\left(1 - 4\bar{x} + 3\bar{x}^2\right),\ 6\bar{x} - 6\bar{x}^2,\ 0,\ L\left(3\bar{x}^2 - 2\bar{x}\right)\right\rangle \tag{3.54a}$$

$$\langle N_c^{vr}\rangle_{,xx} = \frac{1}{L^2}\left\langle 12\bar{x} - 6,\ 0,\ L\left(6\bar{x} - 4\right),\ 6 - 12\bar{x},\ 0,\ L\left(6\bar{x} - 2\right)\right\rangle \tag{3.54b}$$

The last step is to obtain the VBI element equation of motion. In general, the beam element having directly the effect of the wheels can be written as (Yang and Wu, 2001),

$$[m_{bi}]\{\ddot{d}_{bi}\}_{t+\Delta t} + [c_{bi}]\{\dot{d}_{bi}\}_{t+\Delta t} + [k_{bi}]\{d_{bi}\}_{t+\Delta t} = \{f_{bi}\}_{t+\Delta t} + \{f_{bci}\}_{t+\Delta t} \tag{3.55}$$

where $[m_{bi}]$, $[c_{bi}]$, and $[k_{bi}]$ are the *i*th VBI element mass, damping, and stiffness matrices, respectively. In addition, the vector $\{d_{bi}\}$ and its derivatives are due to nodal displacements of the corresponding VBI element, $\{f_{bci}\}$ represents the nodal forces

induced by contact forces according to Eq. 3.46, and finally $\{f_{bi}\}$ includes the effect of other external nodal forces that may be applied on the VBI element.

If one substitutes $\{f_{bci}\}$ of Eq. 3.55 into Eq. 3.46 and also applies Eq. 3.45 in Eq. 3.46 considering Eq. 3.48, 3.52, and 3.53 for the relationship between $\{d_b\}$ and $\{d_c\}$, the new VBI element equation of motion is formulated as:

$$\begin{aligned}&[m_{bi}]\{\ddot{d}_{bi}\}_{t+\Delta t}+[c_{bi}]\{\dot{d}_{bi}\}_{t+\Delta t}+[k_{bi}]\{d_{bi}\}_{t+\Delta t}\\&\quad=\{f_{bi}\}_{t+\Delta t}-\sum_{j=1}^{n}\left([\hat{m}^{*}_{cij}]\{\ddot{d}_{bj}\}+[\hat{c}^{*}_{cij}]\{\dot{d}_{bj}\}+[\hat{k}^{*}_{cij}]\{d_{bj}\}\right)-\{\hat{p}^{*}_{ci}\}_{t+\Delta t}-\{\hat{q}^{*}_{ci}\}_{t}\end{aligned} \tag{3.56}$$

where matrices with an asterisk incorporate the effect of the vehicle contact forces for the VBI element,

$$[\hat{m}^{*}_{cij}]=\left(\{N^{h}_{ci}\}\mu_i+\{N^{v}_{ci}\}\right)\hat{m}_{cij}\langle N^{vr}_{cj}\rangle \tag{3.57a}$$

$$[\hat{c}^{*}_{cij}]=\left(\{N^{h}_{ci}\}\mu_i+\{N^{v}_{ci}\}\right)\left(2v\times\hat{m}_{cij}\langle N^{vr}_{cj}\rangle_{,x}+\hat{c}_{cij}\langle N^{vr}_{cj}\rangle\right) \tag{3.57b}$$

$$[\hat{k}^{*}_{cij}]=\left(\{N^{h}_{ci}\}\mu_i+\{N^{v}_{ci}\}\right)\left(v^2\times\hat{m}_{cij}\langle N^{vr}_{cj}\rangle_{,xx}+\left(a\times\hat{m}_{cij}+v\times\hat{c}_{cij}\right)\langle N^{vr}_{cj}\rangle_{,x}+\hat{k}_{cij}\langle N^{vr}_{cj}\rangle\right) \tag{3.57c}$$

and the equivalent nodal loads are:

$$[\hat{p}^{*}_{ci}]_{t+\Delta t}=\left(\{N^{h}_{ci}\}\mu_i+\{N^{v}_{ci}\}\right)\hat{p}_{ci,t+\Delta t} \tag{3.58a}$$

$$[\hat{q}^{*}_{ci}]_{t}=\left(\{N^{h}_{ci}\}\mu_i+\{N^{v}_{ci}\}\right)\hat{q}_{ci,t} \tag{3.58b}$$

Eqs. 3.56 to 3.58 are the new formulations for VBI element incorporating the effect of vehicle acceleration on the vehicle and bridge responses. Knowing the asterisk matrices for the proposed VBI element, the structural properties (mass, damping, and stiffness) of the bridge can be assembled and updated in each time increment to solve the whole bridge equation of motion. Damping matrix is calculated by Rayleigh method using a linear relationship between mass and stiffness damping.

3.3.6. Working Procedure of Time-History Analysis for VBI Systems Including Acceleration

The step-by-step numerical procedure to analyze a bridge traversed by a moving vehicle with acceleration is as follows:

(a) Construct the structural matrices $[M_b]$, $[C_b]$, and $[K_b]$ for the bridge free of any vehicle. For the calculation of the damping matrix $[C_b]$, Rayleigh method can be used.

(b) Considering vehicle matrices, calculate corresponding constant matrices $[\Psi_{uu}]$, $[\Psi_{wu}]$,$[m_c]$, $[c_c]$, and $[k_c]$ (Appendix A).

(c) Determine time increment Δt, end time of the analysis t_{end} and corresponding vehicle location x_{end}. The parameter x_{end} is needed to determine whether the vehicle is still on the bridge or not. This parameter can be specified for any wheel and its value is vehicle length plus bridge length.

(d) Determine the vehicle geometry matrices $[\Phi_u]$, and $[\Phi_w]$, and also dimensionless matrix of equilibrium $[\Omega]$ for the vehicles, and using proper selection of friction coefficient $[\mu]$, calculate acceleration parameter $[z]$ by Eq. 3.42.

(e) Consider initial conditions for the bridge and vehicle DOFs. Let $t = 0$.

(f) Perform the new time increment $t_{new} = t + \Delta t$. Stop the analysis if $t_{new} \geq t_{end}$ or the position of the first wheel is greater than x_{end}.

(g) Compute interpolation functions $\{N_c^v\}$, $\{N_c^h\}$ using Eq. 3.47, and $\{N_c^{vr}\}$ and its derivatives using Eqs. 3.49 and 3.54 based on wheel positions.

(h) Calculate $\{q_u\}_t$, $\{p_c\}_{t+\Delta t}$, $\{q_c\}_t$, and $\{q_w\}_t$ (Appendix A).

(i) Determine corresponding asterisk matrices $[\hat{m}_c^*]$, $[\hat{c}_c^*]$, and $[\hat{k}_c^*]$ using Eq. 3.57, and also asterisk vectors $\{\hat{p}_c^*\}_{t+\Delta t}$ and $\{\hat{q}_c^*\}_t$ by Eq. 3.58.

(j) Assemble and construct the whole bridge matrices $[M]$, $[C]$, and $[K]$.

(k) Solve bridge equation of motion, by Newmark-β method and find $\{d_b\}$, $\{\dot{d}_b\}$, and $\{\ddot{d}_b\}$ for time $t+\Delta t$.

(l) Find $\{d_c\}$, $\{\dot{d}_c\}$, and $\{\ddot{d}_c\}$ for time $t+\Delta t$ using Eqs. 3.48, 3.52, and 3.53. Consequently, corresponding values for $\{d_w\}$, $\{\dot{d}_w\}$, and $\{\ddot{d}_w\}$ are calculated using Eq. A.3.

(m) Calculate vehicle displacement vectors $\{d_u\}_{t+\Delta t}$, $\{\dot{d}_u\}_{t+\Delta t}$, and $\{\ddot{d}_u\}_{t+\Delta t}$ using Eqs. A.7 to A.9.

(n) Go to Step "f" for the new time increment.

3.3.7 More Vehicle Examples

Formulation of acceleration forces was only shown for one simple vehicle in Section 3.3.1(a). In order to demonstrate how the generalized procedure in Section 3.3.2 works, more vehicle examples should be studied. To formulate the vector of acceleration forces (see Eq. 3.32), matrices $[\Phi_u]$, $[\Phi_w]$, $[\Omega]$, and $[\mu]$ need to be specified. Matrix $[\mu]$ is a diagonal matrix with the value of the friction coefficient of each wheel as its entries. In this section, the other three matrices are determined for three vehicle examples. The first studied model is a car model resembling the one shown in Fig. 3.2 including the effect of tires. The effect of tire in the formulation is studied. The second model is a more

complex model of a car also having the effect of tires in the modeling. The last vehicle model is a train model with two bogies and four wheelsets.

(a) Effect of tire in the modeling (a car model with 6 DOFs)

Consider the model shown in Fig. 3.5 that represents a 2-axle vehicle incorporating the effect of the tires. Each tire is modeled by a spring and a damper under the wheel. The tire DOFs are in direct contact with the bridge and they are assumed to have no mass.

The free body diagram of dynamic forces for the car body is similar to that shown in Fig. 3.3, whereas the free body diagram for the wheels and tires are shown in Fig 3.6.

The equations of motions for tires are:

$$\mu_i V_i - F_{ti} = 0 \qquad i = 1, 2 \tag{3.59a}$$

$$V_i' + SP_{ti} = 0 \qquad i = 1, 2 \tag{3.59b}$$

and for wheels are:

$$F_{ti} - m_{wi} a - F_{wi} = 0 \qquad i = 1, 2 \tag{3.60a}$$

$$SP_{wi} - SP_{ti} - m_{wi} \ddot{r}_m = 0 \qquad i = 1, 2 \tag{3.60b}$$

and for the car body:

$$F_{w1} + F_{w2} - m_c a = 0 \tag{3.61a}$$

$$SP_{w1} + SP_{w2} + m_c \ddot{r}_1 = 0 \tag{3.61b}$$

$$I_c \ddot{r}_2 + SP_{w2} d_2 - SP_{w1} d_1 = -(F_{w1} + F_{w2}) h_1 \tag{3.61c}$$

where a is the vehicle horizontal acceleration. Hence, the vector of acceleration forces is determined as:

$$\{f_a\} = \langle 0, -(F_{w1} + F_{w2}) h_1, 0, 0, 0, 0 \rangle^T \tag{3.62}$$

Consequently, considering internal horizontal acceleration forces $\{F\}$ as:

$$\{F\} = \langle F_{w1}, F_{w2}, F_{t1}, F_{t2} \rangle^T \tag{3.63}$$

the geometry matrix $[\Phi]$ is obtained as:

$$[\Phi] = \begin{bmatrix} 0 & 0 & 0 & 0 \\ -h_1 & -h_1 & 0 & 0 \\ 0 & 0 & 0 & 0 \\ 0 & 0 & 0 & 0 \\ 0 & 0 & 0 & 0 \\ 0 & 0 & 0 & 0 \end{bmatrix} \tag{3.64}$$

Then, using equilibrium equations of horizontal forces (i.e. Eq. 3.59a and 3.60a), the dimensionless matrix of equilibrium $[\Omega]$ is obtained as:

$$[\Omega] = \begin{bmatrix} 1-\frac{m_{w1}}{M_t} & -\frac{m_{w1}}{M_t} \\ -\frac{m_{w2}}{M_t} & 1-\frac{m_{w2}}{M_t} \\ 1 & 0 \\ 0 & 1 \end{bmatrix} \tag{3.65}$$

And finally, the vector of acceleration forces will be calculated using Eq. 3.29.

Correspondingly, the geometry matrix $[\Phi_w]$ due to tire DOFs is a 2×4 zero matrix and $[\Phi_u]$ for upper DOFs is obtained as:

$$[\Phi_u] = \begin{bmatrix} 0 & 0 & 0 & 0 \\ -h_1 & -h_1 & 0 & 0 \\ 0 & 0 & 0 & 0 \\ 0 & 0 & 0 & 0 \end{bmatrix} \tag{3.66}$$

(b) Half-car planar vehicle model of 8 DOFs

Consider the model shown in Fig. 3.7 that represents a vehicle model of a half-car planar vehicle while incorporating the effect of the tires. This model was used by Esmailzadeh and Jalili (2003). Each tire is modeled by linear spring-dampers under each wheel. The tire DOFs are in direct contact with the bridge without any mass.

The equations of motion for tires are:

$$\mu_i V_i - F_{ti} = 0 \qquad i = 1, 2 \tag{3.67a}$$

$$V_i' + SP_{ti} = 0 \qquad i = 1, 2 \tag{3.67b}$$

and for wheels are:

$$F_{ti} - m_{wi} a - F_{wi} = 0 \qquad i = 1, 2 \tag{3.68a}$$

$$SP_{wi} - SP_{ti} - m_{wi} \ddot{r}_j = 0 \qquad i = 1, 2 \;\; ; \;\; j = 5, 6 \tag{3.68b}$$

and for the two upper masses (passenger and driver masses):

$$F_i - m_{pi} a = 0 \qquad i = 1, 2 \tag{3.69a}$$

$$SP_i - m_{pi} \ddot{r}_i = 0 \qquad i = 1, 2 \tag{3.69b}$$

and for the vehicle body:

$$F_{w1} + F_{w2} - F_1 - F_2 - m_s a = 0 \tag{3.70a}$$

$$SP_{w1} + SP_{w2} - SP_1 - SP_2 + m_s \ddot{r}_3 = 0 \tag{3.70b}$$

$$J\ddot{r}_4 + SP_2 d_2 - SP_1 d_1 + SP_{w1} b_1 - SP_{w2} b_2 = (F_1 + F_2) h_1 + (F_{w1} + F_{w2}) h_2 \tag{3.70c}$$

where a is the vehicle horizontal acceleration. Hence, the vector of acceleration forces is an 8×1 vector, and is determined as:

$$\{f_a\} = \langle 0, 0, 0, (F_1 + F_2) h_1 + (F_{w1} + F_{w2}) h_2, 0, 0, 0, 0 \rangle^T \tag{3.71}$$

Consequently, considering internal horizontal acceleration forces $\{F\}$ as:

$$\{F\} = \langle F_1, F_2, F_{w1}, F_{w2}, F_{t1}, F_{t2} \rangle^T \tag{3.72}$$

the geometry matrix $[\Phi_w]$ due to tire DOFs is a 2×6 zero matrix and $[\Phi_u]$ for upper DOFs is obtained as:

$$[\Phi_u] = \begin{bmatrix} 0 & 0 & 0 & 0 & 0 & 0 \\ 0 & 0 & 0 & 0 & 0 & 0 \\ 0 & 0 & 0 & 0 & 0 & 0 \\ h_1 & h_1 & h_2 & h_2 & 0 & 0 \\ 0 & 0 & 0 & 0 & 0 & 0 \\ 0 & 0 & 0 & 0 & 0 & 0 \end{bmatrix} \tag{3.73}$$

Then, using equilibrium equations of horizontal forces (i.e. Eq. 3.67a and 3.68a), the dimensionless matrix of equilibrium $[\Omega]$ is obtained as:

$$[\Omega] = \begin{bmatrix} \frac{m_{p1}}{M_t} & \frac{m_{p1}}{M_t} \\ \frac{m_{p2}}{M_t} & \frac{m_{p2}}{M_t} \\ 1 - \frac{m_{w1}}{M_t} & -\frac{m_{w1}}{M_t} \\ -\frac{m_{w2}}{M_t} & 1 - \frac{m_{w2}}{M_t} \\ 1 & 0 \\ 0 & 1 \end{bmatrix} \tag{3.74}$$

And finally, the vector of acceleration forces will be calculated using Eq. 3.29.

(c) Train model of 10 DOFs

Consider a car of a train that has four wheels, two bogies and a car body, where the suspension system is comprised of spring and dampers that are presented in Fig. 3.9 with

the shown dynamic DOFs. The free body and kinetic diagrams for the car body, one bogie and one wheel are shown in Fig. 3.10. Notations are similar to those in Fig 3.3. Equilibrium for wheels implies that:

$$\mu_i V_i - m_{wi} a - F_{wi} = 0 \qquad i = 1 to 4 \tag{3.75a}$$

$$V_i' + SP_{wi} - m_{wi} \ddot{r}_j = 0 \qquad i = 1 to 4 \;;\; j = 7 to 10 \tag{3.75b}$$

As a sample of equilibrium equations for bogies, bogie #1 is considered here and bogie #2 can be treated similarly:

$$F_{w1} + F_{w2} - F_{b1} - m_{b1} a = 0 \tag{3.76a}$$

$$m_{b1} \ddot{r}_3 + SP_{w1} + SP_{w2} - SP_{b1} = 0 \tag{3.76b}$$

$$I_{b1} \ddot{r}_4 + SP_{w2} d_2 - SP_{w1} d_1 = -F_{b1} h_2 - (F_{w1} + F_{w2}) h_3 \tag{3.76c}$$

and for the car body:

$$F_{b1} + F_{b2} - m_c a = 0 \tag{3.77a}$$

$$m_c \ddot{r}_1 + SP_1 + SP_2 = 0 \tag{3.77b}$$

$$I_c \ddot{r}_2 + SP_2 l_2 - SP_1 l_1 = -(F_{b1} + F_{b2}) h_1 \tag{3.77c}$$

Hence, the vector of the acceleration forces for upper part DOFs is determined as:

$$[f_{ua}] = \begin{Bmatrix} 0 \\ -(F_{b1} + F_{b2}) h_1 \\ 0 \\ -F_{b1} h_2 - (F_{w1} + F_{w2}) h_3 \\ 0 \\ -F_{b2} h_2 - (F_{w3} + F_{w4}) h_3 \end{Bmatrix} \tag{3.78}$$

while for the wheel part DOFs, the vector $[f_{wa}]$ is a 4×1 zero vector. Consequently, considering internal horizontal acceleration forces $\{F\}$ as:

$$\{F\} = \langle F_{b1}, F_{b2}, F_{w1}, F_{w2}, F_{w3}, F_{w4} \rangle^T \tag{3.79}$$

the geometry matrix $[\Phi_u]$ for the upper part or non-contact DOFs is obtained as:

$$[\Phi_u] = \begin{bmatrix} 0 & 0 & 0 & 0 & 0 & 0 \\ -h_1 & -h_1 & 0 & 0 & 0 & 0 \\ 0 & 0 & 0 & 0 & 0 & 0 \\ -h_2 & 0 & -h_3 & -h_3 & 0 & 0 \\ 0 & 0 & 0 & 0 & 0 & 0 \\ 0 & -h_2 & 0 & 0 & -h_3 & -h_3 \end{bmatrix} \tag{3.80}$$

whereas the matrix $[\Phi_w]$ for wheel DOFs is a 4×6 zero matrix.

Consequently, using equilibrium equations of horizontal forces (i.e. Eqs. 3.75a and 3.76a) and Eq. 3.25, one can determine the dimensionless equilibrium matrix $[\Omega]$,

$$[\Omega] = \begin{bmatrix} 1-A_1 & 1-A_1 & -A_1 & -A_1 \\ -A_2 & -A_2 & 1-A_2 & 1-A_2 \\ 1-\frac{m_{w1}}{M_t} & -\frac{m_{w1}}{M_t} & -\frac{m_{w1}}{M_t} & -\frac{m_{w1}}{M_t} \\ -\frac{m_{w2}}{M_t} & 1-\frac{m_{w2}}{M_t} & -\frac{m_{w2}}{M_t} & -\frac{m_{w2}}{M_t} \\ -\frac{m_{w3}}{M_t} & -\frac{m_{w3}}{M_t} & 1-\frac{m_{w3}}{M_t} & -\frac{m_{w3}}{M_t} \\ -\frac{m_{w4}}{M_t} & -\frac{m_{w4}}{M_t} & -\frac{m_{w4}}{M_t} & 1-\frac{m_{w4}}{M_t} \end{bmatrix} \tag{3.81}$$

where $A_1 = \dfrac{m_{w1} + m_{w2} + m_{b1}}{M_t}$ and $A_1 = \dfrac{m_{w3} + m_{w4} + m_{b2}}{M_t}$. The matrix of the friction coefficients $[\mu]$ is also a diagonal matrix of the corresponding friction coefficients for each wheel.

3.4 NUMERICAL VERIFICATIONS

3.4.1 Moving Sprung Mass Model

Consider a simply supported girder subjected to a moving sprung mass as illustrated in the Fig. 3.11. This case was lately used for verification by several researchers such as Yang and Wu (2001), Zhang et al. (2001), and Majka and Hartnett (2008). Vehicle required matrices are presented in Appendix B.1. The required data are: Young's modulus E=2.87 GPa, Poisson's ratio ν=0.2, moment of inertia I=2.90 m^4, mass per unit length m=2303 kg/m, girder length L=25m, sprung mass M_v=5.75 ton, wheel mass M_w=0, and suspension spring constant k_v=1595 kN/m. No damping is included in the system. The span is divided into 10 Euler-Bernoulli beam elements.

The results of the sprung mass system are compared in Figure 3.12 with the analytical solution presented by Biggs (1964) and the moving load model response. The results show perfect match between the two methods. In addition, the moving load response is obtained using the same MATLAB (ref) code by using gravitational loading of the vehicle as the constant moving load.

3.4.2 Suspended Rigid Beam Model

The second verification case is a rigid beam comprised of two DOFs supported by two wheels. Each wheel is connected to the rigid beam by a spring and damper. This model shown in Fig. 3.13 was used by Yang and Wu (2001). The matrices simulating the vehicle's model are presented in Appendix B.2. Properties for the beam are: Young's modulus E=2.943 GPa, Poisson's ratio ν=0.2, moment of inertia I=8.65 m^4, mass per

unit length m=36 t/m, and beam length L_B=30m. The moving beam properties are: sprung mass M_v=540 ton, wheel masses are zero, rotatory mass I_v=13800 t.m^2, and suspension spring constant k_v=41350 kN/m. No damping is included in the system. Wheel to wheel distance is 17.5 m. Vehicle speed is 27.78 m/s. The beam is modeled as 10 elements each is 3 m. The result presented by Yang and Wu (2001) is depicted in Fig. 3.14 together with results obtained from the proposed element and also from moving load model. Again, a very close match is obtained for the proposed element and the one proposed by Yang and Wu (2001).

3.4.3 Half-Car Planar Model Including the Effect of Tires

Consider a vehicle model of a Half-car planar vehicle having the effect of the tires in the model shown in Fig. 3.7. Each tire is modeled by a spring-damper under the wheel. The tire DOFs are in direct contact with the bridge without any mass. In the original study by Esmailzadeh and Jalili (2003), no DOF was considered for tires; their effects were considered in the formulation developed by those researchers. In their model, there are the total of 6-DOF used for the vehicle model. However, for the element presented in this study, two extra DOFs with zero mass are required in the locations of tires (see Fig 3.7), in order to include the tire stiffness and damping in the vehicle model. Vehicle and bridge properties are tabulated in Tables 3.1 and 3.2, respectively.

Vehicle required matrices are presented in Appendix B.4. Results obtained from Esmailzadeh and Jalili (2003) together with those obtained from the new VBI element for three constant velocities of 56, 72, and 88 km/h are demonstrated in Figs. 3.15 and 3.16.

Mid-span deflection is shown in Fig 3.15, and driver bouncing in Fig 3.16 illustrating very close results.

3.5 LIMITATIONS AND ASSUMPTIONS

The suspension units (dashpot and springs) of vehicle models used in the development of VBI elements should retain linear properties. Majority of the vehicle models used by researchers in the analysis of bridge dynamics were linear models. This is particularly common in the VBI analysis using vehicle models comprised of dozens of DOFs, such as those used in the modeling of high-speed trains. However, there are few studies that adopted nonlinear properties (Hwang and Nowak, 1991). Although the actual suspension properties for majority of highway vehicles are nonlinear but they operate closely to linear behaviour, hence they can be approximated as linear.

The VBI element developed for vehicles experiencing acceleration is formulated based on the friction coefficient. It is assumed that the friction coefficients are known and they are one of the inputs. However, the developed element is versatile such that it can model a pre-defined scheme of a varying friction coefficient. Appendix C presents a review on the available models to include friction in multibody dynamic systems, and models considered in VBI analysis.

3.6 SUMMARY

In this chapter, new modified numerical VBI (Vehicle–Bridge Interaction) elements were developed for the calculation of complicated VBI problems that incorporate the

effect of the dynamic parameters (e.g. vehicle speed, acceleration, etc.), more realistically. The general common notations were kept the same as the VBI element proposed by Yang and Wu (2001) presented in Appendix A for easier comparison between the two methods. The new formulation and the mathematical background are presented comprehensively in this chapter.

In the development of the VBI element for vehicles with constant velocity, the available formulation obtained by Yang and Wu (2001) is used to formulate the contact forces. Those forces are related to beam element nodal forces by Hermitian cubic interpolation functions. Suitable interpolation functions between the beam element displacement vector and those for contact points are considered. The velocity and the acceleration of the contact point are then obtained by the first and second derivative of the corresponding displacement vector. The result is a new formulation proposed for the structural properties of a VBI element capable of capturing bridge and vehicle responses more realistically. The final applicable formulas for numerical analysis as the properties of the new VBI element are summarized in Eqs. 3.16 to 3.18 for vehicles with constant velocity.

For vehicles experiencing acceleration or deceleration, a key step is to formulate acceleration forces based on vertical contact forces. The term ‘acceleration forces’ is used referring to those forces exerted on the vehicle because of the vehicle longitudinal (or horizontal) acceleration. Using vehicle equations of motion, the vector of acceleration forces is formulated numerically by defining suitable dimensionless matrices and vectors, after which, vertical contact forces are formulated by the new vector of external forces. A new factor called acceleration parameter is defined assisting the formulation in a practical

and concise form. This parameter simulates the effect of the horizontal acceleration and is constant throughout the analysis. New formulation for the vertical contact forces, and also the effect of horizontal contact forces will result in a new VBI element capable of modeling intricate vehicle models and bridges. Final formulations obtained for this VBI element are presented in Eqs. 3.56 to 3.58.

A new model was coded using MATLAB® programming language (2008) to perform the time-history analysis of vehicle-bridge interaction. Three numerical models are used in this chapter to verify the developed numerical VBI elements and the coded MATLAB program. The numerical verification models comprise sprung mass model, rigid beam model, and half-car planar vehicle model. Results generally demonstrated a close match confirming the validity of the developed numerical elements.

Table 3.1 properties of the half-car planar vehicle model and the bridge (Esmailzadeh and Jalili 2003)

m_s	1794.4	kg	k_1	66824.4	N/m
m_{t1}	87.15	kg	k_2	18615.0	N/m
m_{t2}	140.4	kg	$k_{t1}=k_{t2}$	101115	N/m
$m_{p1}=m_{p2}$	75	kg	$k_{p1}=k_{p2}$	14000	N/m
J	3443.05	$kg.m^2$	c_1	1190	N.s/m
b_1	1.271	m	c_2	1000	N.s/m
b_2	1.716	m	$c_{t1}=c_{t2}$	14.6	N.s/m
d_1	0.481	m	c_{p1}	50.2	N.s/m
d_2	1.313	m	c_{p2}	62.1	N.s/m

Table 3.2 Bridge properties for the half-car planar model (Esmailzadeh and Jalili 2003)

L	100	m
E	207	GPa
I	0.174	m^4
ρ	20,000	kg/m
c	1750	N.s/m

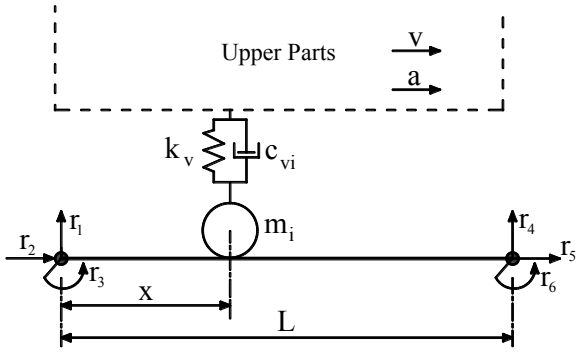

Fig. 3.1 Two-dimensional VBI element

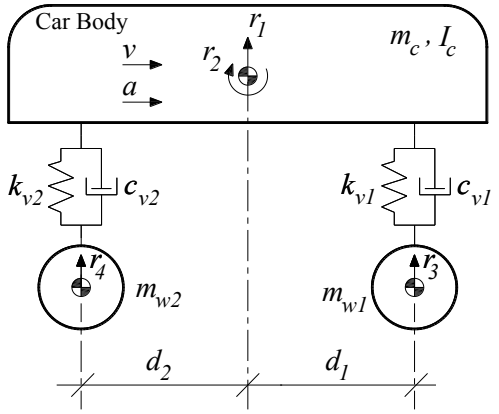

Fig. 3.2 A car model of 4-DOF

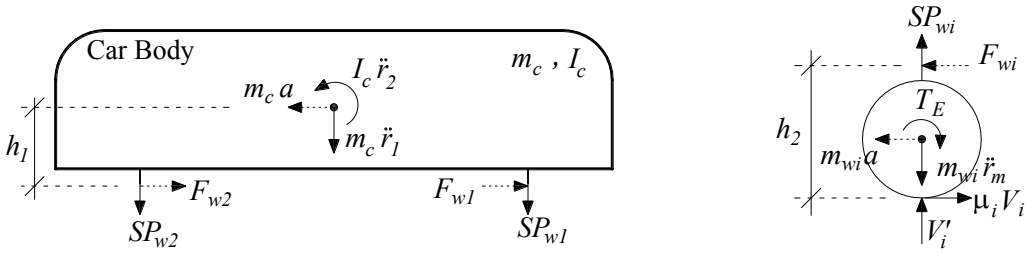

(a) (b)

Fig. 3.3 Free body diagrams of 4-DOF car model of: (a) the car body, (b) wheels

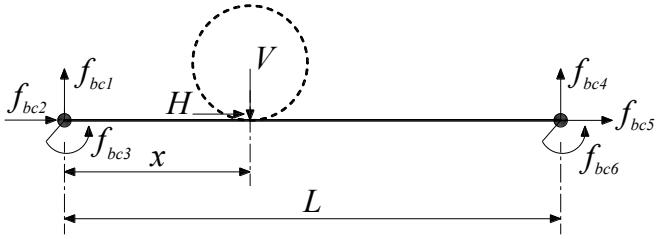

Fig. 3.4 Two-dimensional VBI element for vehicles with acceleration

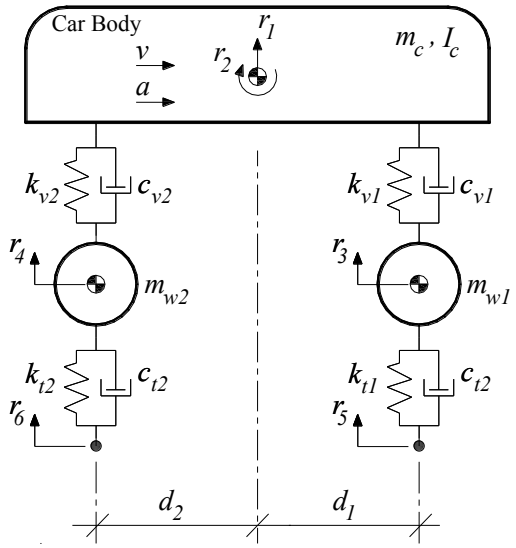

Fig. 3.5 A car model of 6-DOF having the effect of tires

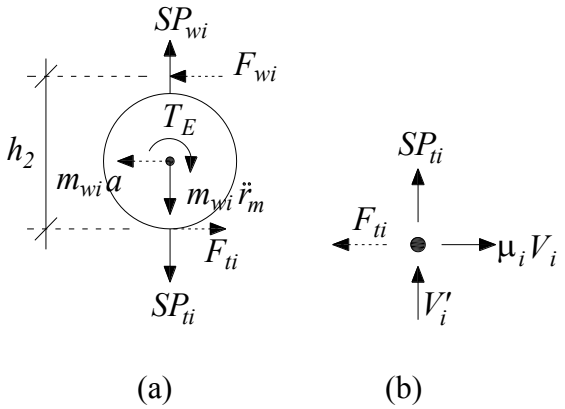

Fig. 3.6 Free body diagrams of 6-DOF car model for (a) wheels (b) tire

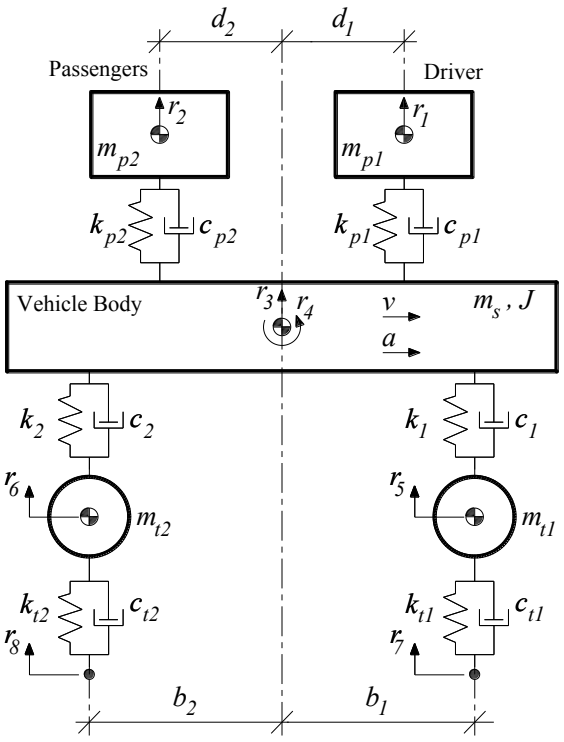

Fig. 3.7 A Half-car planar Vehicle model of 8-DOF having the effect of tires

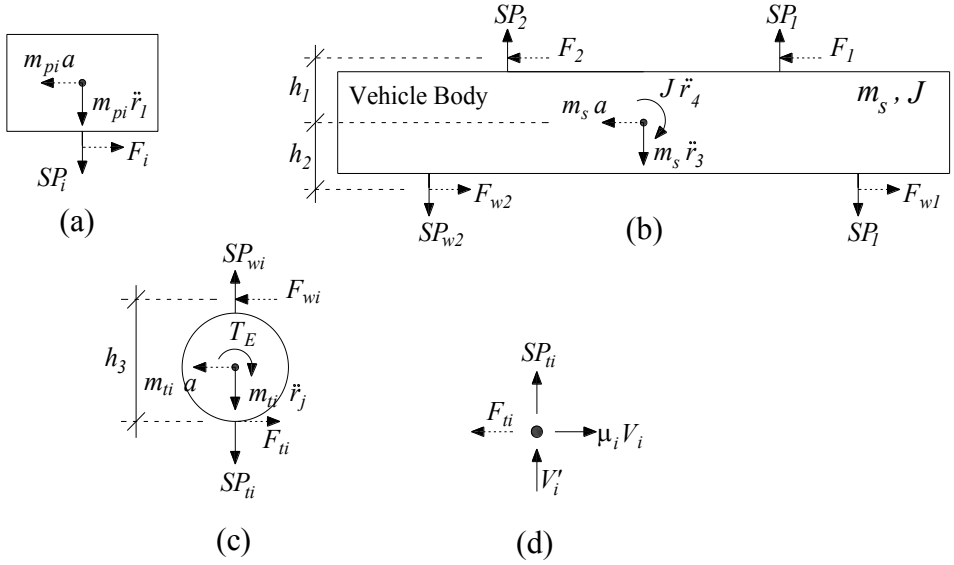

Fig. 3.8 Free body diagrams of the half-car planar model for (a) passenger or driver (b) vehicle body (c) wheels (d) tires

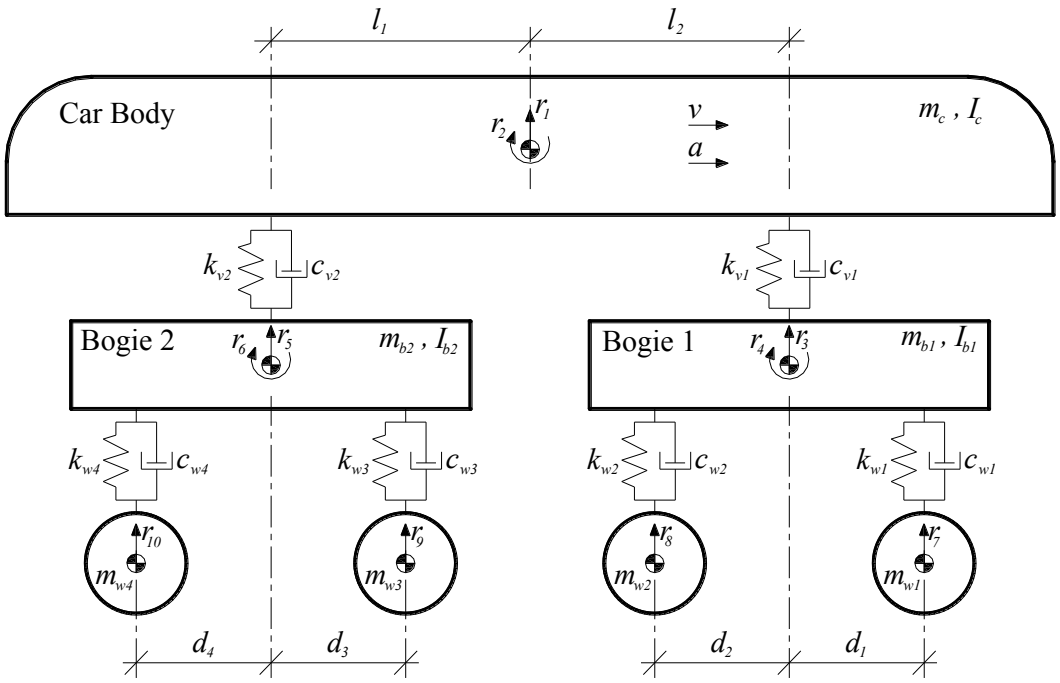

Fig. 3.9 Four-wheel model of one car of a train

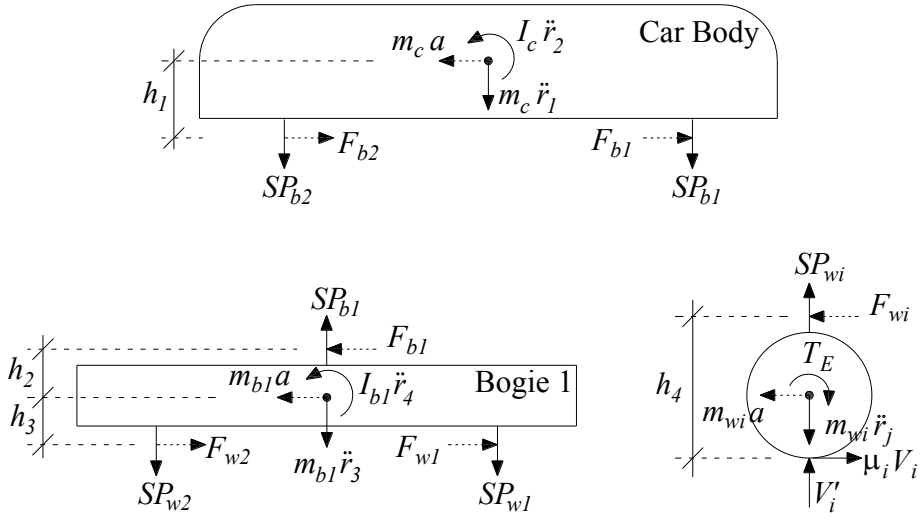

Fig. 3.10 Free body diagram of the car body, a bogie, and a wheel

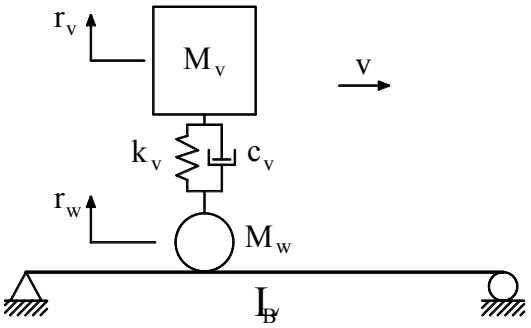

Fig. 3.11 Numerical verification, moving sprung mass model

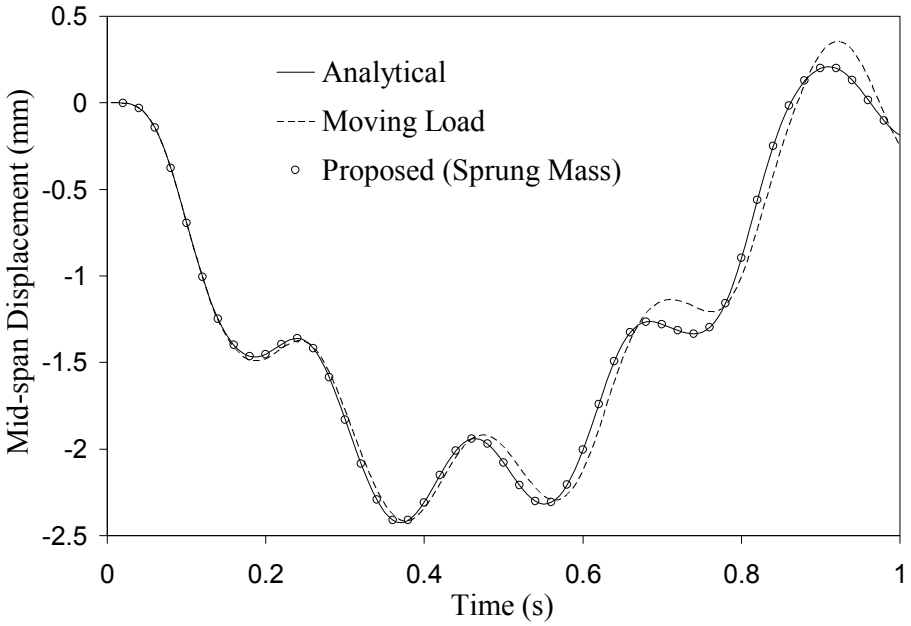

Fig. 3.12 Displacement at the beam mid-span, numerical verification using moving sprung mass model

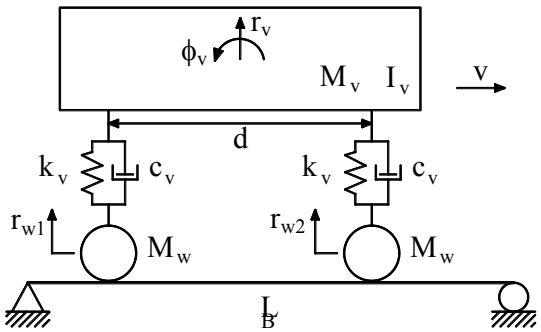

Fig. 3.13: Numerical verification, suspended rigid beam model

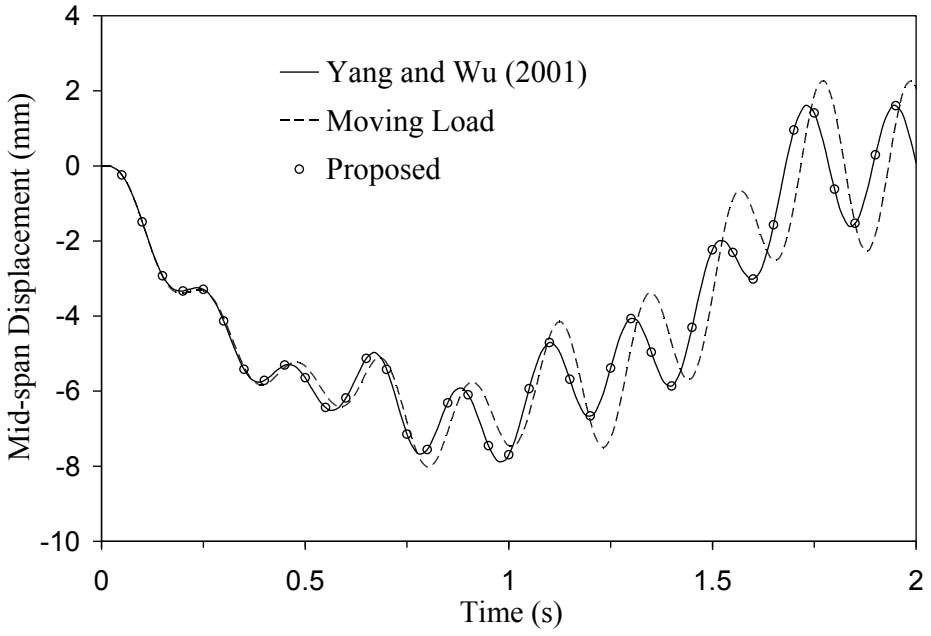

Fig. 3.14: Displacement at mid-span of the beam, numerical verification using suspended rigid beam model

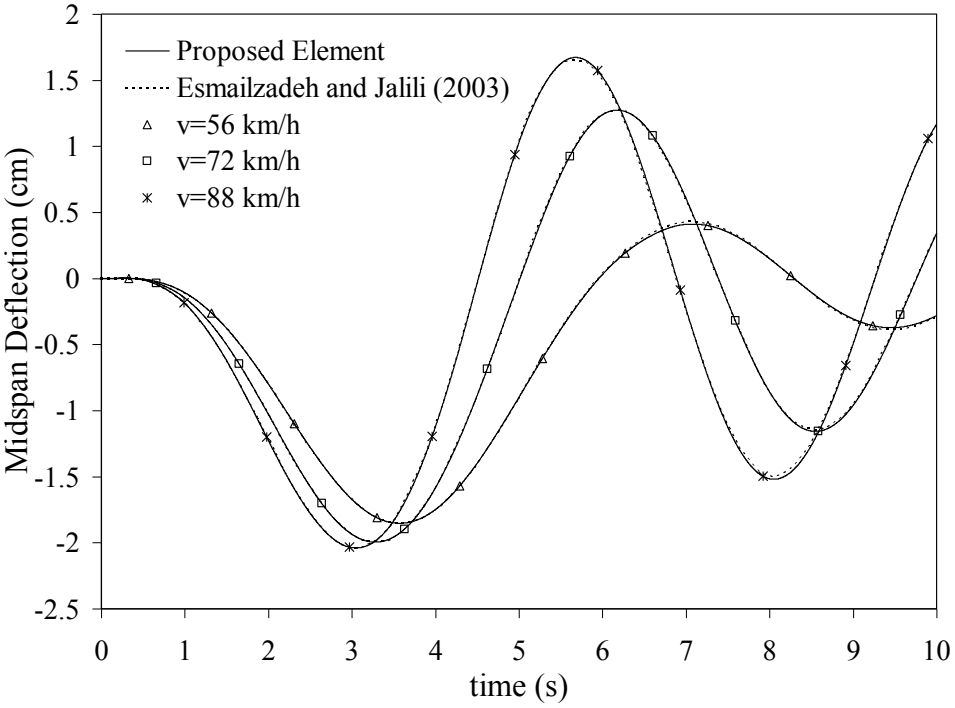

Fig. 3.15 Displacement at mid-span of the bridge for half-car planar model

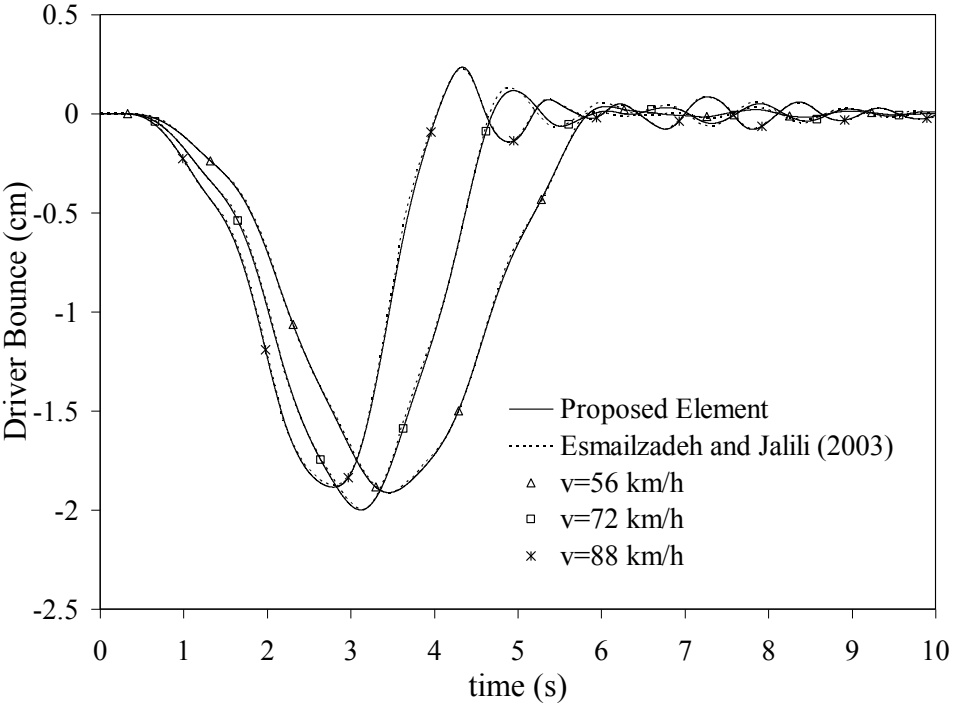

Fig. 3.16 Driver bouncing for half-car planar model

CHAPTER 4

EFFECT OF SHEAR DEFORMATION AND CONSISTENT MASS ON VBI ANALYSIS

4.1 GENERAL

Effect of shear deformations and rotary inertia can be neglected in many applications of structural dynamics and the accuracy of simple beam based on Euler-Bernoulli bending theory is sufficient (Archer, 1963). However, in some cases, relying only on that simple formulation may lead to misrepresenting results. An example of small difference is in the lowest modal frequencies of long and thin beams. Example of significant errors can include thicker beams (lower span-to-depth ratio), and higher modal frequencies of any beam (Thomas et al., 1973). Effect of shear deformations and rotary inertia can be included in the analysis by using Timoshenko beam theory.

The Timoshenko beam theory is also known as the first-order shear deformation theory. The formulation of a specific finite element depends on the choice of the interpolation functions used for the transverse deflection and rotation. For all first-order finite elements, the transverse shear strain is assumed constant with respect to the thickness coordinate. However, the real shear strain distribution is not constant. Therefore, shear correction factors are considered to compensate for this assumption and to adjust the calculated shear force with the actual shear force (Reddy, 1997a).

Consequently, higher-order shear deformation theories were developed to provide a more realistic modeling of transverse shear strains. For instance, Levinson (1981) and Reddy (1984, 1997b) developed third-order shear deformation theories to capture the true

variation of transverse shear strain and stresses; this is because the actual transverse shear strain is quadratic through the beam height. Therefore, there is no need to use a shear correction factor when using a third-order shear deformation theory.

In the application of thick plates and particularly in the laminated plates, higher order shear deformation theories needed to be considered to calculate stress transferred between the two material used in the laminated plate. However, higher-order plate theories provide a slight increase in the accuracy in comparison with the first-order solution, but at the expense of a significant increase in the computational effort. Therefore in many practical applications, the first-order element is used since it provides the best compromise between economy, simplicity, and accuracy in prediction of the global response (Urathaler and Reddy, 2008). Therefore in the current thesis, the Timoshenko beam theory is used, which provides fairly acceptable results for comparison between those obtained by Euler-Bernoulli beam element.

The effects of shear deformations are studied based on two groups according to the bridge mass matrices. In the first group, the mass matrix is modeled by lumped masses, while the second group applies to the consistent mass matrix. In addition, the effects of consistent masses are investigated also in two categories. The first category covers bridge models that have flexural stiffness only (i.e. Euler-Bernoulli beam elements), whereas the second category bridge models accounts for the effect of shear deformations. Chopra (2001) reported that the lumped mass matrix formulation is used in many ordinary engineering applications leading to satisfactory results. Despite the fact that the effect of the consistent mass and rotary inertia used to be ignored in the vibration analysis of simply supported beams, that effect was kept in the formulation in order to

maintain generality knowing that it will not add much complication to the analysis. As expected, in some cases, it was shown that the consistent mass and rotary inertia affect the bridge response as will be discussed in this chapter.

4.2 BRIDGE AND VEHICLE MODELING

Since the analysis is two-dimensional, the bridge model can be modeled by 6-DOF beam elements including 3-DOF at each node, vertical, rotational, and axial DOFs. Utilizing the direct stiffness matrix for a fixed-fixed Euler-Bernoulli beam element, the stiffness matrix is obtained (Zienkiewicz and Taylor, 2005)

$$K = \frac{EI}{L^3}\begin{bmatrix} 12 & 0 & 6L & -12 & 0 & 6L \\ & a & 0 & 0 & -a & 0 \\ & & 4L^2 & -6L & 0 & 2L^2 \\ & & & 12 & 0 & -6L \\ & Sym. & & & a & 0 \\ & & & & & 4L^2 \end{bmatrix} \tag{4.1}$$

where E is the Young's modulus, I is the moment of inertia, and L is the length of the beam element. In addition, a is $\frac{A}{I}L^2$ where A is the cross-sectional area.

The foregoing formula includes only the effect of the flexural deformations. However, for a short beam element, the effect of the shear deformations can be noticeable. In order to include the effect of shear deformations, the Timoshenko beam element can be used. A simple Timoshenko beam element is the beam element used in two dimensional analysis having two nodes with three DOF per node representing translational, longitudinal and rotational movements. There are other types of beam elements depending on the DOFs assumed at each node. The formulation for such an

element for a uniform beam was first driven by McCalley (1963). Later, Przemieniecki (1968) obtained the stiffness matrix for a uniform beam as:

$$K = \frac{EI}{L^3(1+\phi)} \begin{bmatrix} 12 & 0 & 6L & -12 & 0 & 6L \\ & \alpha & 0 & 0 & -\alpha & 0 \\ & & L^2(4+\phi) & -6L & 0 & L^2(2-\phi) \\ & & & 12 & 0 & -6L \\ & Sym. & & & \alpha & 0 \\ & & & & & L^2(4+\phi) \end{bmatrix} \tag{4.2}$$

where E is the Young's modulus, I is the moment of inertia, L is the element length, and:

$$\phi = \frac{12EI}{GkAL^2} \tag{4.3a}$$

$$\alpha = \frac{A(1+\alpha)L^2}{I} \tag{4.3b}$$

where G is the shear modulus, A is the cross-sectional area, and k is the shear coefficient (or Timoshenko shear coefficient) and is calculated based on the geometry of the beam cross-section.

Cowper (1966) obtained the formulas of shear coefficients for various cross-sectional shapes. For a thin-walled I-section the formula is:

$$k = \frac{10(1+\nu)(1+3m)^2}{p_1 + p_2 + 30n^2(m+m^2) + 5\nu n^2(8m+9m^2)} \tag{4.4}$$

where ν is the Poisson's ratio, $m = \frac{2bt_f}{ht_w}$, $n = \frac{b}{h}$ (see Fig. 4.1) , and p_1 and p_2 are

$$p_1 = 12 + 72m + 150m^2 + 90m^3 \tag{4.5a}$$

$$p_2 = \nu(11 + 66m + 135m^2 + 90m^3) \tag{4.5b}$$

The overall bridge stiffness matrix can be constructed with the standard assembling of the member stiffness matrices. The procedure is elaborated elsewhere

(Zienkiewicz and Taylor, 2005). Bridge mass matrix can be constructed assuming the bridge mass as lumped masses on the element nodes. This is an accepted assumption leading to satisfactory results (Chopra, 2001). However, later in this chapter, the effect of consistent masses will be studied. The structural damping is calculated using Rayleigh damping formula (Chopra 2001) as linear combination of the mass and stiffness matrices based on the frequencies of the bridge first two modes.

Two vehicle models are used in this chapter which are sprung mass model and suspended rigid beam model. These models were employed before for numerical validation of the MATLAB program and new VBI elements. The sprung mass model comprised two masses connected by spring-damper suspension system. One mass acts as the wheel which is in the direct contact with the bridge shown in Fig. 3.11. The suspended rigid beam model includes one rigid beam connected to two wheels by a suspension system illustrated in Fig. 3.13. The required vehicle matrices for those models can be consulted from Appendix B. However, the vehicle properties are different and will be given in corresponding sections in this chapter.

4.3 EFFECT OF SHEAR DEFORMATION ON BEAM NATURAL FREQUENCIES

To study the effect of shear deformations on the natural frequencies of beams and also to validate the numerical model coded in MATLAB programming language, a sample 20.0 m individual steel beam that has a W840x226 section is assumed without additional mass. The stiffness matrix is assembled by using the direct stiffness method and two types of element local stiffness matrices; the first type comprises only flexural

effects and the second type includes shear effects in addition to flexural effects. The mass matrix is obtained by the lumped mass approach. By the solution of the Eigen value problem, the frequencies of the first three modes of vibration are compared with the results obtained from linear finite element obtained by SAP2000 in Table 4.1 for three element lengths of 5.0, 2.5, and 1.0 m. Closer results to linear FEM are observed when incorporating the effect of shear deformations.

Modal frequencies depicted in Table 4.1 are modal angular frequencies of the undamped system obtained by the solution of Eigenvalue problem depending only on the mass and the stiffness of the system. The closeness in results between those obtained by shear + flexural effects and those calculated by SAP2000 is mainly due to the closeness of stiffness matrices. There is no difference in the mass matrix which is modeled by lumped mass approximation in all methods.

In addition, comparison of results obtained for each method individually (i.e. SAP2000 only) in Table 4.1 shows an increasing trend for lower element lengths. This is mainly due to the effect of mass in the calculation of modal frequencies. Although the element lengths are changed, the stiffness is not affected noticeably since beam elements are used to assemble global stiffness matrix for each element length. On the other hand, since lumped mass is used, the mass distribution is not consistent (e.g. half of the mass in the two side elements is not included in the analysis) and it is affected by the element lengths. The mass distribution is such that the equivalent modal mass decreases when the element length decreases, and consequently the modal frequencies increases. This effect is reduced when many numbers of elements are used comparing the results of lower element lengths.

4.4 EFFECT OF SHEAR DEFORMATIONS ON TWO NUMERICAL MODELS

Two numerical models are studied in this section, which are moving sprung mass model and suspended rigid beam vehicle models as described in Sections 3.4.1 and 3.4.2. The stiffness matrix is constructed by Eq. 4.1 or 4.2, and the lumped mass matrix is used. The sprung mass model was first studied by Biggs (1964). This case was also used by many researchers such as Majka and Hartnett (2008), Zhang et al. (2001), and Yang and Wu (2001). The required data for the bridge and vehicle models can be consulted from Section 3.4.1. Results are shown in Fig. 4.2 which demonstrates clear and noticeable difference between responses.

The second numerical model is the suspended rigid beam model shown in Fig. 3.13 which was used by Yang and Wu (2001). The required data for the bridge and vehicle models can be consulted from Section 3.4.2. Results presented in Fig. 4.3 show that the effect of shear deformations is less on this model compared to the sprung mass model.

4.5 EFFECT OF SHEAR DEFORMATION ON SAMPLE RAILWAY BRIDGES AND VEHICLES

4.5.1 Bridge and Vehicle Models and Methodology

One of the key parameters affecting the contribution of the shear deformations is the bridge span-to-depth ratio. To study the significance of the effect of the bridge span, several double plate-girder open-deck railway bridges were designed following the requirements of AREMA (American Railway Engineering and Maintenance-of-Way

Association) manual, chapter 15 (AREMA 2007). The moment of inertia and cross-sectional area of bridges were determined to sustain the Cooper-E 80 loading or alternate live load considering overall deflection and local buckling requirements. Appropriate impact loads and rocking effects were also added to the live loads. The summary of the bridge properties is tabulated in Table 4.2. In addition to the self-weight of the girders, a 297 kg/m was considered in the bridge mass accounting for the weight of the track structure and lateral bracings. The girder center to center spacing was selected as 1.8 m to be placed almost under each rail of the track.

These bridges were traversed by a sample vehicle with a sprung mass model similar to Fig. 3.11 as a generic moving vehicle. This model has been used frequently by researchers studying the fundamental behaviour of vehicle and bridge in the VBI analysis (Delgado *et al.*, 2009, Calçada *et al.*, 2009). The properties of the vehicle are based on parameters presented by Lei and Noda (2002) which are due to a TGV (French high-speed train) locomotive, similar to Amtrak Acela Express high-speed train operating between Boston and Washington. Vehicle properties used for this sprung mass model are: M_v= 30.01 ton, M_w=4 ton, k_v=6560 kN/m, c_v=180 kN.s/m.

The designed bridges were modeled by different element lengths traversed by the sample vehicle with different velocities ranging from 0.5 m/s to 150 m/s. The vehicle-bridge interaction numerical dynamic analysis, using the developed VBI element, is performed for each bridge model subjected to the moving vehicle with one specified speed at a time. The important bridge and vehicle responses considered here are bridge mid-span deflection, bridge mid-span acceleration, and vehicle vertical acceleration. Then, maximum responses for mid-span deflection, mid-span acceleration, and vehicle

acceleration are obtained due to each vehicle velocity. Maximum responses are calculated, since in the design procedure the maximum values are used.

Mid-span deflection is the key response to calculate bridge impact factor for the majority of bridge design manuals. For high-speed trains, there are other considerations to be met. First criterion is the vehicle vertical acceleration which is a design criterion for riding comfort. Second criterion is the bridge acceleration which is an essential parameter for stability of ballasted railway tracks. The bridge mid-span acceleration may also be important caused by regular vehicles passing through relatively short bridges. The values for accelerations are obtained using absolute values regardless of the sign of the acceleration.

4.5.2 Bridge Mid-Span Deflection

Figs. 4.4a to 4.4c show mid-span deflection obtained from bridge models including or excluding the effect of shear deformation in the bridge modelling with spans of 6, 12, and 20 m. The bridge element lengths are selected such that they do not affect the accuracy of the response. For a 6.0 m bridge, the element length was selected as 0.5 m, whereas an element length of 1 m was used for the 12 and 20 m bridges.

The general trend in these figures implies that increasing the vehicle speed would not necessarily augment the mid-span deflection and it may result in lower responses for higher speeds. The first value on the left of the figures is almost equal to the static response of the bridge for which the vehicle speed is 0.5 m/s. These very low vehicle speeds are called crawl speed to obtain static-equivalent responses. The rest of the figure presents the dynamic response of the bridge for higher speeds. As clear in these figures,

the impact factor which is the ratio of dynamic over static deflection could become even less than one for some high vehicle speeds. For example, for vehicle speeds of 100 m/s in Fig. 4.4b, the dynamic deflection at 100 m/s is less than the static (or crawl) deflection on the vertical axis.

Figs. 4.4a to 4.4c also demonstrate that the deflection is greater for models including the effect of shear deformation. This is attributed to the fact that the stiffness of the bridge model comprising the effect of shear deformations is less than the model excluding such effects. It means that the bridge is more flexible, which eventually will result in more deflection.

A significant difference between these two bridge modeling schemes (i.e. including or excluding the effect of shear deformations) is seen while decreasing the bridge span. However, the general behaviour looks similar. For the studied bridge models and the sample vehicle with the speed ranges mentioned, the differences between bridge deflections including or excluding shear deformation are summarized in Fig. 4.5. The maximum difference in mid-span deflection is calculated for each bridge by the passage of the sample vehicle with speeds ranging from 0.5 m/s to 150 m/s. Fig. 4.5 shows that, as expected, the effect of shear deformation is greater on shorter spans and the difference rapidly increases to reach up to 18% for 4.0 m span while for longer spans the difference reduces to be around 8%.

As shown in Figs. 4.4a to 4.4b, the response pattern of two models (i.e. including or excluding the effect of shear deformation) are generally similar, but the pattern of curves including shear deformation is shifted to the left in comparison with the other

curves. This can be attributed to the driving frequency of the vehicle which is defined as (Fryba, 1996)

$$\Omega = \frac{\pi v}{L_B} \tag{4.6}$$

where v is the vehicle speed and L_B is the bridge span. As mentioned above, employing shear deformations in the stiffness matrix will decrease the bridge stiffness. This will eventually reduce the bridge natural vibration frequencies. As expected, the maximum responses occur when the vehicle driving frequency is close to the bridge natural frequencies. Therefore, if the bridge natural frequencies are less, those responses occur for less vehicle driving frequencies. Considering Eq. 4.6, the driving frequency decreases when vehicle speed is reduced. Hence, the maximum responses happen for lower vehicle speeds, concluding that the response curve is shifted to the left.

4.5.3 Bridge Mid-Span Acceleration

Another essential bridge response is the mid-span acceleration which is an important factor in the stability of the ballast in ballasted railway bridges. Similar bridges with similar sample vehicle models were analyzed to study the importance of the effect of shear deformation on the bridge mid-span acceleration. Results are shown in Figs. 4.6a to 4.6c which are maximum absolute values of mid-span acceleration. The figures imply that for shorter bridge spans with high-speed vehicles, the differences between two curves increase rapidly.

On of the reasons of the rapid increase can be attributed to the changes in the bridge natural frequency resulting from modified bridge stiffness matrix. The dynamic interaction between bridge and the vehicle is greater for higher vehicle speeds since

driving frequency is more for those speeds (Eq. 4.6). Therefore, the dynamic response between two methods of bridge modelling varies more when vehicle speed increases which can be seen in Fig. 4.6.

In addition, the results imply that the effect of shear deformation is more significant for bridges with shorter spans. It should be noted that, maximum values of mid-span acceleration are used in Fig. 4.6 which are very sensitive to the jagged oscillating nature of bridge mid-span acceleration. Furthermore, the overall vibration of the bridge should also be considered while using values presented in Fig. 4.6.

4.5.4 Vehicle Vertical Acceleration

Despite the fact that accounting for shear deformations affects only the stiffness of the bridge model, this might affect the vehicle response as well. Fig. 4.7 shows the vehicle vertical acceleration for three bridge spans. Vehicle vertical acceleration is an important criterion for riding comfort of vehicles particularly for high-speed trains. The comparison between response of bridges with 6 m and 20 m spans shows that the vehicle on shorter spans are affected more by the effect of shear deformation even for low vehicle velocities. The reason can be attributed to the different bridge natural frequencies interacting with vehicle natural frequencies and also vehicle driving frequency.

4.6 EFFECT OF CONSISTENT MASS CONSIDERING FLEXURAL EFFECTS ONLY

In general, construction of stiffness matrix in Finite Element (FE) modeling is done using the strain energy by the application of assumed appropriate shape functions.

Kinetic energy can be used for obtaining the mass matrix. However, in many ordinary engineering applications, lumped mass method is used. If kinetic energy is used to obtain the mass matrix, the result will be dependent on the chosen shape functions. If similar shape functions applied for stiffness matrix are used to derive the mass matrix, the resulted mass matrix is called consistent mass matrix which basically is consistent with the stiffness matrix. For an Euler-Bernoulli beam element usually Hermitian cubic functions are used which will yield to the following consistent mass matrix (Przemieniecki, 1985)

$$M_C = \frac{\rho AL}{420}\begin{bmatrix} 140 & 0 & 0 & 70 & 0 & 0 \\ & 156 & 22L & 0 & 54 & -13L \\ & & 4L^2 & 0 & 13L & -3L^2 \\ & & & 140 & 0 & 0 \\ & Sym. & & & 156 & -22L \\ & & & & & 4L^2 \end{bmatrix} \tag{4.7}$$

To study the effect of the consistent mass matrix, the generic sprung mass model used in Section 4.5 together with the 6 m railway bridge model is used. The properties of the vehicle are based on parameters presented by Lei and Noda (2002) given in Section 4.5. The railway bridge model of 6 m was traversed by the sprung mass model for various ranges of vehicle speeds. Numerous analyses were carried out to determine maximum responses for each vehicle speeds. Midspan deflection, midspan acceleration and vehicle vertical acceleration are calculated as the main vehicle and bridge responses for vehicle-bridge dynamic interaction.

Results for maximum midspan deflection, maximum vehicle vertical acceleration and maximum midspan acceleration are shown in Figs. 4.8 to 4.10. The bridge element lengths were chosen 0.5 m for 6 m span bridge, and 1 m for 12 and 20 m bridges, and

they only include the effect of flexural deformations. Each point in those figures is the maximum value of the corresponding response of the passage of the vehicle through bridge with the associated velocity. The speed parameter is used as the horizontal axis. The speed parameter is a ratio of the driving frequency of the vehicle to the fundamental circular frequency of the bridge. That is a parameter depending on the vehicle velocity, v, the bridge fundamental frequency, ω, and the bridge length, L_B, defined as:

$$S = \frac{\pi v}{\omega L_B} \tag{4.8}$$

Speed parameter is a dimensionless parameter. The maximum midspan deflection and the maximum vehicle vertical acceleration are not affected by the application of the consistent mass matrix for all speed ranges. However, the maximum midspan acceleration is affected for higher speeds as shown in Fig. 4.10. For speed parameters more than 0.5 in Fig. 4.10, results are affected by the application of the consistent mass. Nevertheless, for low vehicle speeds due to insignificant dynamic content of the bridge oscillation, the effect is not considerable. The effect of consistent mass reduces rapidly for longer bridges.

In conclusion, for Euler-Bernoulli beam element having flexural stiffness only, the effect of consistent mass can be neglected in the analysis of vehicle-bridge interaction even for high-speed trains. Special attentions should be given to short bridges where the bridge acceleration is important (e.g. ballasted railway bridges) at high vehicle speeds.

4.7 EFFECT OF CONSISTENT MASS CONSIDERING FLEXURAL AND SHEAR EFFECTS

4.7.1 Mass Matrices

The application of various types of mass matrices may be important in the bridge modeling while incorporating the effect of shear deformations. The consistent mass matrix including the effect of shear deformation is (Przemieniecki, 1985)

$$M_{CS}=\frac{\rho AL}{(1+\phi)^2}\begin{bmatrix} m_1 & 0 & m_2 & m_3 & 0 & m_4 \\ & \frac{1}{3}(1+\phi)^2 & 0 & 0 & \frac{1}{6}(1+\phi)^2 & 0 \\ & & m_5 & -m_4 & 0 & m_6 \\ & & & m_1 & 0 & -m_2 \\ & Sym. & & & \frac{1}{3}(1+\phi)^2 & 0 \\ & & & & & m_5 \end{bmatrix} \tag{4.9}$$

where

$$m_1=\frac{13}{35}+\frac{7\phi}{10}+\frac{\phi^2}{3} \tag{4.10a}$$

$$m_2=\left(\frac{11}{210}+\frac{11\phi}{120}+\frac{\phi^2}{24}\right)L \tag{4.10b}$$

$$m_3=\frac{9}{70}+\frac{3\phi}{10}+\frac{\phi^2}{6} \tag{4.10c}$$

$$m_4=-\left(\frac{13}{420}+\frac{3\phi}{40}+\frac{\phi^2}{24}\right)L \tag{4.10d}$$

$$m_5=\left(\frac{1}{105}+\frac{\phi}{60}+\frac{\phi^2}{120}\right)L^2 \tag{4.10e}$$

$$m_6=-\left(\frac{1}{140}+\frac{\phi}{60}+\frac{\phi^2}{120}\right)L^2 \tag{4.10f}$$

where the definition of bridge parameters (i.e. A, L, etc.) is given in Section 4.2.

The effect of rotary mass may also be important induced by the beam cross-sectional rotary inertia. This effect can be important in short beams with big cross sections, i.e. for beams with low span-to-depth ratios. If one wants to incorporate the effect of rotary masses, another mass matrix is obtained as (Przemieniecki, 1985)

$$M_{CR} = \frac{\rho AL}{(1+\phi)^2}\left(\frac{r}{L}\right)^2 \begin{bmatrix} m_7 & 0 & m_8 & -m_7 & 0 & m_8 \\ & 0 & 0 & 0 & 0 & 0 \\ & & m_9 & -m_8 & 0 & m_{10} \\ & & & m_7 & 0 & -m_8 \\ & Sym. & & & 0 & 0 \\ & & & & & m_9 \end{bmatrix} \tag{4.11}$$

where

$$m_7 = \frac{6}{5} \tag{4.12a}$$

$$m_8 = \left(\frac{1}{10} - \frac{\phi}{2}\right)L \tag{4.12b}$$

$$m_9 = \left(\frac{2}{15} + \frac{\phi}{6} + \frac{\phi^2}{3}\right)L^2 \tag{4.12c}$$

$$m_{10} = \left(-\frac{1}{30} - \frac{\phi}{6} + \frac{\phi^2}{6}\right)L^2 \tag{4.12d}$$

Subsequently, the total consistent mass matrix including the effect of rotary inertia is:

$$M = M_{CS} + M_{CR} \tag{4.13}$$

4.7.2 Bridge and Vehicle Models and Methodology

In order to study the effect of these types of consistent masses including the effect of shear deformations, the generic sprung mass vehicle model used in the preceding

section is applied here with two bridge lengths of 6 m and 20 m. These bridges are chosen as representatives of a short span bridge and comparatively a medium span bridge, respectively. Three important dynamic responses are obtained using the developed MATLAB program for numerical time history dynamic analysis. These responses are midspan deflection, midspan acceleration, and vehicle vertical acceleration. The new VBI element is used to analyze the vehicle-bridge interaction.

Stiffness matrix can be constructed by the flexural effects only (Eq. 4.1), or with flexural plus shear effects (Eq. 4.2). Mass matrix can be assembled using lumped masses or consistent masses, which in the case of the Timoshenko beam it will include the effect of rotary masses as well (Eq. 4.13). Three types of bridge models are considered here which are based on two types of stiffness and mass matrices. The first model is the basic model of Euler-Bernoulli beam element having **f**lexural stiffness with **l**umped mass denoted as **FL** model. The second model is named **FSL** model for the Timoshenko beam having the effect of **s**hear deformation in the **s**tiffness matrix and **l**umped masses. The last model is called **FSCR** model which is the Timoshenko beam with the stiffness and **c**onsistent mass matrix including the effect of **f**lexure and **s**hear deformations and also the effect of **r**otary mass in the mass matrix. These assigned names are used in Figs. 4.11 to 4.16.

4.7.3 Bridge Model of 6.0 m Span

The midspan acceleration, which is the most sensitive response to the various bridge characteristics, is shown in Fig. 4.11 for four vehicle speed parameters. In all four sub-figures, the vehicle leaves the bridge at the vehicle location of 6 m since the bridge

length is 6 m. The free vibration of the bridge is also shown which can be seen in all sub-figures from the vehicle location of 6 m to 12 m. The effect of 2% bridge damping is evident in Fig. 4.11 (a) and also in the rest of figures. In Fig. 4.11 (a) regarding speed parameter S=0.05, the maximum midspan acceleration occurs right before the vehicle leaves the bridge. In contrast, for S=0.3, 0.6, and 1.0, the maximum value of midspan acceleration happens in the free vibration. This is because the vehicle passage is like a pulse exerted on the bridge; due to its magnitude and duration, the bridge may not have enough time to respond completely while the vehicle is on the bridge. Therefore, the maximum response will happen in the first peak of the bridge vibration after the vehicle leaves the bridge. It happens always in the first peak of vibration due to decreasing nature of the free vibration as a result of the bridge damping.

The effect of various methods of constructing the bridge stiffness matrix and the bridge mass matrix is illustrated in Fig. 4.11. For relatively low vehicle velocities shown in Fig 4.11 (a), the response of midspan acceleration is almost the same for the bridge models constructed by the FSL model compared to bridges using FSCR model. The discrepancies between the two models increase for higher vehicle speeds which can be clearly observed from Fig. 4.11 (b) to (d). This is attributed to the fact that the effect of the consistent masses and particularly the rotary inertia increases while frequency of the excitation is augmented. The length of the bridge plays an important role, as well. Therefore, as expected, the effects of consistent and rotary masses are noticeable in higher vehicle speeds for this short bridge.

The comparison between FL model and the other two models imply that the FL model underestimates the midspan acceleration. The difference reaches 70% for the

maximum midspan acceleration for S=0.6 shown in Fig. 4.11 (c). The reason is mainly due to the effect of shear deformations in the stiffness matrix. If one considers those effects in the stiffness matrix, it will result in a less stiff bridge; therefore more responses will occur.

In Figs. 4.12 (a) and (b), the maximum midspan deflection occurs while the vehicle is still on the bridge. However, it happens in the bridge free vibration (when the vehicle is not on the bridge anymore) for higher vehicle speeds of Figs. 4.12 (c) and (d). This implies large impulsive nature of the vehicle passing the bridge which can also be attributed to the very short bridge length. The differences between the results obtained by FSL and FSCR models are much less than those for midspan accelerations. The midspan deflections are very close even for very high vehicle speeds (S=0.6). However for extremely fast movements with driving frequencies close to the bridge fundamental frequency (i.e. S=1.0), the discrepancy in the response can increase shown in Fig. 4.12 (d). In addition, the effect of shear deformations is important in all vehicle speed ranges illustrated in Figs. 4.12 (a) to (d) by comparing FL model with the other models of FSL or FSCR.

Fig. 4.13 shows the vehicle vertical acceleration for 6 m bridge. As illustrated in Figs. 4.13 (a) to (d), the vehicle response is less affected by the various bridge modeling schemes of FSL and FSCR compared to the two previous bridge responses. For all vehicle velocities, there are no noticeable differences between the response obtained by lumped mass matrix (FSL) and those by consistent-rotary mass matrix (FSCR). In contrast, the vehicle vertical acceleration is affected by employing the shear effects in FSL and FSCR models comparing to FL model excluding such effects. Similar to other

responses (i.e. midspan acceleration and midspan deflections) the effect of shear deformations is important in all vehicle speed ranges.

4.7.4 Bridge Model of 20 m Span

The bridge midspan acceleration is shown in Figs. 4.14 (a) to (d). It is expected to have less effects of either shear deformations or consistent-rotary mass on the response for 20 m bridge compared to the shorter bridge of 6 m. The effect of consistent-rotary mass of FSCR model is much less compared to 6 m bridge illustrated in Fig. 4.11. However, that effect becomes more important for higher speeds as it is evident in Fig. 4.14 (d). The effect of shear deformations still plays a significant role in the response of the bridge for midspan acceleration caused by high speed vehicles clearly depicted in Figs. 4.14 (c) and (d). On the other hand, such effects are less important for low vehicle speeds of longer bridges comparing Fig. 4.14 (a) with Fig. 4.11 (a).

For the midspan deflection and vehicle vertical acceleration shown in Figs. 4.15 and 4.16 respectively, the consistent-rotary mass has no effect whatsoever comparing the results for FSL and FSCR models. This is true for all vehicle speed ranges where the results for FSL and FSCR models are identical. In addition, despite the fact that the effects of shear deformations are not negligible for midspan deflection and vehicle vertical acceleration for 20 m bridge shown in Figs. 4.15 and 4.16, their effects are less important compared to those for 6 m bridge shown in Figs. 4.12 and 4.13, respectively.

4.8 SUMMARY

It was shown in this chapter that the effect of shear deformation should be included in the construction of the stiffness matrix and they are not negligible in the VBI analysis particularly for bridges with low span-to-depth ratios. The beam frequencies were calculated for a sample beam including and excluding the effect of shear deformations, which were compared with frequencies obtained from linear FEM analysis. Closer results to linear FEM were observed when considering the effect of shear deformations. In addition, two popular numerical models were analyzed which demonstrated the noticeable effect of shear deformation in the response. Moreover, by the passage of a sample vehicle (French high speed locomotive) over a series of designed double plate-girder open-deck railway bridges, the difference in the mid-span deflection between models including and excluding shear deformation were measured up to 18% for 4.0 m span bridge and around 8% for spans longer than 16.0 m.

If the effect of shear deformation is incorporated in the stiffness matrix, it will decrease the bridge stiffness which will eventually reduce the bridge natural frequencies. The dynamic interaction and maximum responses between vehicle and the bridge mainly depend on the relationship and closeness of bridge natural frequencies and the vehicle driving frequency. When the bridge frequency is less, the maximum response happens for less vehicle driving frequency (i.e. less vehicle speeds). This is as if the response pattern is shifted to the left of the figure which was observed for mid-span deflection, mid-span acceleration and even vehicle vertical acceleration (Figs. 4.4 to 4.7). Therefore, the maximum response due to lower vehicle speed may happen to be within the vehicle

operating speed range which could have been out of that range before considering the effect of shear deformations.

Effect of consistent masses was also studied in this chapter. If the bridge stiffness matrix is constructed by flexural effects only, there is no considerable effect of consistent masses in bridge mid-span deflection and vehicle vertical acceleration for all vehicle speed ranges. However, those effects will slightly change the peak value of bridge midspan acceleration which is a very sensitive response compared to bridge midspan deflection and vehicle acceleration. This is valid only for short bridges and for vehicles with speed parameter $S > 0.5$.

Timoshenko beam element is used to simulate the effect of shear deformation with consistent mass including the effect of rotary mass. Three types of bridge models are considered here which address two types of stiffness and mass matrix. Two plate-girder railway bridges of 6 and 20 m spans were used representing short and medium span girder bridges. Shear effects have a significant influence on all bridge responses of 6 m short bridge particularly for midspan acceleration. The model including flexural effects with lumped masses underestimates the midspan acceleration which can reach up to 70% in the peak midspan acceleration for the speed parameter $S=0.6$. The effects of consistent masses are minor in the midspan deflection and vehicle acceleration for most vehicle ranges; however, midspan acceleration is affected for very high vehicle speeds. For the 20 m medium span bridge, the responses are less affected by the effect of consistent-rotary masses. Yet there is still an effect on the midspan acceleration for high vehicle velocities.

Table 4.1: Modal frequencies (rad/sec) for a simply-supported beam obtained from the computer code compared to linear FEM (obtained by SAP2000)

	Linear FEM			Flexural Effects Only			Shear + Flexural Effects		
	5m	2.5m	1m	5m	2.5m	1m	5m	2.5m	1m
Mode 1	27.207	27.213	27.214	27.322	27.325	27.326	27.180	27.186	27.188
Mode 2	106.7	107.17	107.24	109.03	109.29	109.30	106.60	107.06	107.14
Mode 3	228.34	234.73	235.51	241.37	245.76	245.93	228.12	234.50	235.28

Table 4.2 Structural properties of the designed plate-girder open-deck railway bridges

Bridge span	Moment of inertia	Cross-sectional area	Timoshenko Shear Coefficient
m	m^4	m^2	
4	0.001020	0.01946	0.442
6	0.002806	0.03208	0.431
8	0.006384	0.04704	0.441
10	0.011170	0.06014	0.438
12	0.016496	0.06625	0.468
14	0.024240	0.07510	0.471
16	0.031300	0.08523	0.479
18	0.042020	0.09308	0.490
20	0.057560	0.10072	0.516
25	0.105540	0.12172	0.529
30	0.183480	0.15336	0.485

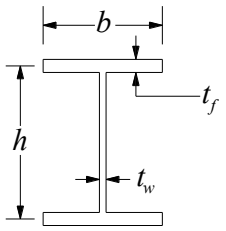

Fig. 4.1 Required designations for Timoshenko shear coefficient

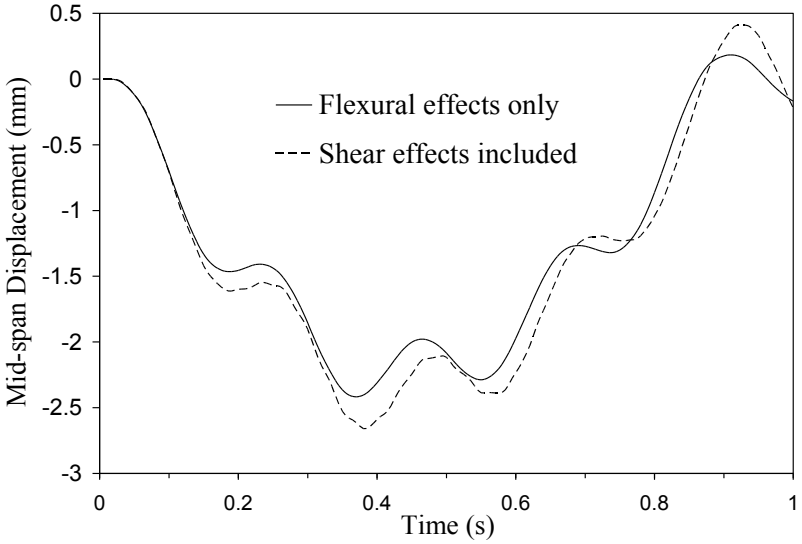

Fig. 4.2 Effect of shear deformations on sprung mass model

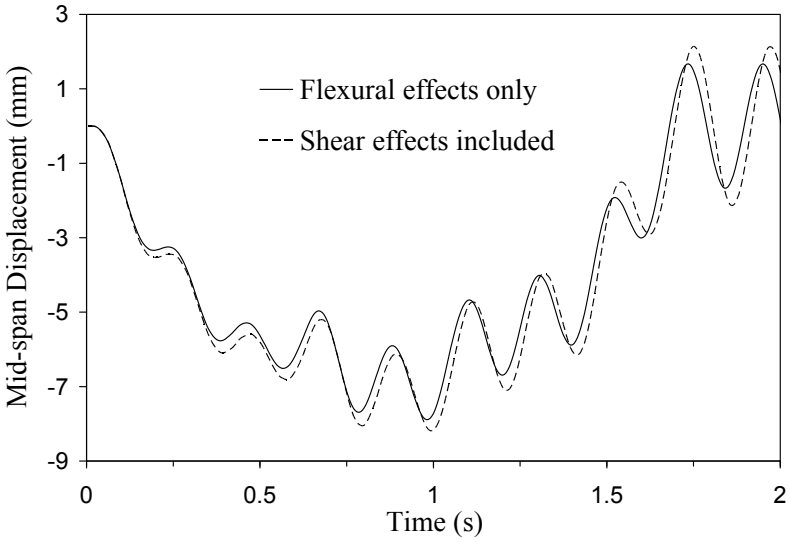

Fig. 4.3 Effect of shear deformations on suspended rigid beam model

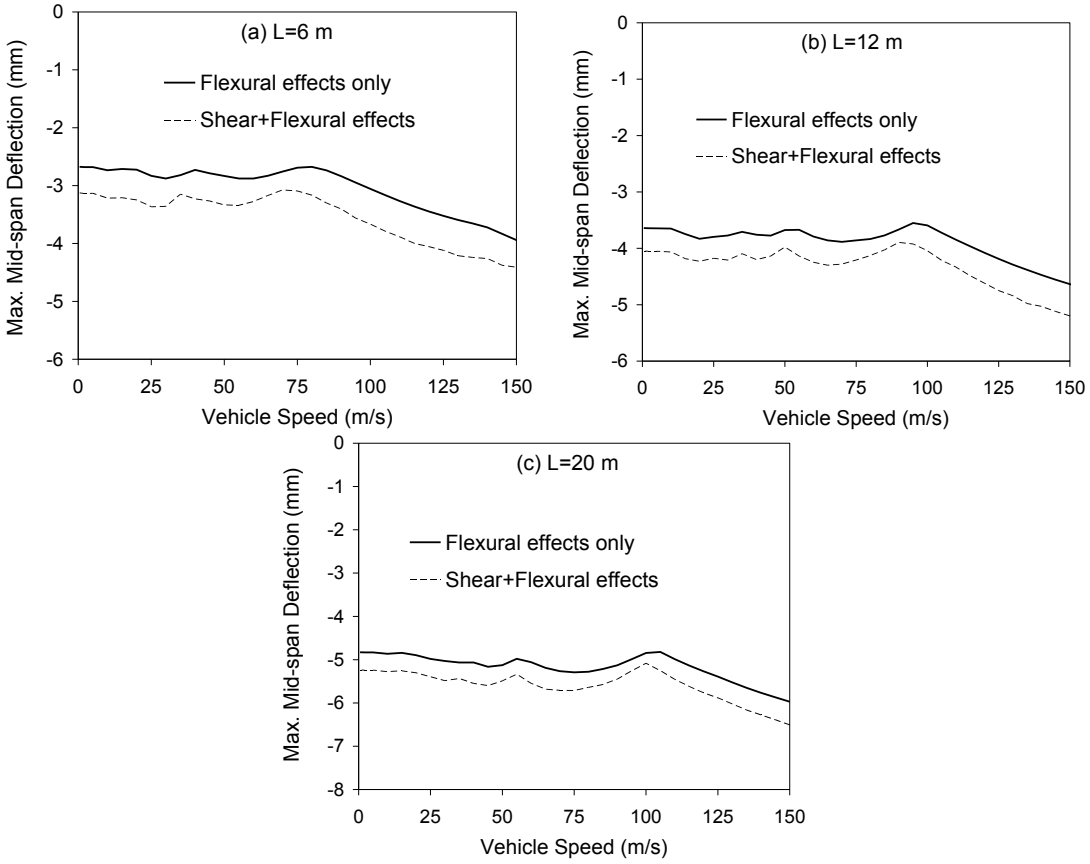

Fig. 4.4: Maximum mid-span deflection for bridge models including or excluding the effect of shear deformations, bridge spans of (a) 6m, (b) 12m, (c) 20m.

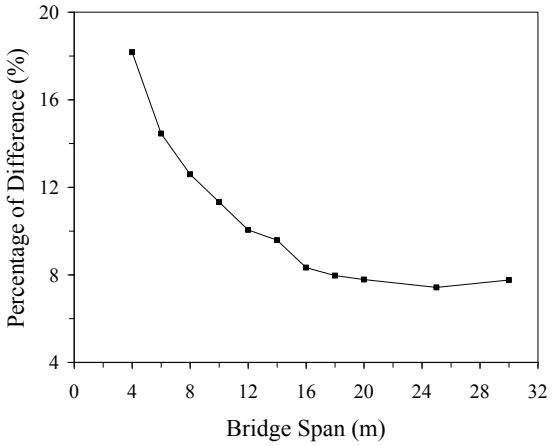

Fig. 4.5 The percentage of difference for mid-span deflection response regarding models including shear deformation effects with respect to models including flexural effects only for various bridge spans.

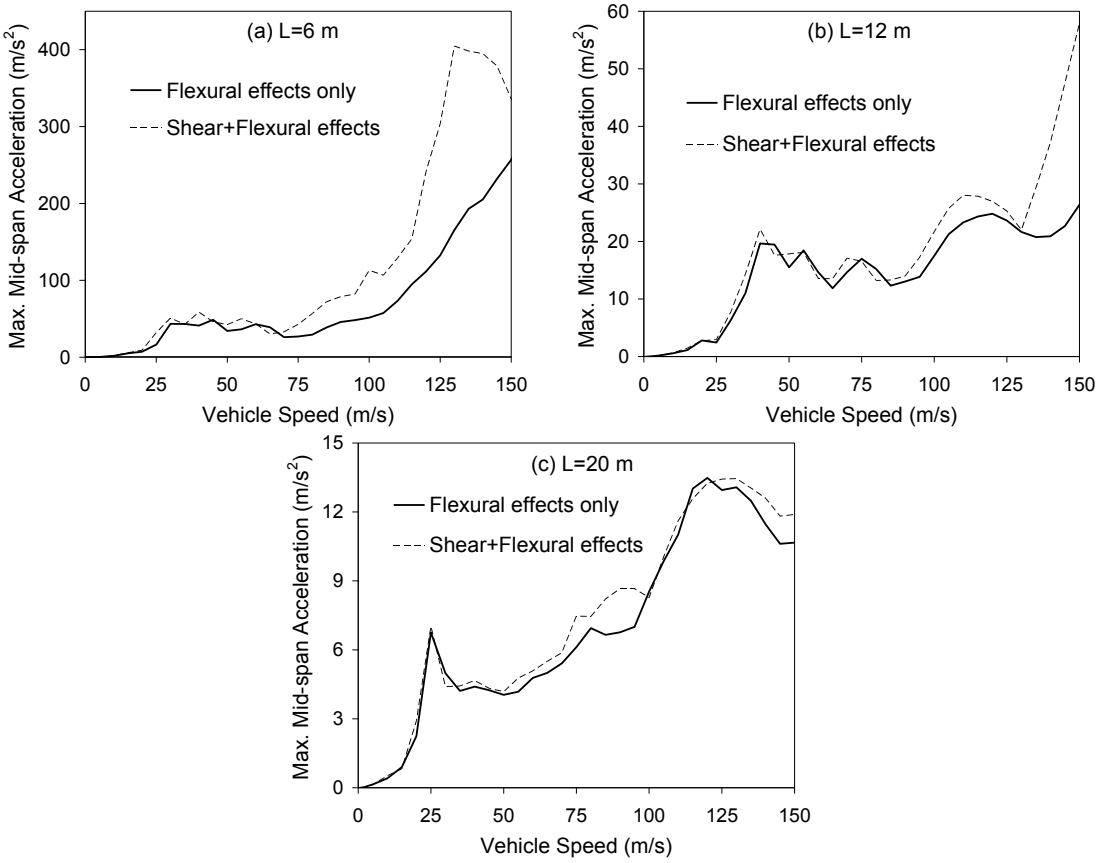

Fig. 4.6 Maximum bridge mid-span acceleration for bridge models including or excluding the effect of shear deformations, bridge spans of (a) 6 m, (b) 12 m, (c) 20 m.

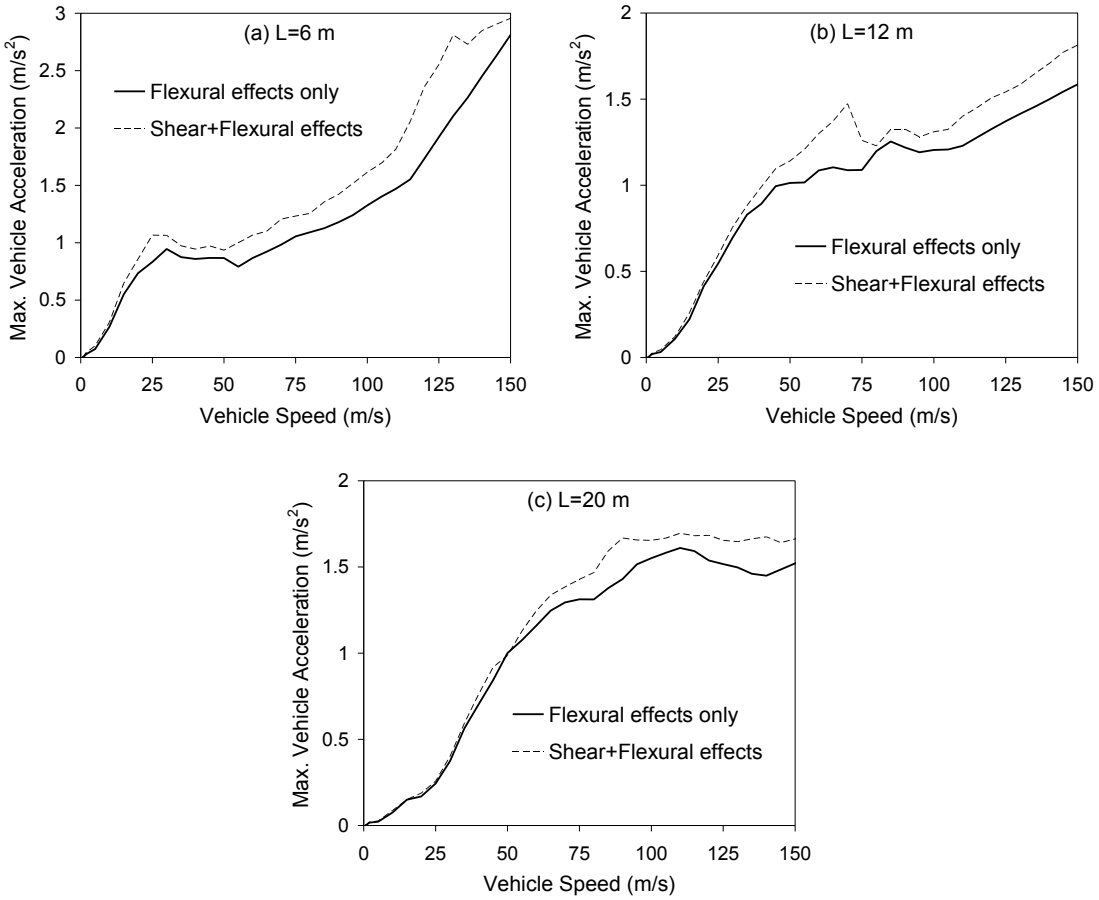

Fig. 4.7 Maximum vehicle vertical acceleration for bridge models including or excluding the effect of shear deformations, bridge spans of (a) 6m, (b) 12m, (c) 20m

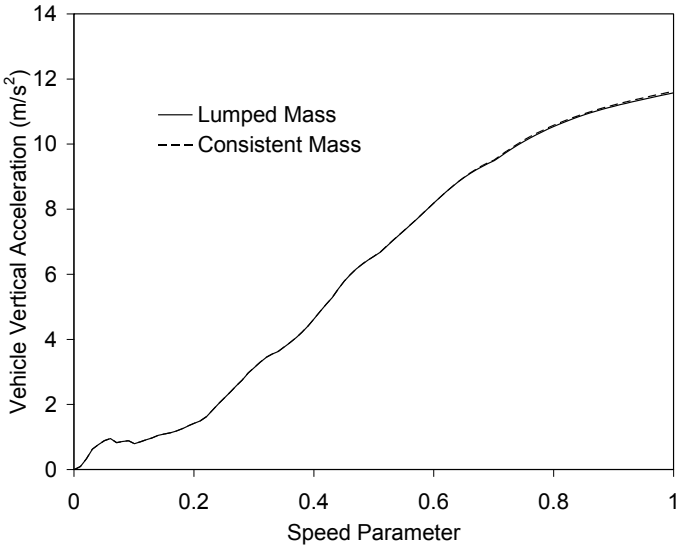

Fig. 4.8 Effect of the consistent mass on the maximum vehicle vertical acceleration for the bridge model of 6 m

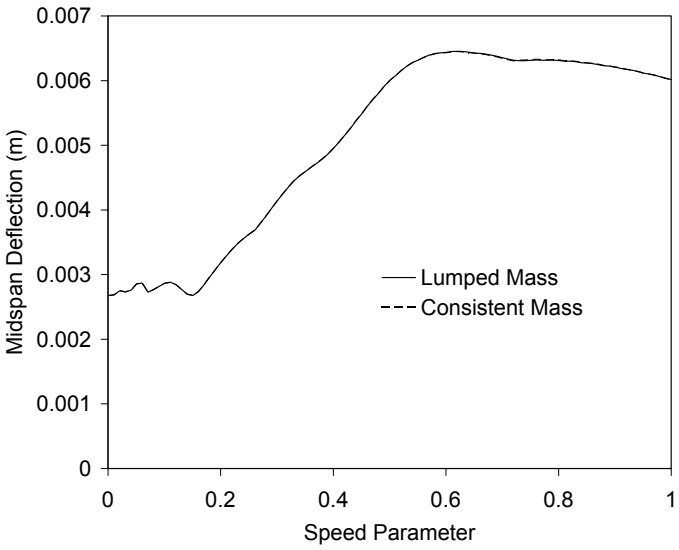

Fig. 4.9 Effect of the consistent mass on the maximum midspan deflection for the bridge model of 6 m

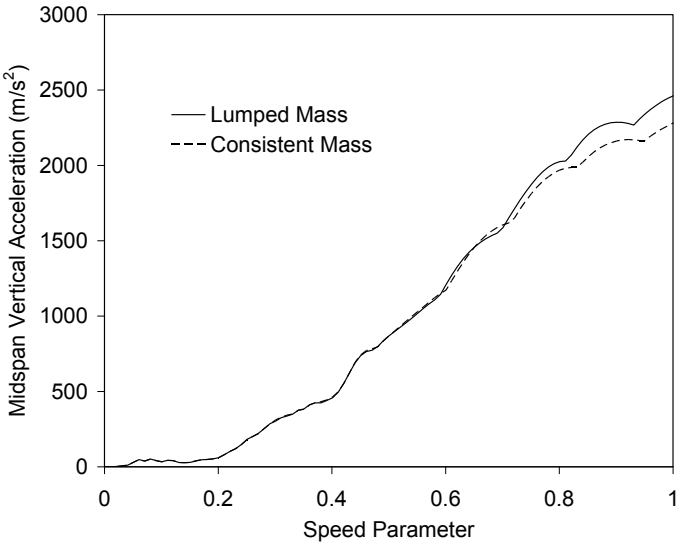

Fig. 4.10 Effect of the consistent mass on the maximum midspan vertical acceleration for the bridge model of 6 m

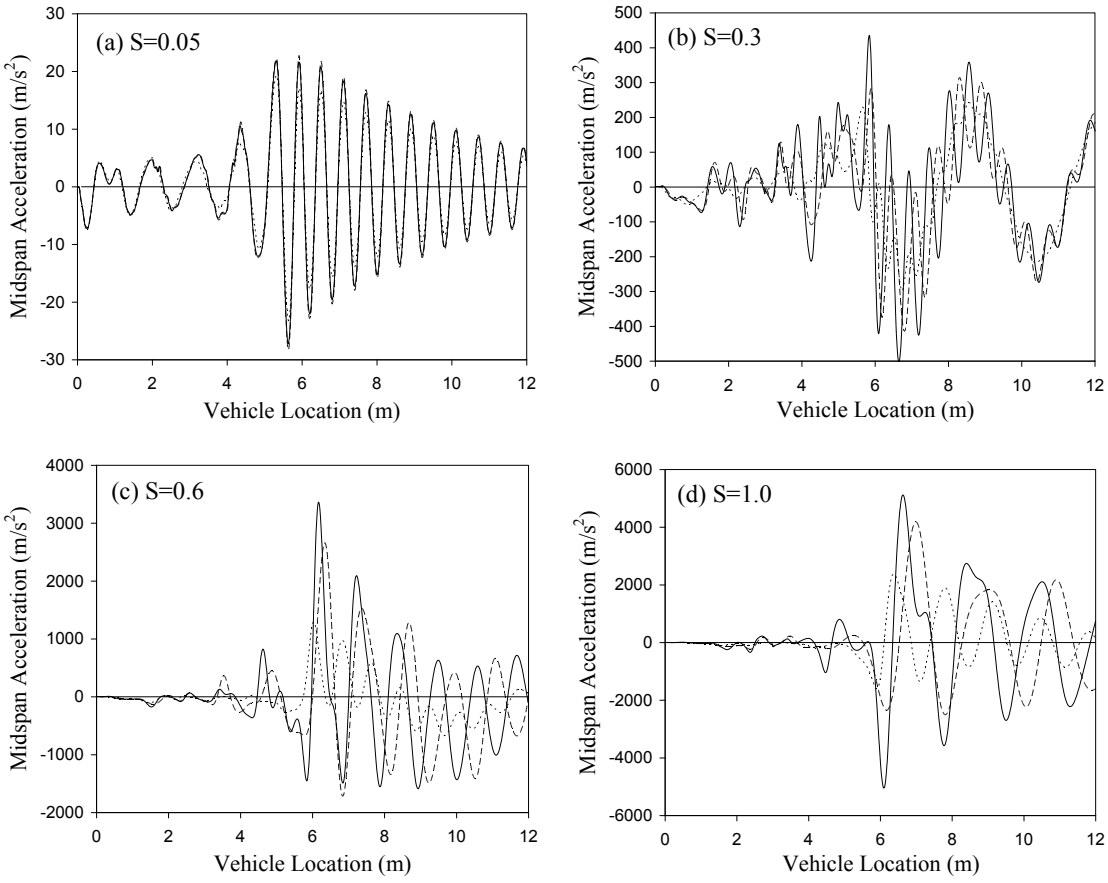

Fig. 4.11 Midspan acceleration in the 6 m bridge for four speed parameters (a) 0.05, (b) 0.3, (c) 0.6, (d) 1.0. ····· Flexural stiffness with lumped mass (FL), ---- Flexural and shear stiffness with lumped mass (FSL), —— Flexural and shear stiffness with consistent-rotary mass (FSCR).

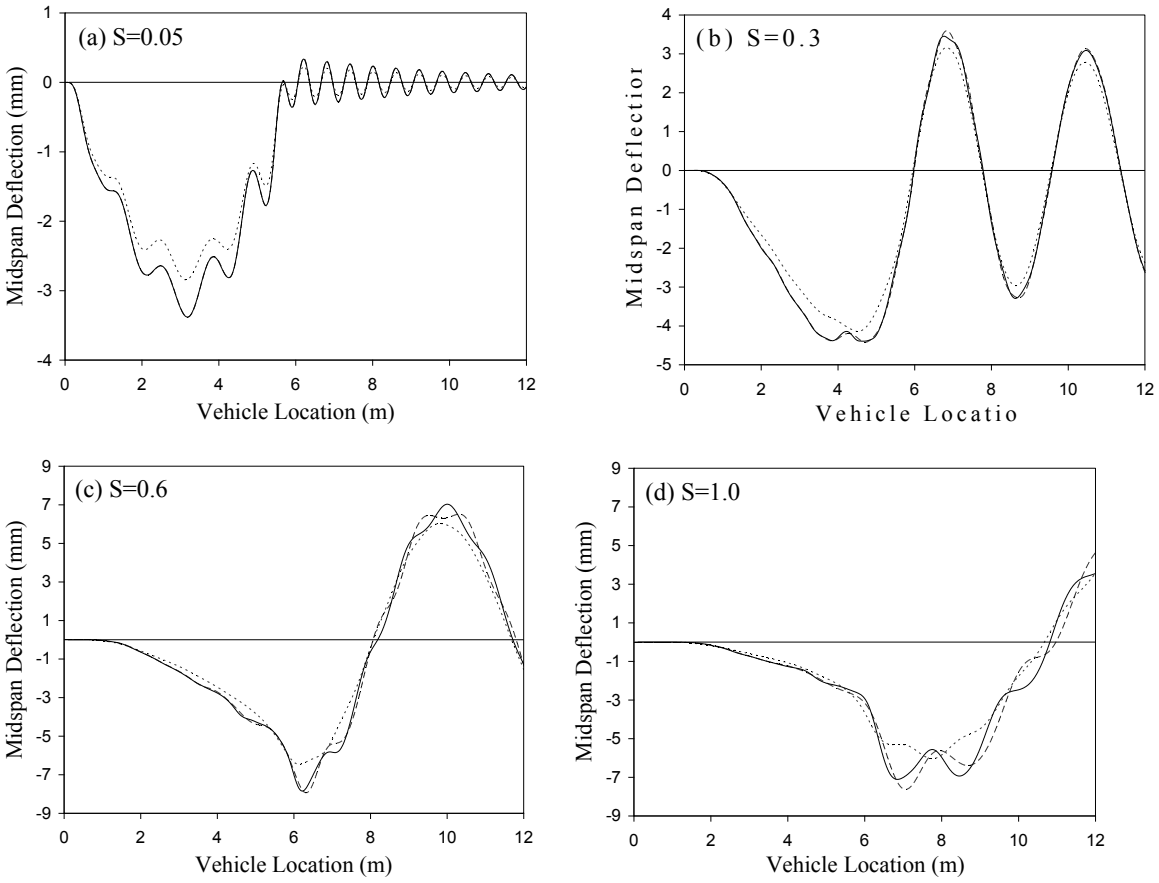

Fig. 4.12 Midspan deflection in the 6 m bridge for four speed parameters (a) 0.05, (b) 0.3, (c) 0.6, (d) 1.0. ····· Flexural stiffness with lumped mass, - - - - Flexural and shear stiffness with lumped mass, —— Flexural and shear stiffness with consistent-rotary mass.

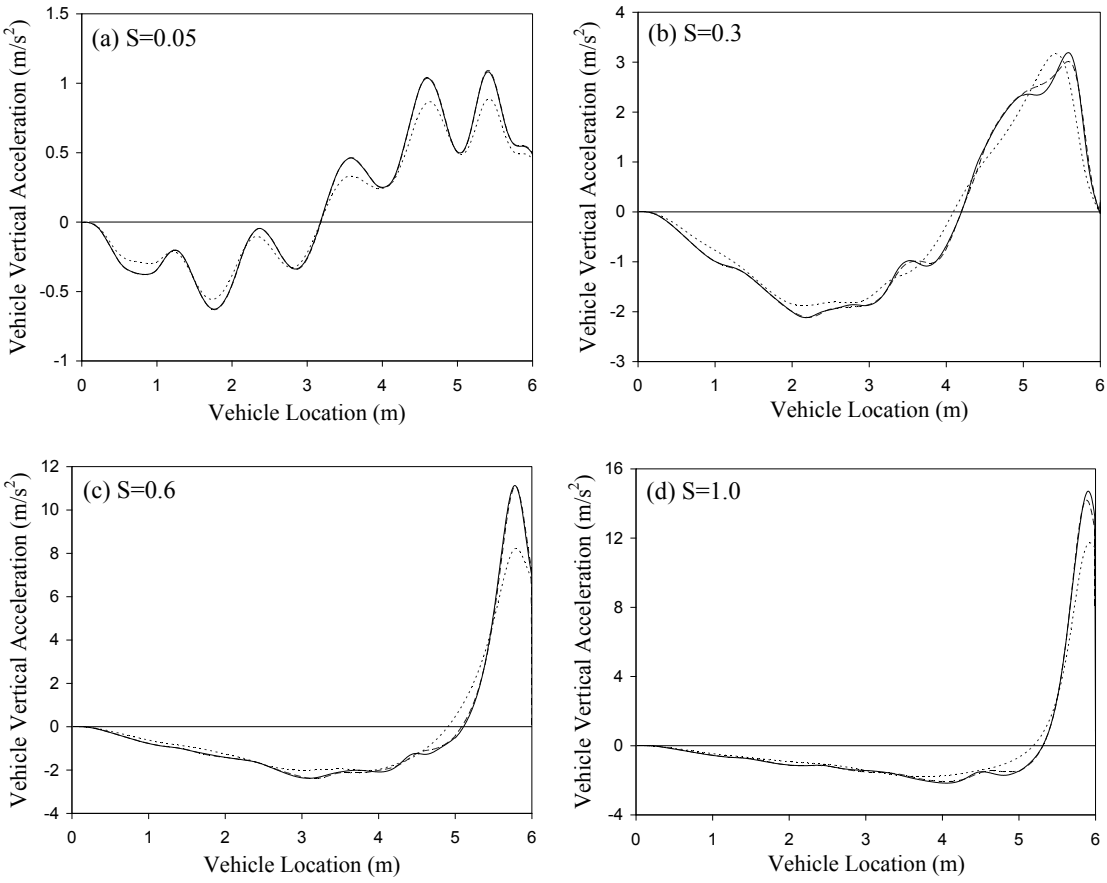

Fig. 4.13 Vehicle vertical acceleration in the 6 m bridge for four speed parameters (a) 0.05, (b) 0.3, (c) 0.6, (d) 1.0. ····· Flexural stiffness with lumped mass, - - - - Flexural and shear stiffness with lumped mass, —— Flexural and shear stiffness with consistent-rotary mass.

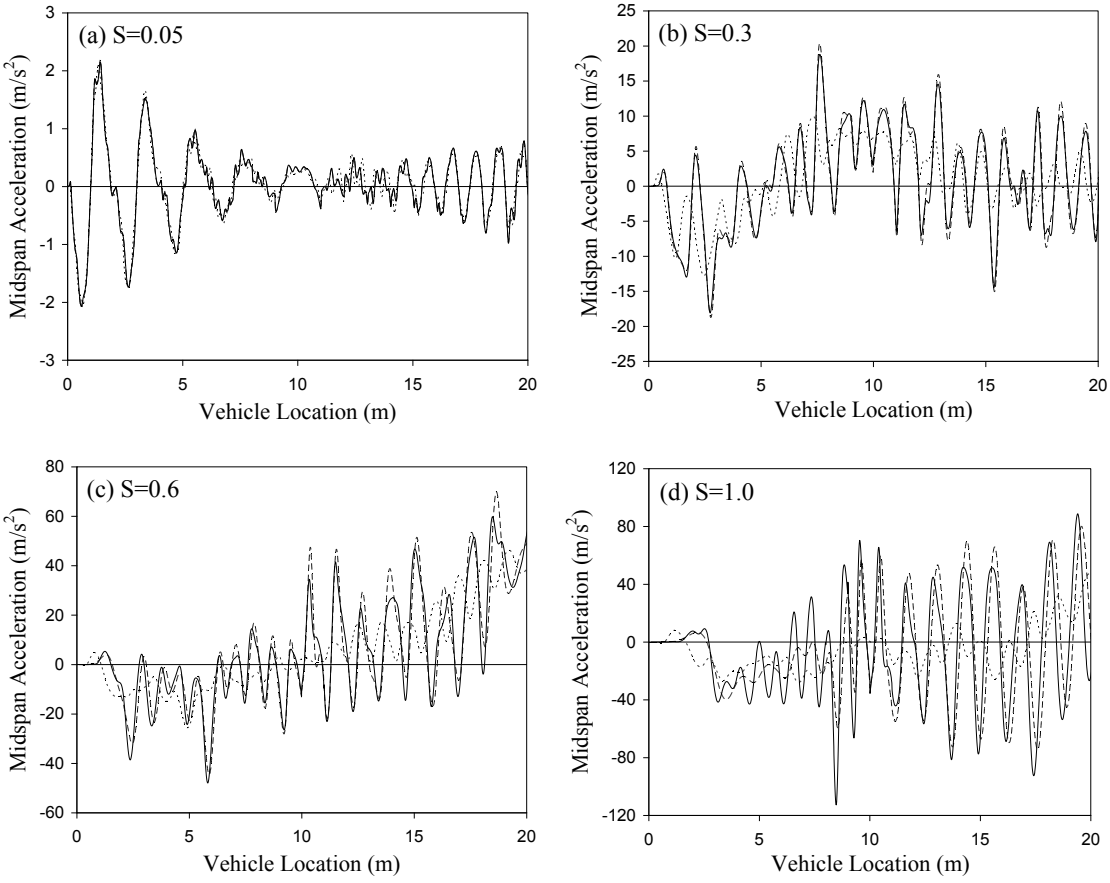

Fig. 4.14 Midspan acceleration in the 20 m bridge for four speed parameters (a) 0.05, (b) 0.3, (c) 0.6, (d) 1.0. ····· Flexural stiffness with lumped mass, - - - - Flexural and shear stiffness with lumped mass, —— Flexural and shear stiffness with consistent-rotary mass.

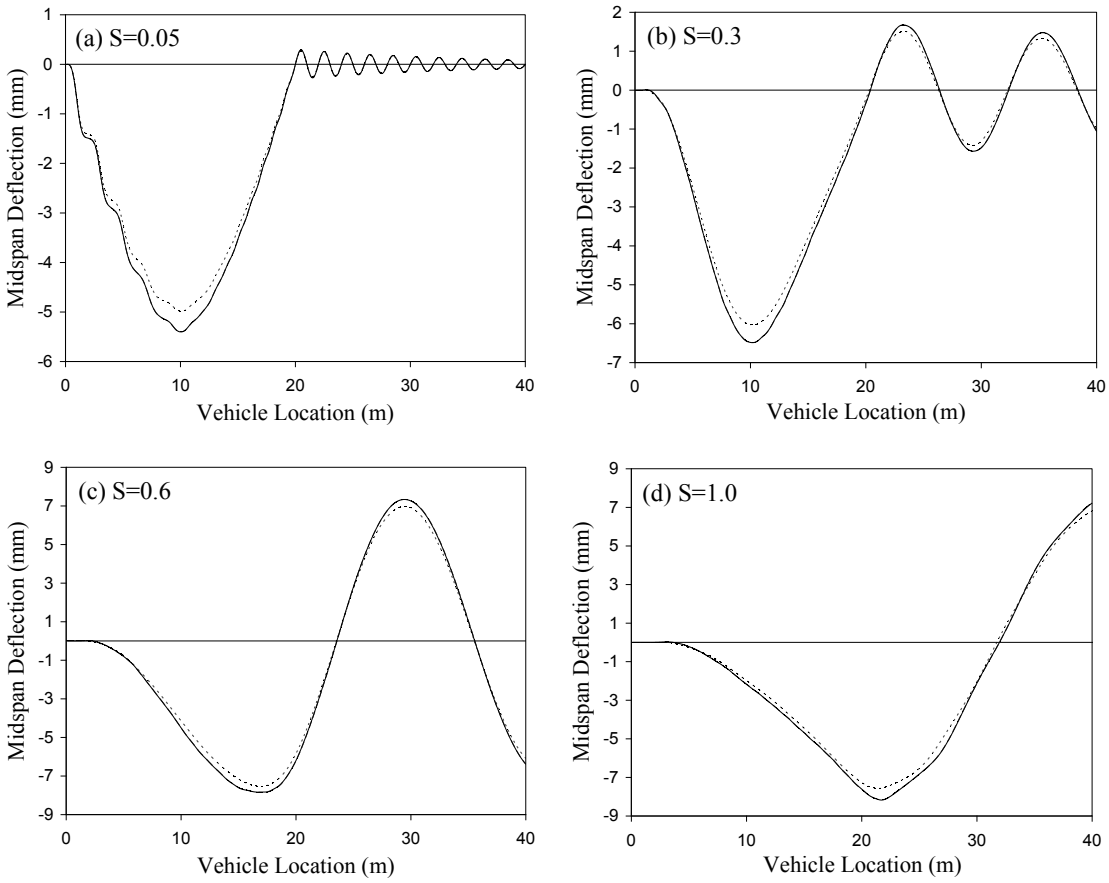

Fig. 4.15 Midspan deflection in the 20 m bridge for four speed parameters (a) 0.05, (b) 0.3, (c) 0.6, (d) 1.0. ····· Flexural stiffness with lumped mass, - - - - Flexural and shear stiffness with lumped mass, —— Flexural and shear stiffness with consistent-rotary mass.

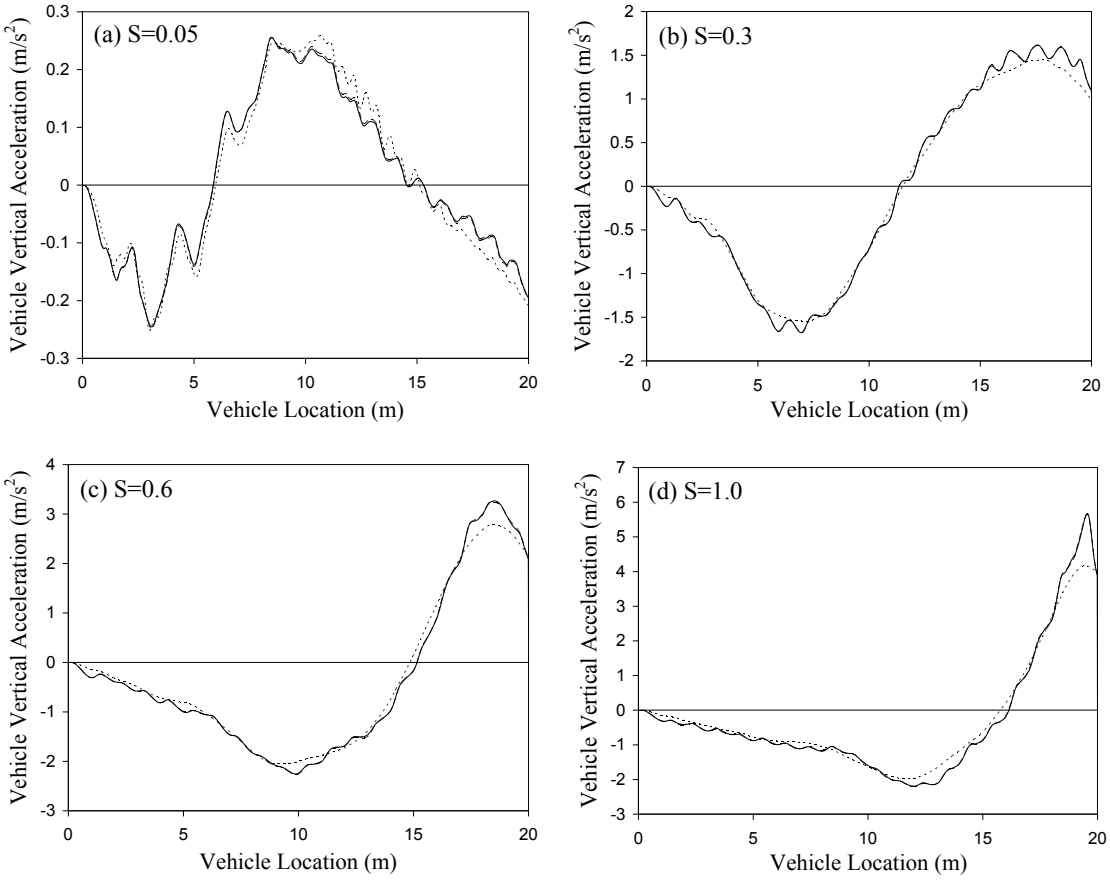

Fig. 4.16 Vehicle vertical acceleration in the 20 m bridge for four speed parameters (a) 0.05, (b) 0.3, (c) 0.6, (d) 1.0. ····· Flexural stiffness with lumped mass, - - - - Flexural and shear stiffness with lumped mass, —— Flexural and shear stiffness with consistent-rotary mass.

CHAPTER 5

EVALUATION AND INVESTIGATION OF THE SIGNIFICANCE OF NEW VBI ELEMENTS

5.1 GENERAL

In the current study, two numerical VBI elements, one for vehicles with constant velocities and the other one for vehicles experiencing acceleration or deceleration, are developed and verified as described in Chapter 3. The effect of shear deformation and consistent mass on the VBI analysis were studied in Chapter 4. In this chapter, the significance of the developed VBI elements is investigated. It should be noted that, since most of the results available in the literature are based on Euler-Bernoulli beam element with flexural stiffness and lumped masses, the same approach is taken in this chapter to have comparable results with those reported in the literature.

For vehicles with constant velocity, the effects of the model parameters are studied. These parameters include bridge and vehicle damping, frequency parameter, system mass parameter, in addition to a new introduced parameter called vehicle mass parameter.

Moreover, the VBI element developed for vehicles with longitudinal (or horizontal) deceleration is studied for three vehicle models: The suspended rigid beam model; unsymmetrical truck model; and a train model. The results are compared with those in the literature demonstrating significant effect on both vehicle and bridge responses.

5.2 EVALUATION OF THE NEW VBI ELEMENT FOR VEHICLES WITH CONSTANT VELOCITY

5.2.1 Parameters to be Investigated and Bridge and Vehicle Models

In order to investigate the efficiency of the new VBI elements, a study on the effect of the model variables is conducted. Non-dimensional parameters used by other researchers (Green and Cebon, 1997; Majka and Hartnett, 2008) are used. A new parameter called vehicle mass parameter, which is the ratio of the wheel mass to the vehicle body mass, is introduced and considered. Non-dimensional parameters to be investigated are the damping of the vehicle and the bridge, frequency parameter, γ, system mass parameter, κ, and vehicle mass parameter, η.

The frequency parameter γ is the ratio of vehicle natural frequency to the bridge natural frequency. For parametric study, various values of γ are obtained by modifying the stiffness of the sprung mass model while the vehicle mass remains constant. System mass parameter κ is the ratio of the total vehicle mass to the total bridge mass. In order to obtain various values of κ for parametric study, vehicle mass and stiffness are modified such that γ remains constant. Parametric study is conducted comparing the results of the new VBI element with models proposed by Yang and Wu (2001) and also Majka and Hartnett (2008). The latter model requires iterations in each time increment, while no iteration is needed in the proposed element.

In order to study the influence of the dimensionless parameters and also to compare the developed VBI element by the model proposed by Yang and Wu (2001), a railway bridge model reported by Foutch et al (1997) is used. The bridge is an open deck plate girder railway bridge with a simply-supported span of 15.24 m. The cross sectional area

is 0.12684 m^2 and mass per unit length is 1428.64 kg/m. The moment of inertia is calculated as 0.05411 m^4 based on the drawings available in the report. In addition, other required bridge properties are assumed which are Young's modulus E=200 GPa, damping ratio 2%, and Poisson's ratio 0.3. The same sprung mass vehicle model is used in this section similar to the one applied in Section 4.5.1.

To compare the new VBI element with Majka and Hartnett (2008) model, the same bridge and vehicle models applied by these researchers are used. The bridge model is a single steel span of 31.5 m. The second moment of inertia is 0.1859 m^4, cross-sectional area is 0.2262 m^2, material density is 7850 kg/m^3, total mass of the bridge is calculated as 55933.6 kg., damping ratio is 1.30%, and Young modulus is 205 GPa. The bridge fundamental frequency is calculated as 7.33 Hz. The vehicle model is the sprung mass model (Fig. 3.11) with the vehicle properties based on the Manchester Benchmark ''Vehicle 1'' train model, reported by Iwnicki (1999). The body mass of the vehicle is 22240 kg with zero mass in the wheel. Stiffness is 7.31×10^6 N/m, and damping is 11.43×10^3 Ns/m. The vehicle natural frequency is obtained as 2.89 Hz.

To carry out the analysis, the dynamic amplification factor (DAF), defined as the ratio of the mid-span dynamic displacement to the static one, is calculated as the most important parameter in the bridge response. In addition to DAF, two other responses are evaluated in this study, namely maximum bridge mid-span acceleration and vehicle vertical acceleration. The bridge acceleration is important in the design of bridges especially ballasted railway bridges, while vehicle acceleration is a design criterion in the design of high speed trains governing the passenger comfort. Results are presented in subsequent sub-sections. Each figure illustrates the effect of each parameter on the bridge

or vehicle response and also shows a comparison of the new proposed element with the models proposed by Yang and Wu (2001) or Majka and Hartnett (2008).

5.2.2 Effect of Bridge and Vehicle Damping

The effect of the bridge damping is shown in Figs. 5.1 to 5.6, and for the vehicle damping, results are presented in Figs. 5.7 to 5.12. The effect of the vehicle damping on the bridge responses is minor, i.e. bridge acceleration and DAF, while the effect of bridge damping is much more, in particular for the bridge acceleration. However, the effect of the vehicle damping is more influential on the vehicle response compared to the bridge damping (Figs. 5.6 and 5.12). Results for DAF are decreasing in several speed regions as shown in Figs. 5.1 and 5.7. The most prominent of which is within the speed range of 75 to 100 m/s. This reduction in DAF is due to the *cancelation* effect of the vehicle and bridge on each other which reduces the magnitude of the oscillation. The reduction could be to the extent that DAF becomes less than one for vehicle speed of 100 m/s as shown in Figs. 5.1 and 5.7.

The comparison between the new proposed element and Yang and Wu (2001) element indicates that the new model results in smaller values of DAF for both bridge and vehicle damping. This effect is more evident for vehicle vertical acceleration. In addition, the general trend shows the growing effect of the proposed element for higher speeds. On the other hand, more results are obtained for proposed element compared with the Yang and Wu (2001) element regarding the vehicle or bridge acceleration.

Results of DAF and vehicle vertical acceleration obtained by the new VBI element show a close match with those obtained by Majka and Hartnett (2008) model for both

vehicle and bridge damping (see Figs. 5.2, 5.6, 5.8, 5.12). However, higher discrepancy is observed for mid-span acceleration which is a sensitive response to the bridge damping as shown in Fig. 5.4.

5.2.3 Effect of Frequency Parameter, γ

The effect of the ratio of the natural frequency of the vehicle over the bridge natural frequency (i.e. parameter γ) is shown in Figs. 5.13 to 5.18. In order to incorporate changes in the frequency parameter, only the stiffness of the moving sprung mass was varied such that the targeted γ was obtained. The results indicate substantial effects in all bridge and vehicle responses. In particular, γ has larger effect on DAF and vehicle acceleration compared to the bridge acceleration, even for lower speed ranges.

The results shown in Figs. 5.13, 5.15, and 5.17, calculated based on proposed and also Yang and Wu (2001) elements, specify that the difference widens while vehicle speed increases. This may be attributed to the fact that the proposed element incorporates more realistically the effect of dynamic parameters such as vehicle velocity which have more effect in higher speeds. However, the two models provide very close results for vehicle vertical acceleration. In contrast to the bridge or vehicle damping, the new proposed element results in greater responses for DAF and smaller values for bridge and vehicle acceleration due to changing frequency parameter.

Figs. 5.14 and 5.18 show a close match between results obtained by Majka and Hartnett (2008) model and the new VBI element for DAF and vehicle vertical acceleration. However, the bridge acceleration is overestimated by Majka and Hartnett

(2008) model for large speed parameters, while it is underestimated for low speed parameters as shown in Fig. 5.16.

5.2.4 The Effect of System Mass Parameter, κ

The last parameter studied is the system mass ratio κ, which is the ratio of the vehicle mass over the bridge mass. It has a significant effect on all bridge and vehicle responses as shown in Figs. 5.19 to 5.21. It is interesting to note that, for speed parameters less than 0.2, the rate of vehicle acceleration is substantially increased when κ is increased and the effect is less for higher speed parameters. The maximum vehicle vertical acceleration is obtained for S=0.2 regardless of the value of κ associated, as shown in Fig. 5.21. The results obtained for the bridge acceleration are as expected, and they are ascending with almost the same rate like κ as demonstrated in Fig. 5.20. In addition, DAF is significantly affected with variation in κ. Fig. 5.19 shows that for speed parameters less than 0.25, DAF is larger for higher values of κ. However, this trend is reversed for higher values of speed parameters. The speed parameter 0.25 corresponds to the vehicle speed of 115 m/s (415 km/hr) for the bridge model assumed which is the speed of the railway traffic (conventional trains or high-speed trains). Therefore, one can conclude that DAF increases with higher values of κ in the railway traffic.

Comparing the bridge and vehicle responses obtained from the new VBI element and Majka and Hartnett (2008) model shown in Figs. 5.19 to 5.21, a trend similar to other dimensionless parameters is observed. Results for vehicle vertical acceleration and DAF are very close, while there are noticeable discrepancies for the bridge acceleration. The reason is attributed to the iterative nature of the Majka and Hartnett (2008) model where

the convergence criterion is written for bridge displacements only. Such criterion will ensure acceptable results for bridge mid-span deflection, but not necessarily for bridge acceleration which experiences oscillations with high frequency.

5.2.5 Effect of a New Parameter Called Vehicle Mass Parameter, η

A new parameter, called vehicle mass parameter, is proposed for the study of the model variables. This parameter, denoted as η, is defined as the wheel mass m_w to the vehicle body mass m_{vb}

$$\eta = \frac{m_w}{m_{vb}} \tag{5.1}$$

Since the wheel mass is constant for a particular vehicle, the upper and lower bound of this parameter is due to the maximum loaded vehicle or an empty one, respectively. However, fully loaded vehicles are usually used for the bridge design yet there are different η values for various vehicles (e.g. cars, trucks, and trains) which affect the discrepancy of the bridge dynamic response with respect to the static analysis. In contrast to the bridge design, the fully loaded passenger cars may not result in maximum design criteria for the passenger comfort which is evaluated by the vehicle acceleration. Partially loaded trains have higher η values, since the mass of the car body is less whilst the wheel mass is the same as for the fully loaded train.

To study the effect of this parameter on the dynamic response, the same bridge and vehicle model used in Section 4.5.1. is utilized here as well. Figs. 5.22 to 5.24 show the sensitivity of the response for various values of this parameter and also verify the different responses obtained from proposed modified VBI element and Yang and Wu

(2001) element. Similar to the bridge and vehicle damping ratio, smaller results for DAF are obtained from the proposed element compared to Yang and Wu (2001) element and greater responses for vehicle and bridge acceleration.

The differences between two models associated with higher values of η are significant for DAF in high-speed vehicles. Accordingly, Fig. 5.22 demonstrates that the effect of the wheel mass is overestimated in the Yang and Wu (2001) element which can result in great DAF values for η=0.5 in high-speed vehicles. All responses of the bridge and vehicle shown in Figs. 5.22 to 5.24 tend to increase when η is augmented. Figs. 5.23 and 5.24 imply that the greater acceleration in both bridge and vehicle is obtained for vehicles with less weight having higher η values. Therefore, using fully loaded vehicles does not necessarily result in upper bound responses for bridge and vehicle acceleration particularly for high-speed vehicles.

5.3 EFFECT OF THE NEW VBI ELEMENT FOR VEHICLES EXPERIENCING ACCELERATION OR DECELERATION

In order to demonstrate the capability, versatility, and significance of the new VBI element, three examples are studied. First model is a vehicle with a symmetrical geometry, and the second one is a truck model with an asymmetrical geometry. In the second model, the effect of tires is also studied. The third model is a train model based on the properties of a high-speed train. Effect of the new element and also some other important parameters are investigated for a number of important bridge and vehicle responses.

5.3.1 A Symmetrical Vehicle Model

As a sample of symmetrical vehicle, the rigid beam model used by Yang and Wu (2001) is used here. Vehicle and bridge properties are based on the model given in Section 3.4.2. Vehicle matrices are given in Appendix B. Results obtained by the new VBI element are compared with those calculated by Yang and Wu (2001) to demonstrate the significance of the VBI element. In addition, the effect of the new VBI element on some important bridge and vehicle responses is studied.

(a) Vehicle Responses and Discussions

The proposed VBI element can predict the fluctuation in the vertical contact forces caused by the rotary or pitching moment. This moment is the result from horizontal vehicle acceleration or deceleration as explained in Chapter 3. Results of vertical contact forces for front and rear wheels are shown in Figs. 5.25 and 5.26. The forces are normalized with respect to static vertical contact forces. As expected, at the beginning of braking, the contact force of the front wheel increases and the rear wheel decreases due to the rotary moment. After this, the vehicle experience the oscillations exerted by the rotary moment resulting in a pitching movement and changes in vertical contact forces. Comparison between results obtained from the two models demonstrates significant differences of contact forces. For instance, by looking at the front wheel of the vehicle with the initial speed of 100 m/s and the initial deceleration of -20 m/s^2 , one can conclude that the new model results in 42% increase, while Yang and Wu (2001) model shows only 10% increase. This huge difference implies that the effect of rotary moments can be considerable and should be included in the analysis.

Considering the alterations in the vertical contact forces, the horizontal acceleration can vary due to Equation 7 where the total mass is constant. One of the assumptions in the proposed model is that the friction coefficient is constant, or even if it is changing, the variation scheme is known prior to the analysis. However, as shown in Figs. 5.25 and 5.26, the vertical contact forces are fluctuating considerably which can introduce alterations in the horizontal acceleration. As the friction coefficients are constant for this vehicle model, fluctuations in horizontal vehicle acceleration is found as follows. Considering Equation 7; Figs. 5.25 and 5.26 are multiplied by the corresponding friction coefficient and added to each other. Then, the summation figure is divided by the total mass of the vehicle. Fig. 5.27 shows the concluded figure demonstrating the alteration in vehicle horizontal deceleration resulting from variation in vertical contact forces. The figure is in the normalized form in which the horizontal deceleration was divided by corresponding $\mu \cdot g$ value, where μ is the friction coefficient and g is the ground acceleration. The vehicle deceleration for the Yang and Wu (2001) model is constant which is the line of normal deceleration equal to 1 in Fig. 5.27.

Fig. 5.27 demonstrates that in addition to the vehicle horizontal deceleration, the vehicle initial speed is also very important. The vehicle experiences up to 10.5% increase in the horizontal vehicle deceleration for the extreme case of vehicle speed and deceleration. However, for another case of 50 m/s and -10 m/s^2 the increase is only up to 3.5%. It also can be concluded that the variation in horizontal deceleration is much less than vertical contact forces comparing the percentage of increases. Less changes in horizontal deceleration, which also corresponds linearly with total vertical contact forces

(considering Eq. 3.25), can be attributed to the fact that while one wheel is experiencing higher contact forces the other one is doing somewhat reverse.

To explain these differences, one can simulate the vertical contact forces of this simple symmetric vehicle with three components. As shown in Fig. 5.28, these three components are (A) two equal static forces F_1, (B) equal but reverse couple F_2 resulting from the vehicle pitching moments and also rotary moments caused by horizontal acceleration, and finally, (C) components of two equal forces F_3 corresponding to the vehicle vertical solid bouncing with no pitching. All the previous forces in each component category are equal due to the symmetry in the vehicle model.

Consider only components (A), assuming that there are no pitching and bouncing effects (e.g. two small moving mass models on a very stiff and even surface). If this model experiences braking, there would be no changes in the total contact forces of $2F_1$, hence the horizontal acceleration will remain constant. Now, consider components (A) and (B) together. This corresponds to the vehicle model moving on a very stiff and even surface. If this vehicle experiences horizontal acceleration, only one rotary moment will be present and no solid vertical bouncing will appear. Since the forces in the components (B) are the same but in the reverse direction, the total contact forces in this case is also constant and it is $2F_1$; therefore, the horizontal acceleration remains constant, as well. Finally, consider all components together which corresponds to the vehicle model moving on a bridge or a non-stiff or uneven surface. In this case due to vertical movement of wheels, the car body will also bounce vertically producing vertical acceleration in the car body. Since these two forces are in the same direction, the total

contact force in this case is $2F_1+2F_3$ which is different from $2F_1$ and will result in alteration in the horizontal acceleration.

Regarding the free body diagrams of vehicle shown in Fig 3.3, consider only those equilibrium equations due to vertical bouncing of the vehicle (Eq. 3.19b and Eq. 3.20b) rewritten as follows:

$$\Delta V_1 + SP_{w1} - m_{w1}\ddot{r}_3 = 0\,;\ \Delta V_2 + SP_{w2} - m_{w2}\ddot{r}_4 = 0\,, \tag{5.2a}$$

$$SP_{w1} + SP_{w2} + m_c\ddot{r}_1 = 0 \tag{5.2b}$$

where ΔV_i are due to changes in the vertical contact forces caused by vertical vehicle bouncing. Omitting suspension forces SP_w, the following total contact force ΔV of the vehicle bouncing is obtained

$$\Delta V = \Delta V_1 + \Delta V_2 = m_{w1}\ddot{r}_3 + m_{w2}\ddot{r}_4 + m_c\ddot{r}_1 \tag{5.3}$$

Since wheel masses are neglected in this model and they are set to zero, ΔV will only be equal to $m_c\ddot{r}_1$. This implies that, for this particular example, the variation of the total vertical contact forces are linearly related to vehicle vertical acceleration; consequently, the vehicle horizontal acceleration is linearly related to vehicle vertical acceleration. This can be concluded from comparison of Fig. 5.27 with those results of vehicle acceleration for the new model presented in Fig. 5.29.

(b) Bridge Responses

Midspan deflection for various vehicle speeds and accelerations is shown in Fig. 5.30. That value is a key response in the calculation of the dynamic amplification factor in bridge design manuals. Using the new VBI element, the midspan deflection rapidly increases due to higher values of the front wheel contact forces. Differences of the new

VBI element and Yang and Wu (2001) model can reach up to 40% for vehicle initial velocity of 100 m/s and initial deceleration of -20 m/s^2. Since these forces are much higher compared to contact forces calculated by Yang and Wu (2001) model, the first peak of the midspan deflection caused by the front wheel force is quickly augmented as shown in Fig. 5.30.

Another important parameter is the midspan acceleration which is essential in the design of nonstructural components installed on the bridge or for the design of the ballast of the ballasted railway bridges. As shown in Fig 5.31, the effect of vehicle velocity is much higher than vehicle horizontal deceleration. However, the effect of the vehicle horizontal deceleration can not be neglected.

Horizontal reaction in the hinge support is also an important response affecting the design of the horizontal restraint of the hinge connection. As shown in Fig. 5.32, in contrast to the differences between results obtained from the new VBI element and the one presented by Yang and Wu (2001), the peak values are almost the same for the two models.

5.3.2 An Unsymmetrical Truck Model

(a) Bridge and truck models

The model discussed in the previous section was symmetric. In this section, an unsymmetrical model of a 3-axle truck is studied considering the effect of tires. To study the response resulting from new VBI element and also the effect of tire in the response, a sample bridge was traversed by a truck model. The Vehicle-Bridge Interaction (VBI) analysis was performed numerically and analyzed for various vehicle velocity and

deceleration conditions. The bridge model is a highway plate girder bridge initially used by Hwang and Nowak (1991) for the development of AASHTO LRFD (1994). Properties of the bridge are: Length=12 m, mass per unit length= 552 kg/m, and equivalent stiffness EI= 4.20×10^6 kN-m^2. Assuming E=200 GPa for steel, corresponding moment of inertia is obtained as 0.021 m^4. Cross sectional area is not given and it is assumed that the bridge consists of plate girders with the total cross sectional area of 0.07 m^2. In addition, Poisson's ratio ν was set to 0.3.

The truck model utilized is similar to the model shown in Fig. 3.2 for the model excluding tire and Fig 3.5 is for the model including tire. Although the truck includes three axles, two axles are beside each other and considered as one axle in the truck model used by Hwang and Nowak (1991). Properties of these models are presented in Table 5.1. Values are used directly from a report by Nowak (1999) or calculated according to that report.

The developed computer program in MATLAB was used to model the bridge and vehicle and also to perform the step-by-step time history numerical analysis. Results are obtained for vehicle initial speed of 50 m/s due to a truck with high speed and two friction coefficients of 0.1 and 0.7 as low and high friction conditions to have somewhat two extreme cases for better comparison. The latter can happen for emergency braking of new tires (Alvarez et al., 2005). Another value for friction coefficient that was previously considered is 0.85 for new tires of trucks having ABS (Anti-lock Braking System), (Shurtz et al., 2006).

(b) Discussion on bridge and vehicle responses

Results of vehicle vertical deceleration for speed vehicles of 50 m/s and friction coefficient μ = 0.1 and 0.7 are presented in Fig. 5.33 and 5.34.

Two types of vehicle models are included; one excluding the effect of tires and the other one including tires. The results are compared with those obtained using Yang and Wu (2001) model. As expected, tires make the ride smoother and reduce the oscillations of the vehicle which brings more riding comfort. This can be seen clearly in Figs. 5.33 and 5.34 comparing results of 'no tire' with those for 'with tire'. Considering the response obtained from the new VBI element, the vertical acceleration increases rapidly while braking forces increases comparing Fig. 5.33 with Fig. 5.34. However, results obtained by Yang and Wu (2001) model are almost the same for two deceleration levels; since the effect of the vehicle horizontal deceleration was only considered at the contact point not on the vehicle itself. Hence, the vehicle responses and vertical contact forces will not change for various vehicle horizontal decelerations. This can be seen in Appendix A, Section A.4.

Considering the vehicle horizontal deceleration shown in Fig. 5.35, it could be seen that there is no clear relationship between vehicle vertical acceleration and vehicle horizontal deceleration as explained in previous section for the vehicle without tires. The reason is associated with the effect of wheel vertical acceleration. Eq. 5.3 is also valid for this model. Since wheel masses are not zero for the truck model used in here, they will contribute in the total vertical contact forces due to Eq. 5.3. Although tires smoothen the ride, they increase the total vertical contact forces which will lead to almost 15% increase in horizontal deceleration for μ = 0.7 and 7% increase for μ = 0.1.

The bridge response is also affected by the vehicle horizontal deceleration. The comparison between Figs. 5.36 and 5.37 acknowledges that the bridge midspan deflection increases for higher braking situations. Similar to the rigid beam model, the increase is due to higher vertical contact forces of the front wheel.

In contrast to the midspan deflection, the midspan acceleration is not affected by the vehicle horizontal deceleration. This can be seen for the results of both truck models comparing Fig. 5.38 with Fig. 5.39. However, discrepancies between results obtained by the new VBI element and those by Yang and Wu (2001) model increases while increasing vehicle horizontal deceleration.

5.3.3 A Sample Train Model

In order to study the influence of the vehicle braking on the response of bridges and trains, a railway bridge model is used reported by Foutch et al (1997) whose properties are given in Section 5.2.1. The train model used by Wu et al. (2001) which is a high-speed train of SKS series 300 model is used as the vehicle model. The train model is similar to the model shown in Fig. 3.9 and associated properties are tabulated in Table 5.2. Required vehicle matrices for numerical analysis are given in Appendix B.

(a) Contact forces

The vertical contact forces for all wheels are shown in Figs. 5.40 and 5.41 for vehicle initial speed of 50 and 100 m/s. Considering the vehicle model of Fig. 3.9, the wheels are numbered from right to left, where the first one at right is the first wheel and the last one at the very left is the fourth wheel. These designations are used in Figs. 5.40 and 5.41.

The friction coefficient of μ = 0.1 and 0.7 are used here representing low and high braking situations. The value of 0.7 for friction coefficient is extremely high and it is the highest value that was reported by Olofsson and Telliskivi (2003). They concluded that, the friction coefficient varies between 0.5 and 0.6 for pure non-lubricated sliding tests which can reach 0.7 in some cases. If the rail is lubricated, the friction coefficient reduced to values between 0.2 to 0.4.

As shown in Figs. 5.40 and 5.41, the results obtained by Yang and Wu (2001) model are not able to track the fluctuation in the vertical contact force. This is due to the fact that they used the contact force formulation of the vehicle with constant velocity for the case of vehicles with acceleration, which is not capable of modeling the pitching moment caused by the vehicle horizontal acceleration or deceleration. Significant variations in the contact forces are observed for all vehicle speeds in Figs. 5.40 and 5.41. The maximum contact force in each case is affected slightly by the vehicle velocity and it is more a function of friction coefficient or severity of the braking. The first wheel and the second wheel are under bogie #1 and the other two wheels are under bogies #2. Due to the pitching moment on the bogie #1, the first wheel experiences growth in the contact force and the other wheel is vice versa. Similar behaviour is observed for the third and the forth wheel under the bogie #2.

(b) Midspan deflection

The midspan deflection is shown in Fig. 5.42 for vehicle initial speed of 50 m/s. Results for all cases are very close. It is usually expected to have a direct relationship between the exerted forces on the bridge and the amount of resulting deflection.

However, the current example contradicts that clear fact at the first glance. As shown in Figs. 5.40 and 5.41, significant fluctuations in contact forces are observed for all wheels with no exception, but midspan deflections for all cases are only slightly different. The reason is attributed to the spacing of the forces and how they are applying on the bridge. The spacing between the first wheel and the second wheel is 2.5 m and they are under the bogie #1 (see Fig. 3.9). Therefore compared to the bridge length which is 15.24 m, first and second wheels are relatively close to each other. Although the contact force in the first wheel is growing, it is decreasing in the second wheel. Hence, the resultant force, which is a summation of the first and the second wheels, is not fluctuating as significantly as individual wheels.

Results for the summation of the vertical contact forces for the first and last two wheels are shown in Fig. 5.43 for the vehicle initial speed of 50 m/s. For two wheels under the bogie #1 (i.e. first and second wheels) shown in Fig. 5.43 (a), the increase in contact forces is only around 7% and for the bogie #2 the decrease is around 10% shown in Fig. 5.43 (b). These slight changes are due to the pitching moment in the vehicle body itself. The car body pitching moment is resisted by the inertial effect of the vehicle body rotary inertia and two vertical spring-dampers supporting the vehicle body. Although, the amount of the pitching moment is larger compared to that for the two bogies, the rotary inertia of the car body is much higher than bogies; consequently, the pitching of the car body is much less than that for bogies shown in Fig. 5.44. In addition to the pitching, the vehicle bouncing is also important which is shown in Fig. 5.45 confirming the previous results.

(c) Vehicle horizontal deceleration

Vehicle horizontal deceleration is presented in Fig. 5.46 for three levels of vehicle speeds and three levels of friction coefficients. The deceleration is obtained using Eq. 3.25 for each friction coefficient of 0.1 and 0.7 as shown in Fig. 5.46. In addition to the friction coefficients that are constant for each analysis, the total vehicle mass M_t is also constant throughout the analysis; therefore considering Eq. 3.25, the vehicle horizontal acceleration or deceleration is a function of summation of all vertical contact forces. It is observed from Fig. 5.46 that, the vehicle horizontal deceleration is very much affected by the vehicle initial velocity not the friction coefficient. For the vehicle initial velocities of 50 and 100 m/s, the maximum change in the horizontal deceleration is almost 2% which is very low and cannot be felt by the passengers sitting on that train. However for the very high speed vehicle velocity of 200 m/s, fluctuations grow to 13% which may be felt by the passengers.

(d) Other important responses

Vehicle vertical acceleration shown in Fig. 5.47, is also an important parameter that governs the level of passenger comfort. It is not affected considerably by the various values of friction coefficients. The results for Yang and Wu (2001) model and the new VBI element are very close, implying the fact that the vehicle horizontal acceleration or deceleration has no noticeable effect on the vehicle vertical acceleration for train models.

The bridge midspan acceleration is demonstrated in Fig. 5.48 for two vehicle initial speeds of 50 m/s and 100 m/s. As clearly shown in Fig. 5.48, the midspan acceleration is very much affected by the vehicle velocity not the vehicle horizontal

deceleration. Hence, similar to the vehicle horizontal deceleration, the midspan acceleration does not depend on friction coefficients (i.e. severity of braking); however, the vehicle initial velocity plays a governing role.

Fig. 5.49 shows the hinge support reaction which is not affected noticeably by the severity of braking, and the peak values are only 5% different. The response can be divided into two parts in Fig. 5.49; the first part from zero to 18 m and the second part from 18 m to 35 m. the first part is basically the response due to the first two wheels and the second part is due to the last two wheels. Since the fluctuations of the last two wheels are more than the first two wheels shown in Fig. 5.43, the second part of Fig. 5.49 demonstrates more differences between μ=0.1 and 0.7 compared to the first part of the figure. Finally, the peak values of the hinge support reaction are 10% different in the second part of Fig. 5.49 which should be considered in the design practices.

5.4. SUMMARY

In order to investigate the effect of the new VBI element for vehicles with constant velocity compared with the VBI element proposed by Yang and Wu (2001) and Majka and Hartnett (2008) model, a study on the influence of some important parameters was carried out. Parameters available in the literature considered in this study were vehicle and the bridge damping, total vehicle mass to the bridge mass κ, and the ratio of the vehicle first mode frequency over the bridge natural frequency γ. In addition, a new parameter η was introduced in this study which is the ratio of the wheel mass to the vehicle body mass. The dynamic amplification factor, as the ratio of the mid-span displacement of the dynamic analysis to the static one, was considered as the most

important bridge response for the study on the model variables. Bridge and vehicle accelerations were also obtained from the analysis important for high-speed trains.

Results of vehicle with constant velocity obtained by the new VBI element compared with those obtained by Yang and Wu (2001) generally imply that the new VBI element results in different DAF values increasing when vehicle speed increases. For vehicle and bridge acceleration, different responses are observed for all vehicle speeds. These differences can be attributed to the effects of dynamic parameters (e.g. vehicle speed) presented in the formulation proposed for the new modified VBI element compared to that of Yang and Wu (2001) model.

Results of DAF and vehicle vertical acceleration obtained by the new VBI element show a close match with those obtained by Majka and Hartnett (2008) model. However, higher discrepancy is observed for mid-span acceleration. The reason is attributed to the iterative nature of the Majka and Hartnett (2008) model where the convergence criterion is written for bridge displacements only. Such criterion will ensure acceptable results for bridge mid-span deflection, but not necessarily for bridge acceleration which experiences oscillations with high frequency.

In addition, studying the effect of dimensionless parameters demonstrates that the greatest sensitivity is observed for the vehicle mass parameter η and κ for any vehicle speed and also for frequency parameter γ regarding high speed vehicles. Results indicate that using fully loaded vehicles having less η values will not always result in upper bound responses for bridge and vehicle acceleration, particularly for high-speed vehicles. Finally, the analyses showed that the dynamic amplification factor (DAF) is not always increasing with vehicle velocity and can be even less than one for medium speed vehicles

due to the *cancellation* effect between the vehicle and the bridge. This region of decreasing DAF can be shifted if longer bridges with different natural frequency are applied.

The effect of the new VBI element for vehicles experiencing deceleration was studied for three types of vehicle models, symmetrical and unsymmetrical vehicles, and a train model. As a sample of the first group, a vehicle model of 4-DOF called rigid beam model was used and available results in the literature were compared with those obtained from the new VBI element. Large differences were observed for vertical contact forces, vehicle vertical acceleration, and also bridge midspan deflection. However, the effect of the new VBI element to Yang and Wu (2001) model is not prominent for bridge midspan acceleration and horizontal support reactions.

As a representative for unsymmetrical vehicles, a sample truck model on a simply-supported highway bridge is studied including and excluding the effect of tires. Two friction coefficients of 0.1 and 0.7 are used representing common and extreme braking forces. Results show almost the same conclusions obtained for the symmetric model, however due to different properties of the bridge and the vehicle, the order of differences was smaller particularly for midspan deflection. Moreover, the effect of tires were considerable on both bridge and vehicle responses, and as expected, much greater on vehicle responses.

The last model that was used to investigate the effect of the new VBI element for vehicles experiencing deceleration is a train model. Vertical contact forces are greatly affected and they can be augmented 50% for an extreme braking situation. The two vertical contact forces under each bogie act reversely, meaning that, if one contact force

increases the other one will decrease because of pitching moment exerted on the bogie. Although the vertical contact forces vary significantly, the midspan deflection is affected slightly. This is because the two wheels under each bogie are relatively close and they cancel the effect of each other. The car body vertical acceleration is affected slightly by the vehicle horizontal deceleration. In addition, midspan acceleration is not very sensitive to the vehicle horizontal deceleration, but it is very sensitive to the vehicle velocity which determines vehicle driving frequency.

Table 5.1 Properties of the unsymmetrical truck model

m_c	25	ton
m_{w1}	1	ton
m_{w2}	2	ton
I_c	80	ton.m^2
k_{v1}	280	kN/m
k_{v2}	350	kN/m
$k_{t1}=k_{t2}$	880	kN/m
$c_{v1}=c_{v2}$	50	kN.s/m
$c_{t1}=c_{t2}$	1.5	kN.s/m
d_1	3.41	m
d_2	2.09	m
h_1	0.25	m
h_2	0.75	m

Table 5.2 Properties of the train model

m_c	41.75	ton
$m_{b1}=m_{b2}$	3.04	ton
$m_{w1}=m_{w2}=m_{w3}=m_{w4}$	1.78	ton
I_c	2080	ton.m^2
$I_{b1}=I_{b2}$	3.93	ton.m^2
$k_{v1}=k_{v2}$	1180	kN/m
$k_{w1}=k_{w2}=k_{w3}=k_{w4}$	530	kN/m
$c_{v1}=c_{v2}$	39.2	kN.s/m
$c_{w1}=c_{w2}=c_{w3}=c_{w4}$	90.2	kN.s/m
$l_1=l_2$	8.75	m
$d_1=d_2=d_3=d_4$	1.25	m
h_1	0.75	m
h_2	0.42	m
h_3	0.20	m
h_4	0.455	m

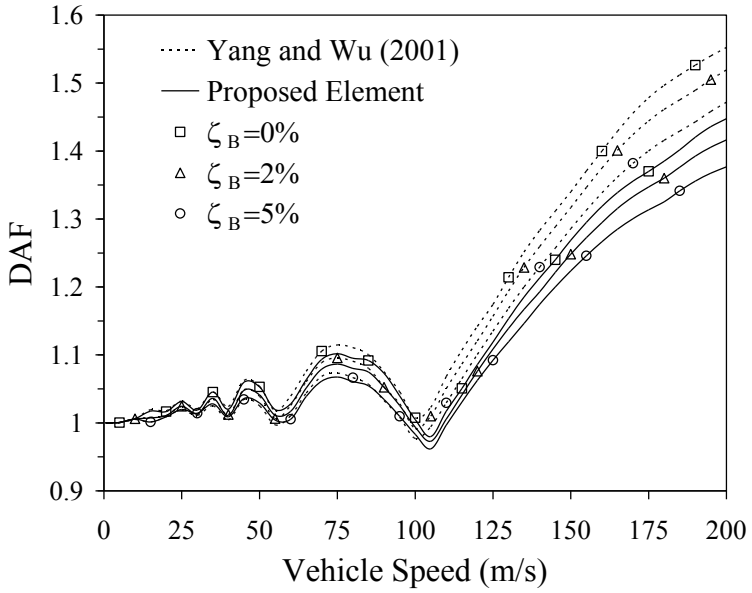

Fig. 5.1 The comparison of the effect of the bridge damping ζ_B on DAF with Yang and Wu (2001) model

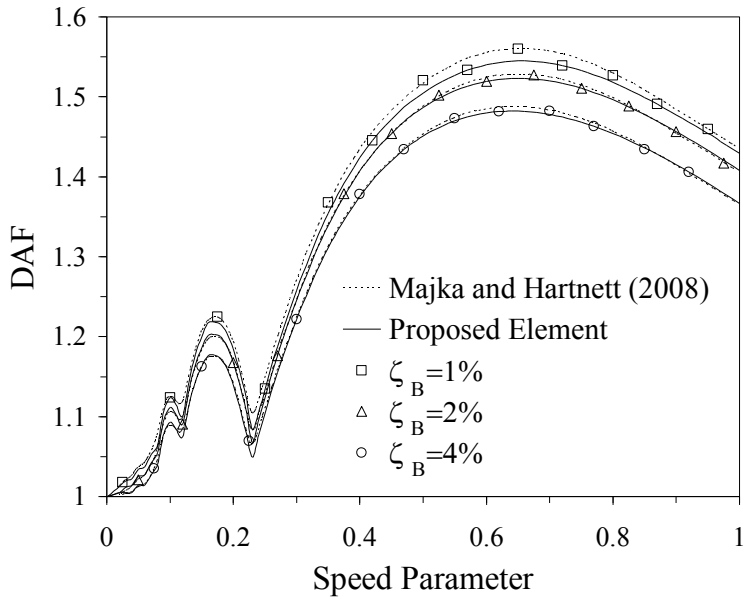

Fig. 5.2 The comparison of the effect of the bridge damping ζ_B on DAF with Majka and Hartnett (2008) model

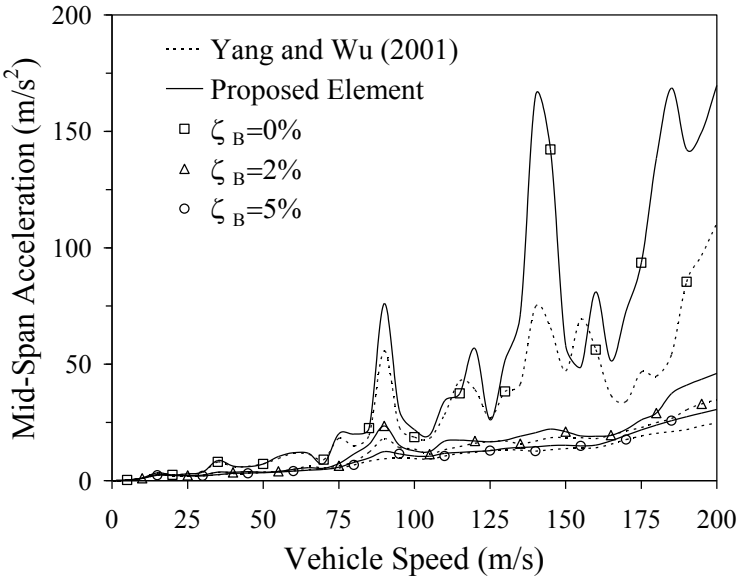

Fig. 5.3 The comparison of the effect of the bridge damping ζ_B on the bridge mid-span acceleration with Yang and Wu (2001) model

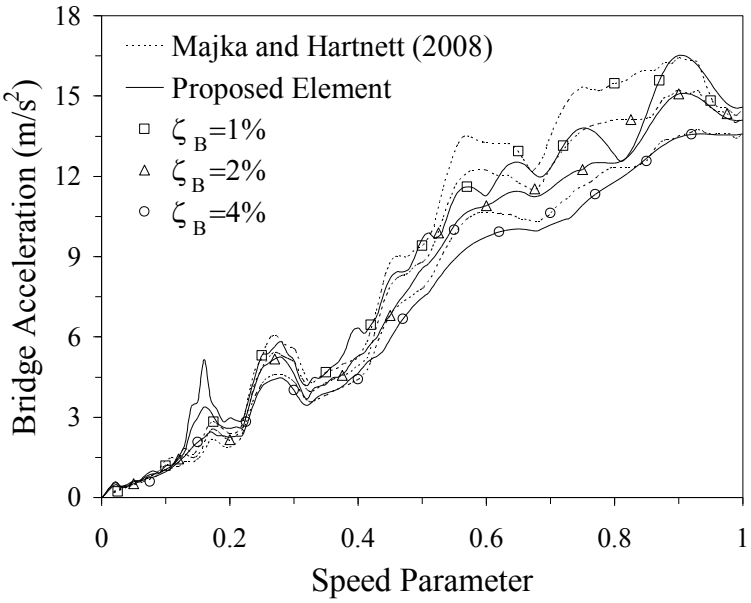

Fig. 5.4 The comparison of the effect of the bridge damping ζ_B on the bridge mid-span acceleration with Majka and Hartnett (2008) model

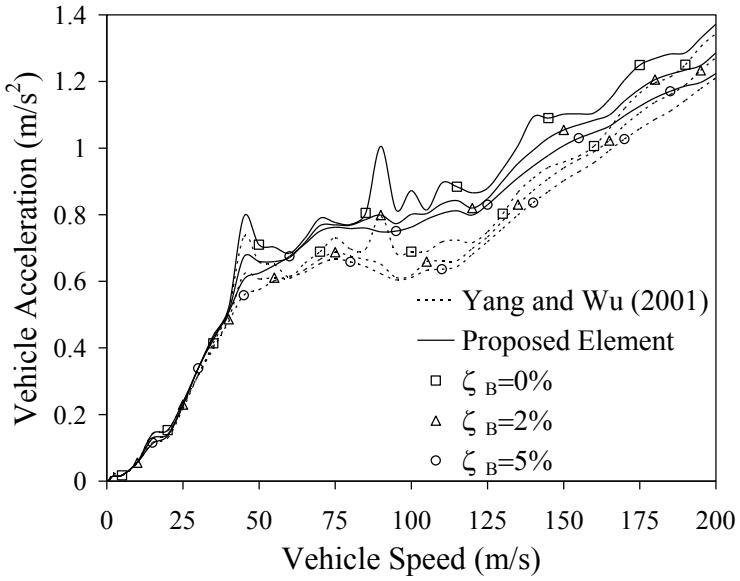

Fig. 5.5 The comparison of the effect of the bridge damping ζ_B on the vehicle vertical acceleration with Yang and Wu (2001) model

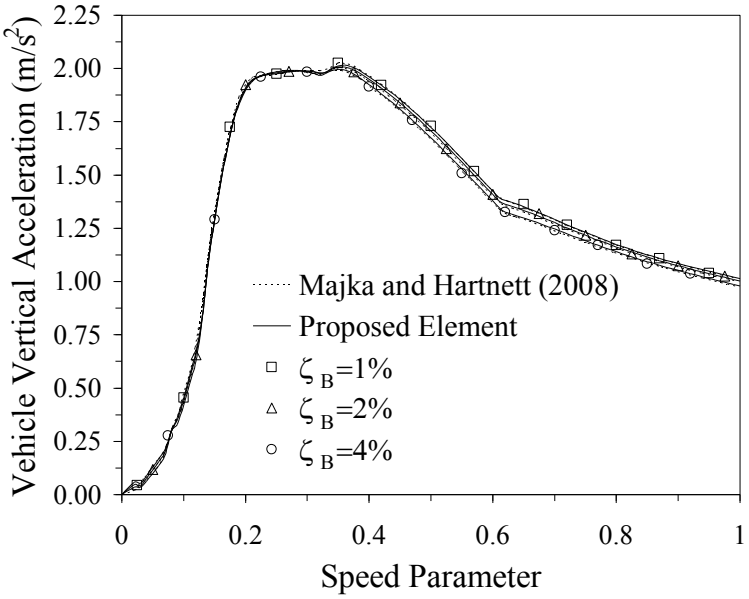

Fig. 5.6 The comparison of the effect of the bridge damping ζ_B on the vehicle vertical acceleration with Majka and Hartnett (2008) model

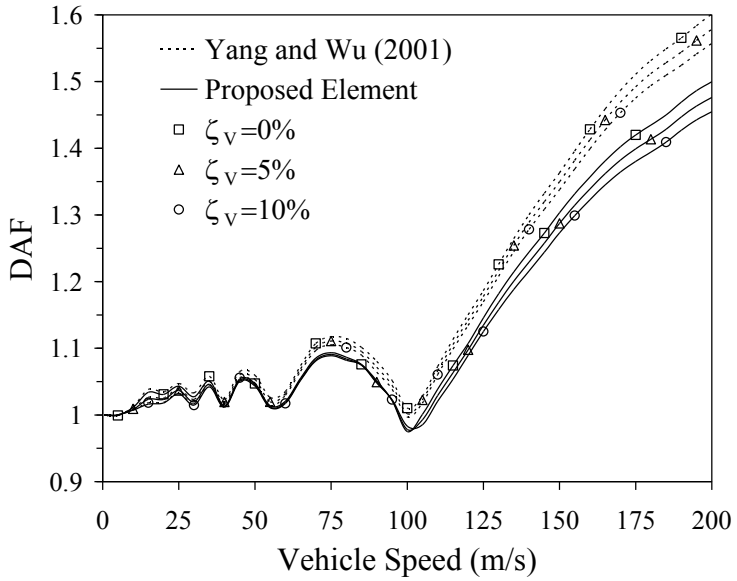

Fig. 5.7 The comparison of the effect of the vehicle damping ζ_V on DAF with Yang and Wu (2001) model

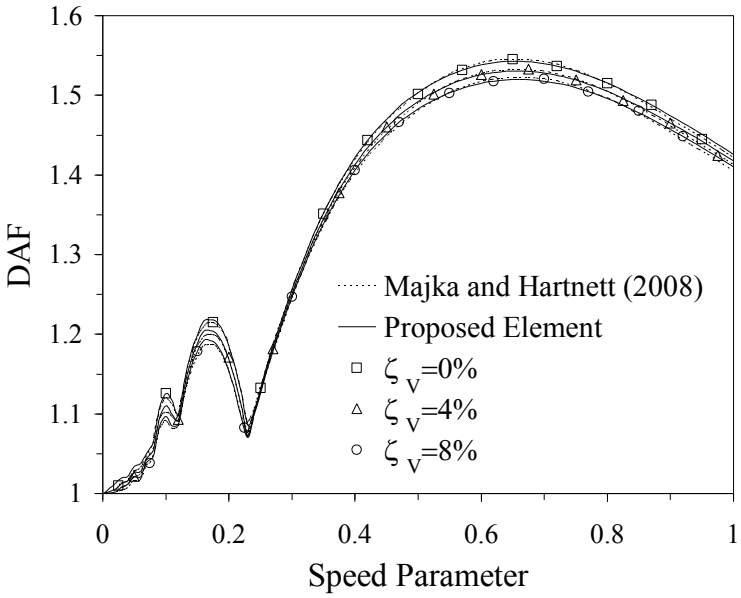

Fig. 5.8 The comparison of the effect of the vehicle damping ζ_V on DAF with Majka and Hartnett (2008) model

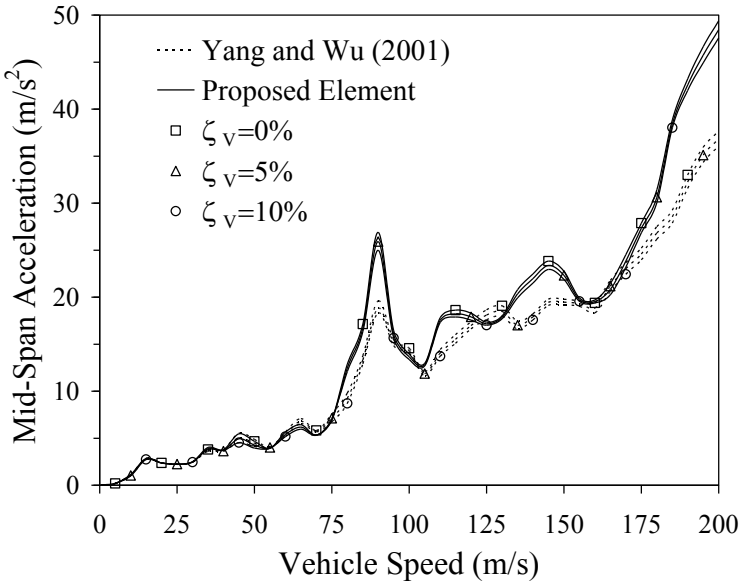

Fig. 5.9 The comparison of the effect of the vehicle damping ζ_V on the bridge mid-span acceleration with Yang and Wu (2001) model

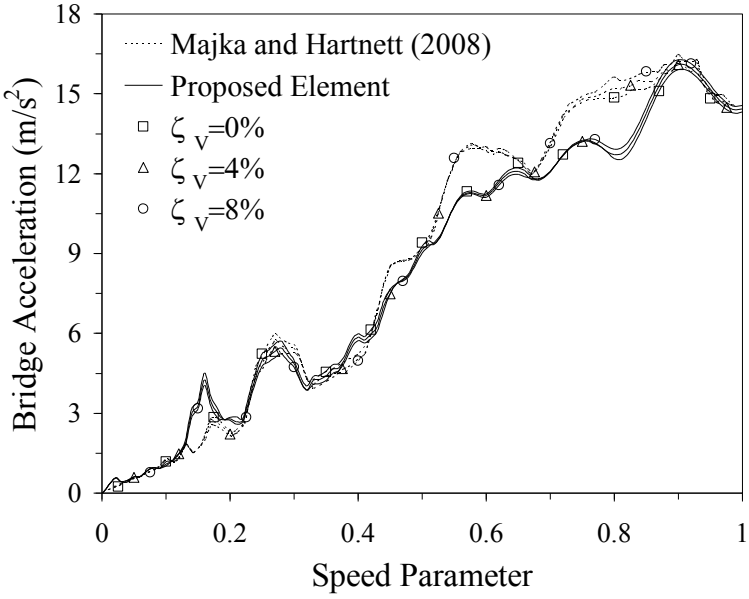

Fig. 5.10 The comparison of the effect of the vehicle damping ζ_V on the bridge mid-span acceleration with Majka and Hartnett (2008) model

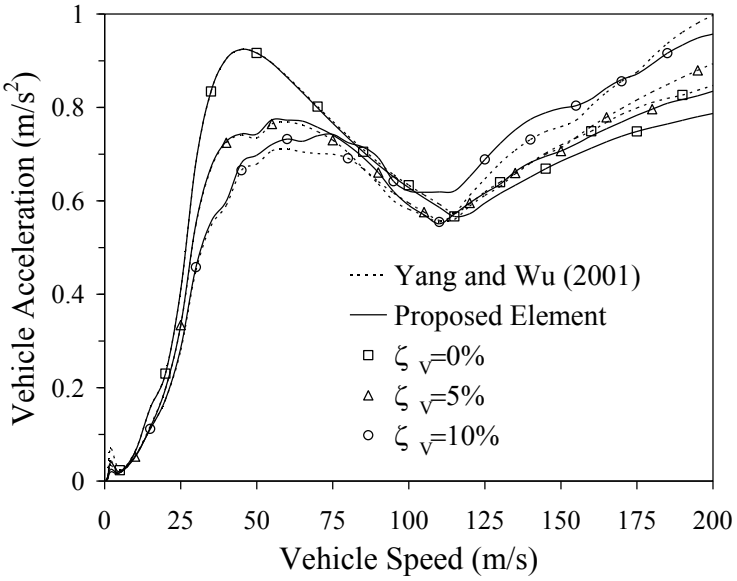

Fig. 5.11 The comparison of the effect of the vehicle damping ζ_V on the vehicle vertical acceleration with Yang and Wu (2001) model

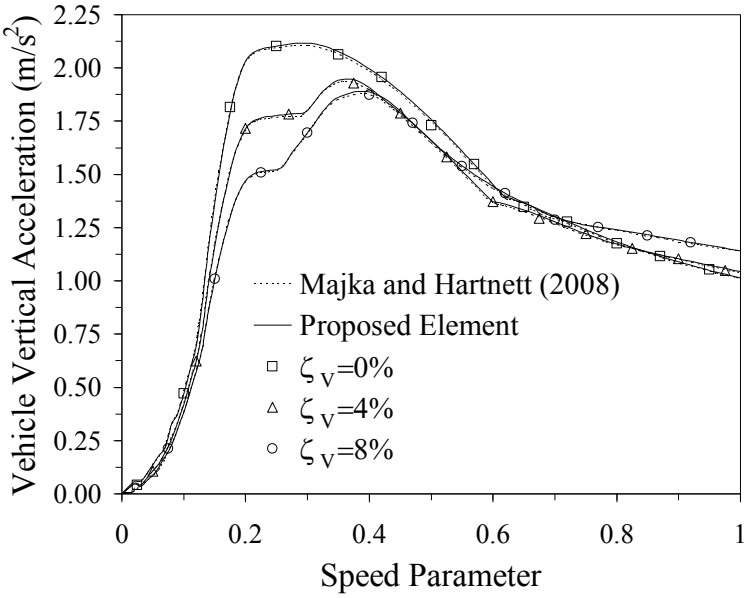

Fig. 5.12 The comparison of the effect of the vehicle damping ζ_V on the vehicle vertical acceleration with Majka and Hartnett (2008) model

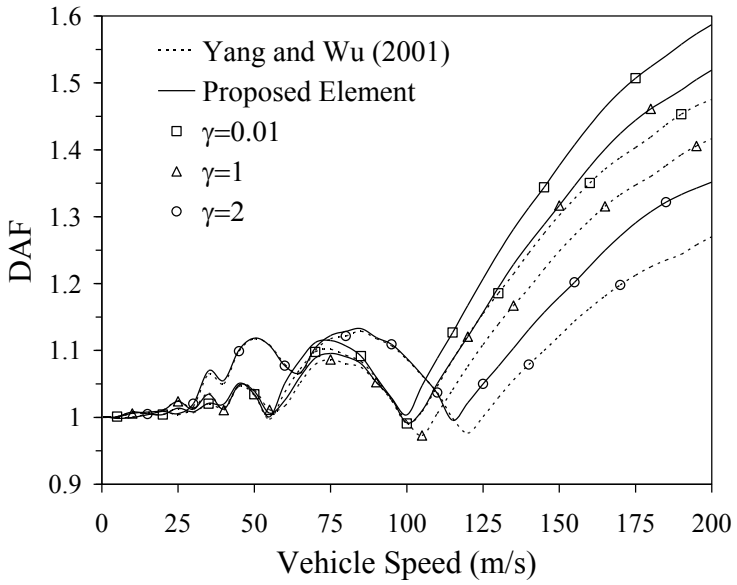

Fig. 5.13 The comparison of the effect of the frequency parameter γ on DAF with Yang and Wu (2001) model

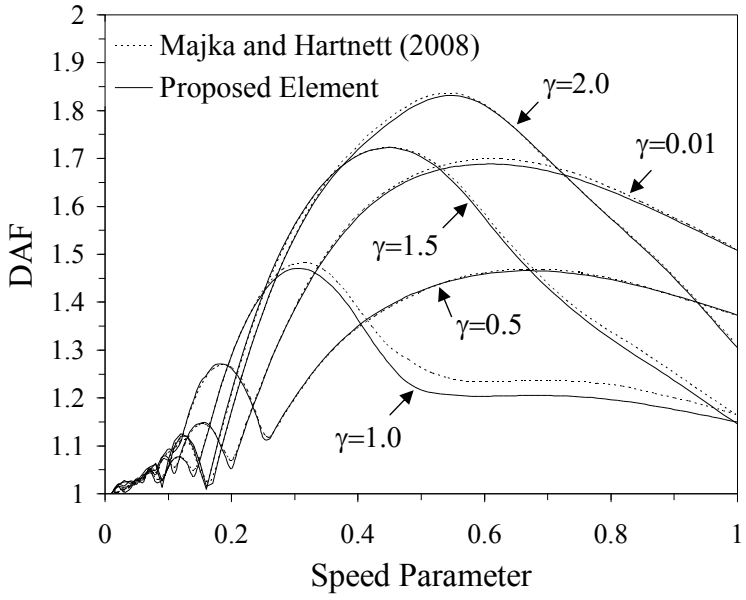

Fig. 5.14 The comparison of the effect of the frequency parameter γ on DAF with Majka and Hartnett (2008) model

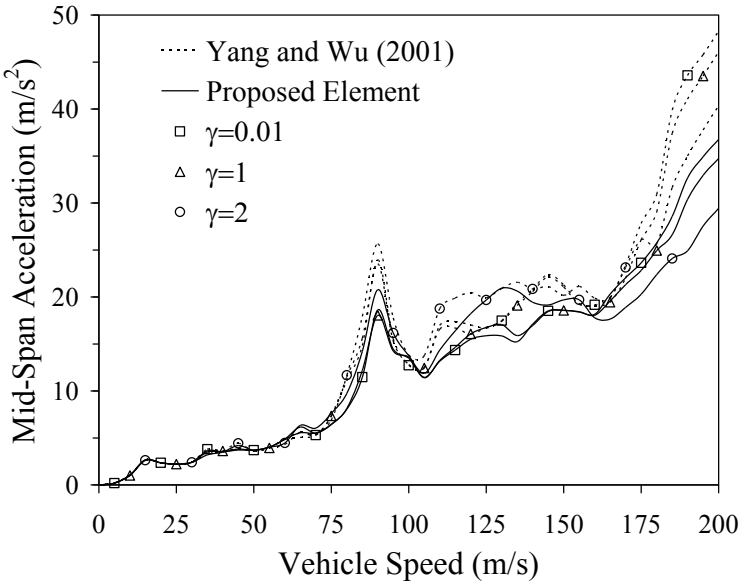

Fig. 5.15 The comparison of the effect of the frequency parameter γ on the bridge mid-span acceleration with Yang and Wu (2001) model

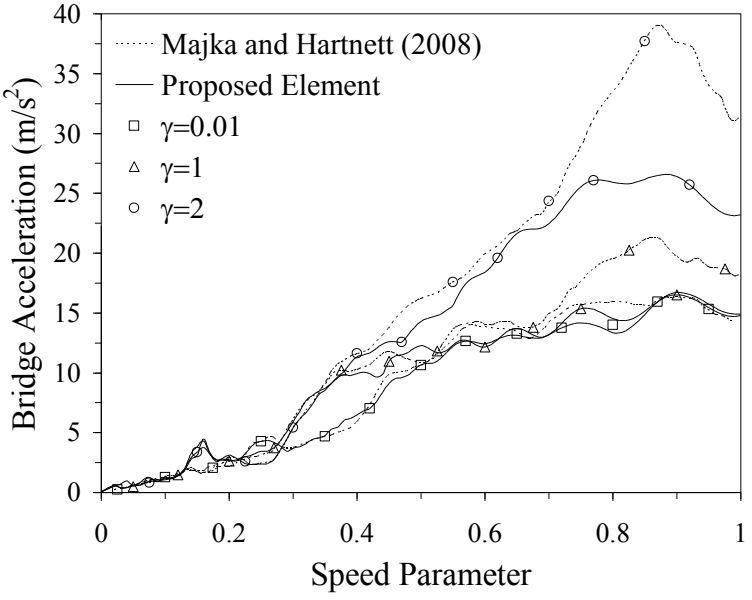

Fig. 5.16 The comparison of the effect of the frequency parameter γ on the bridge mid-span acceleration with Majka and Hartnett (2008) model

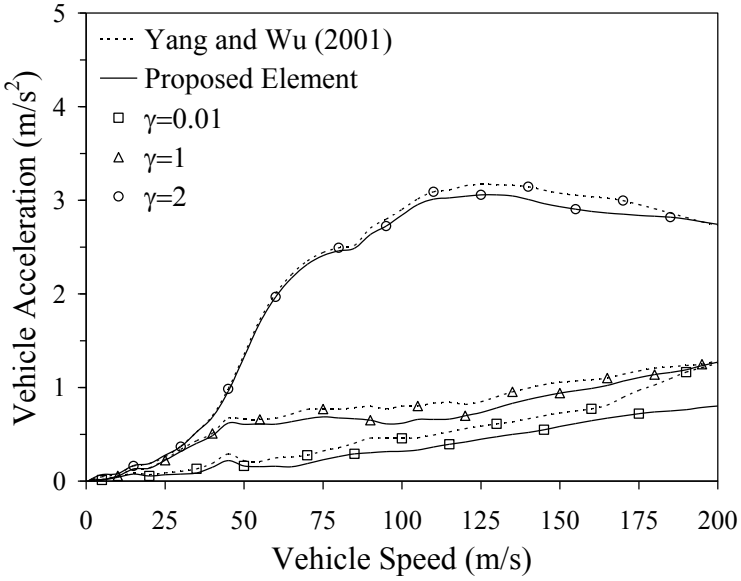

Fig. 5.17 The comparison of the effect of the frequency parameter γ on the vehicle vertical acceleration with Yang and Wu (2001) model

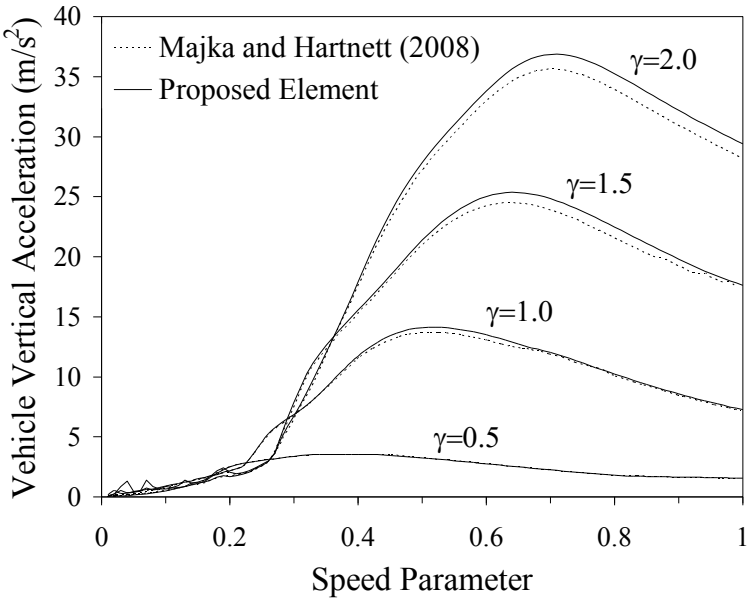

Fig. 5.18 The comparison of the effect of the frequency parameter γ on the vehicle vertical acceleration with Majka and Hartnett (2008) model

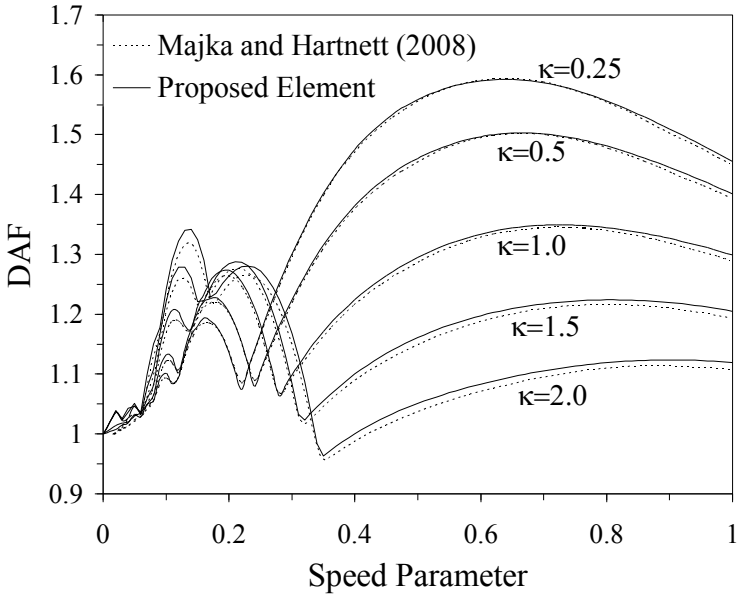

Fig. 5.19 The comparison of the effect of the system mass parameter κ on DAF with Majka and Hartnett (2008) model

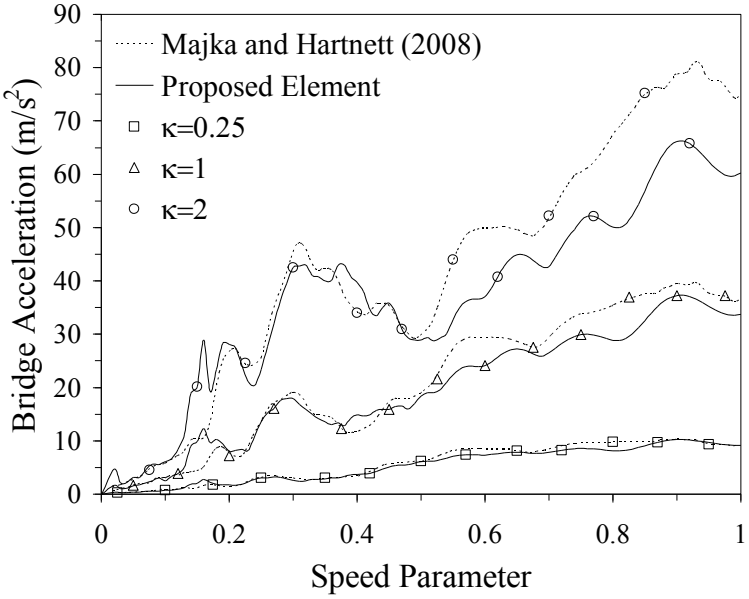

Fig. 5.20 The comparison of the effect of the system mass parameter κ on the bridge mid-span acceleration with Majka and Hartnett (2008) model

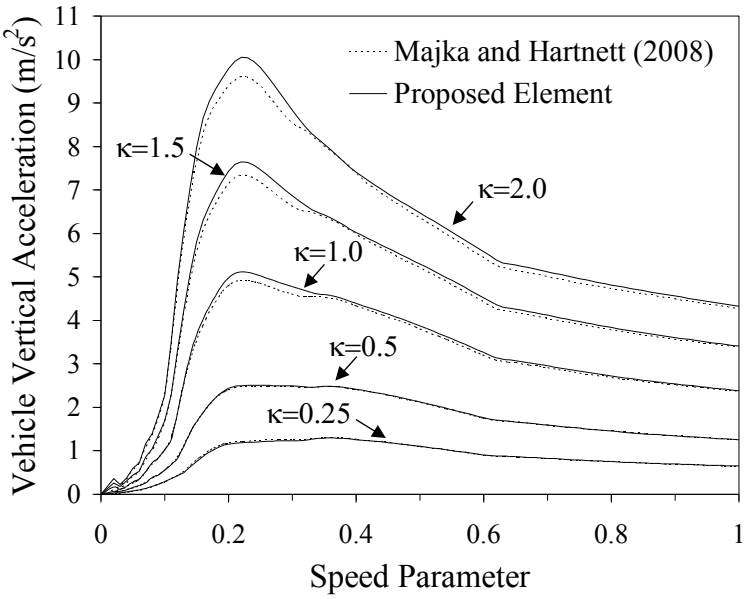

Fig. 5.21 The comparison of the effect of the system mass parameter κ on the vehicle vertical acceleration with Majka and Hartnett (2008) model

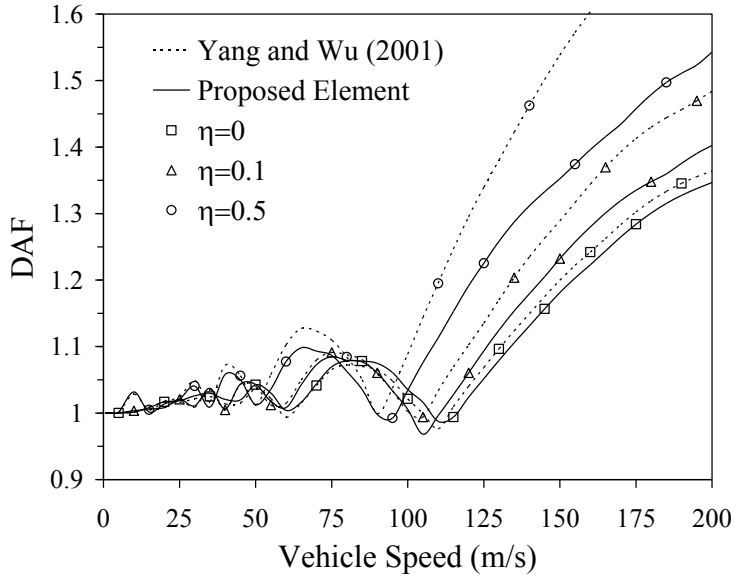

Fig. 5.22 The comparison of the effect of the vehicle mass parameter η on DAF with Yang and Wu (2001) model

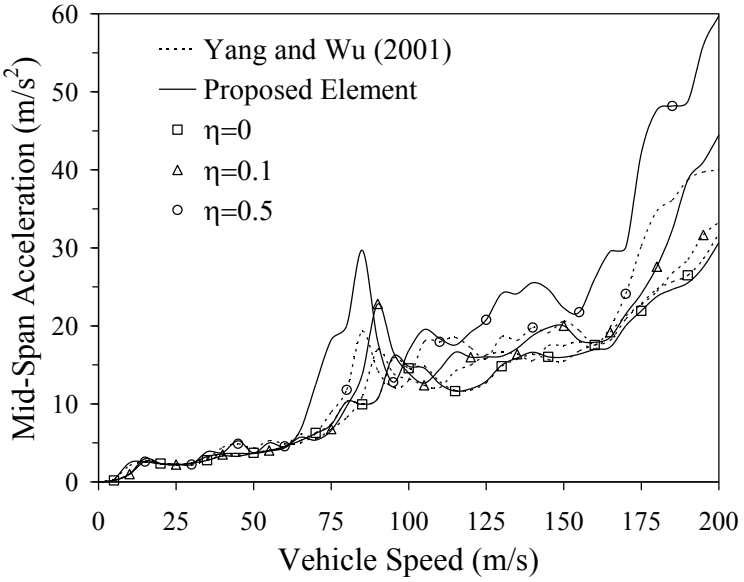

Fig. 5.23 The comparison of the effect of the vehicle mass parameter η on the bridge mid-span acceleration with Yang and Wu (2001) model

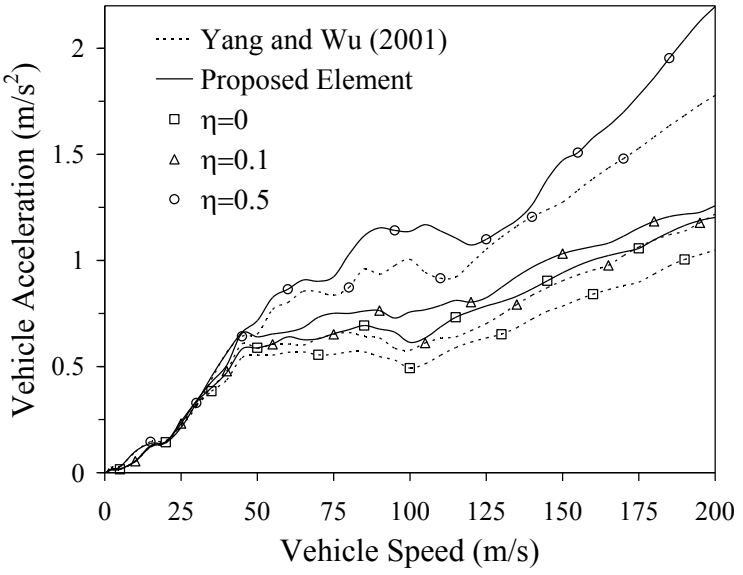

Fig. 5.24 The comparison of the effect of the vehicle mass parameter η on the vehicle vertical acceleration with Yang and Wu (2001) model

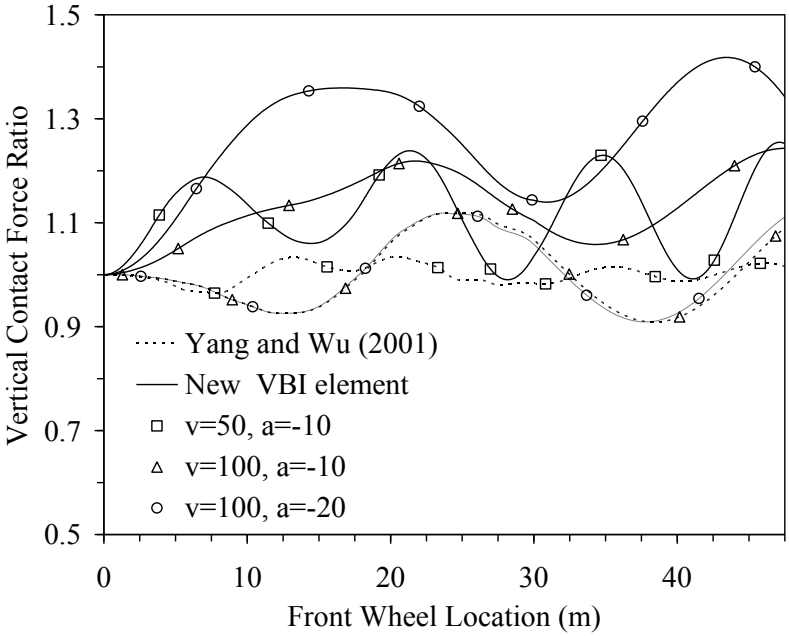

Fig. 5.25 Ratio of vertical contact forces over static contact forces in the front wheel of the rigid beam model

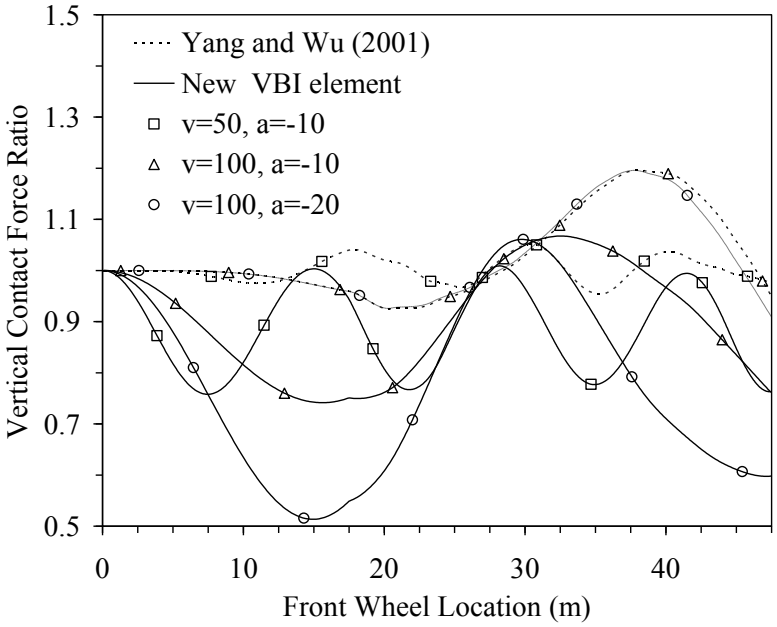

Fig. 5.26 Ratio of vertical contact forces over static contact forces in the rear wheel of the rigid beam model

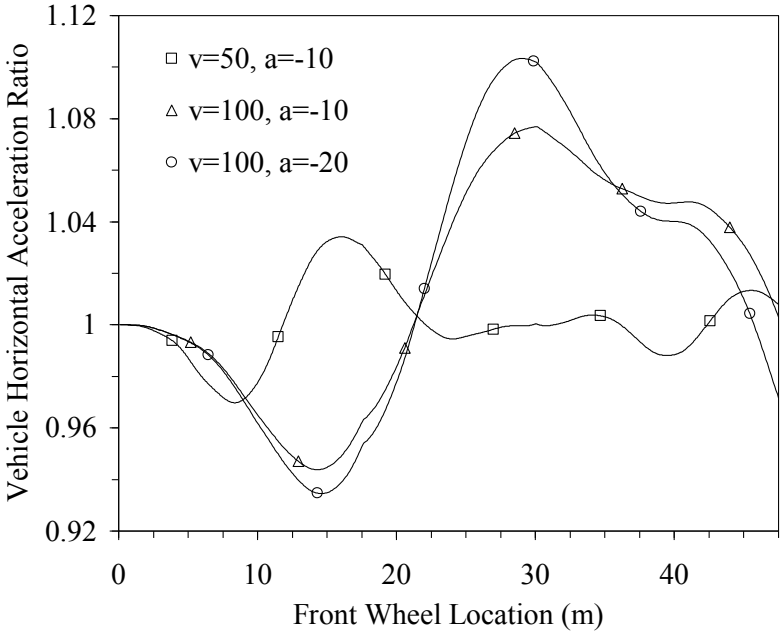

Fig. 5.27 Ratio of horizontal acceleration over initial acceleration of the rigid beam model

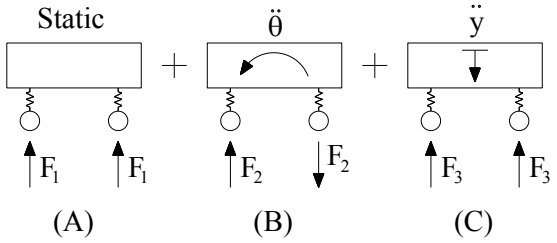

Fig. 5.28 Simplified illustration of the vehicle model dynamics

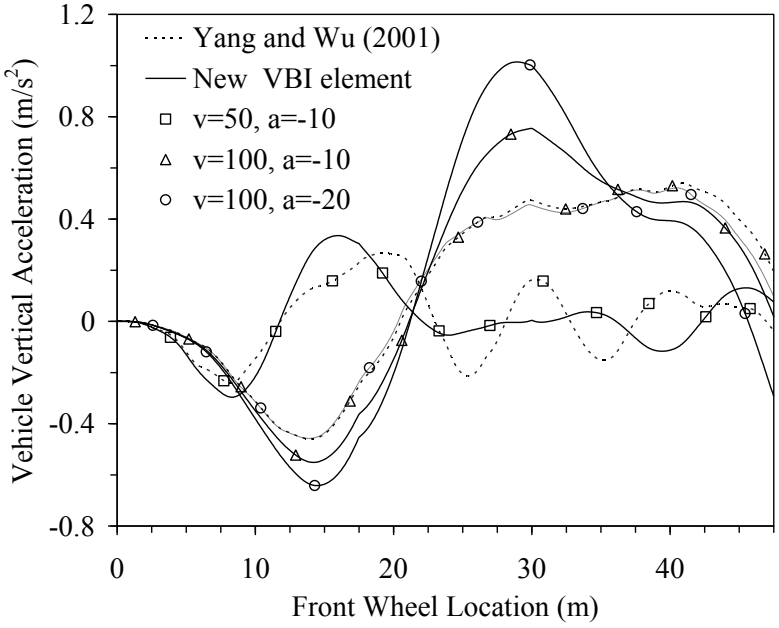

Fig. 5.29 Vehicle vertical acceleration of the rigid beam model

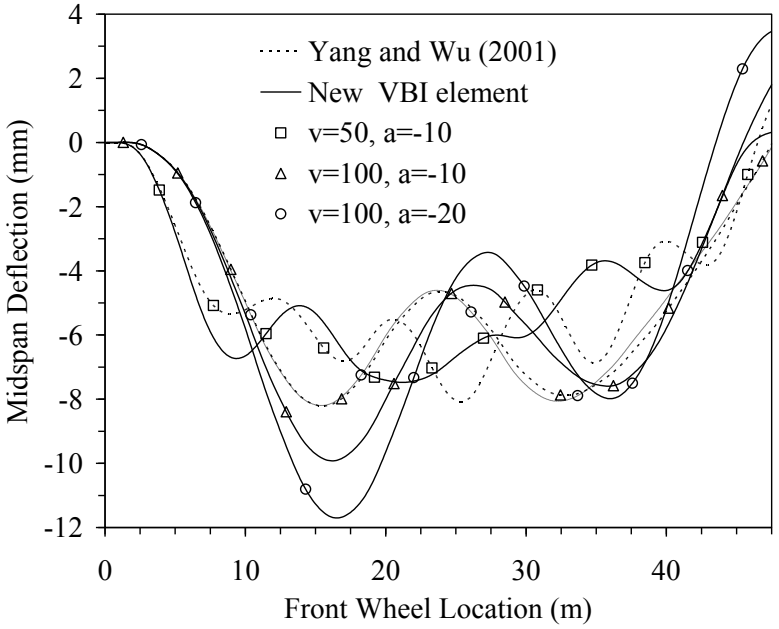

Fig. 5.30 Bridge midspan deflection of the rigid beam model

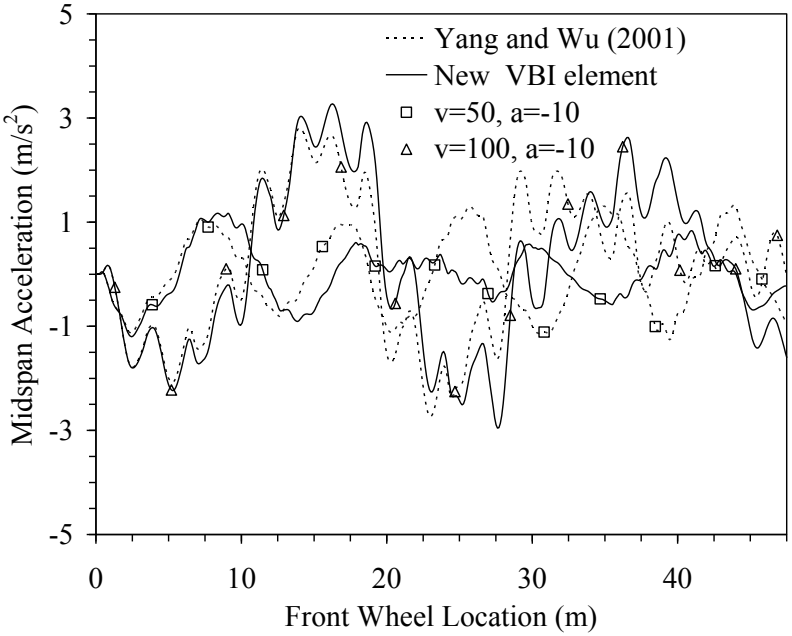

Fig. 5.31 Bridge mid-span vertical acceleration of the rigid beam model

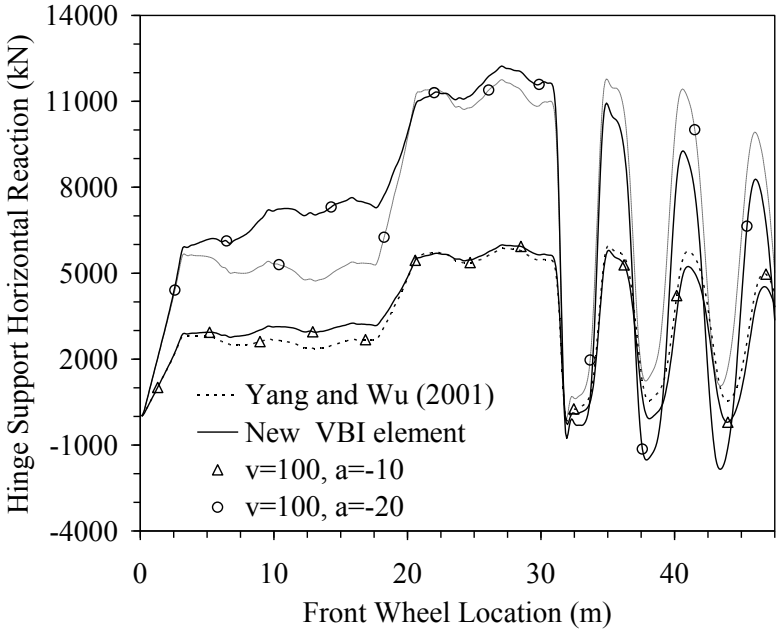

Fig. 5.32 Hinge support horizontal reaction of the rigid beam model

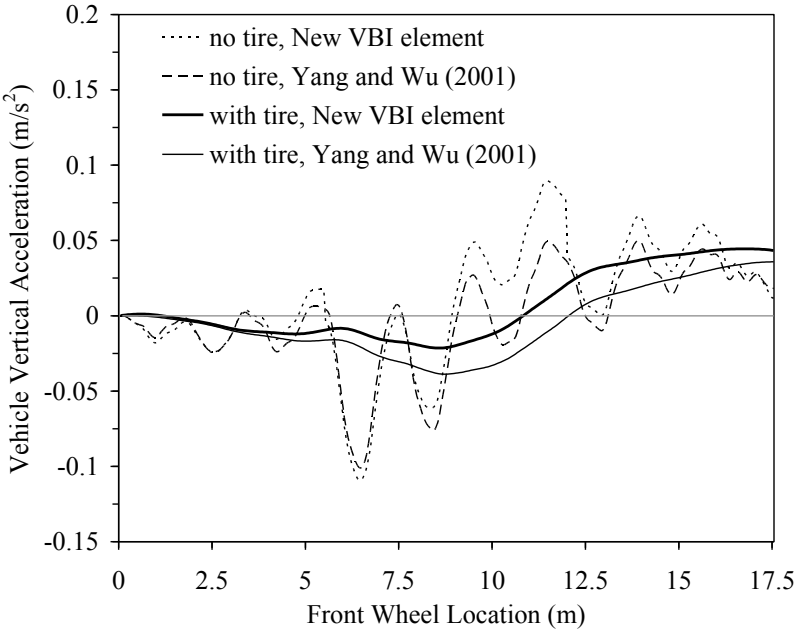

Fig. 5.33 Truck model vertical acceleration for μ=0.1

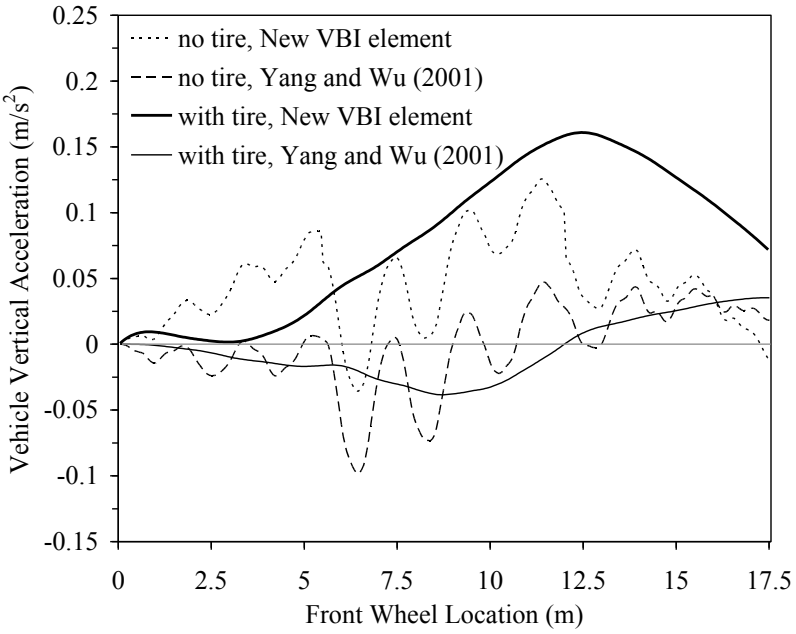

Fig. 5.34 Truck model vertical acceleration for μ=0.7

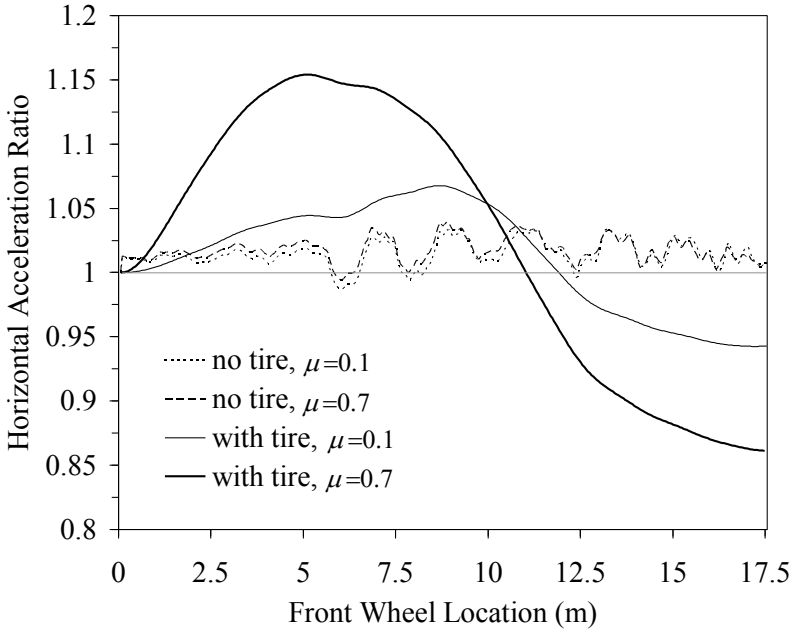

Fig. 5.35 Ratio of horizontal deceleration over initial deceleration for the truck model

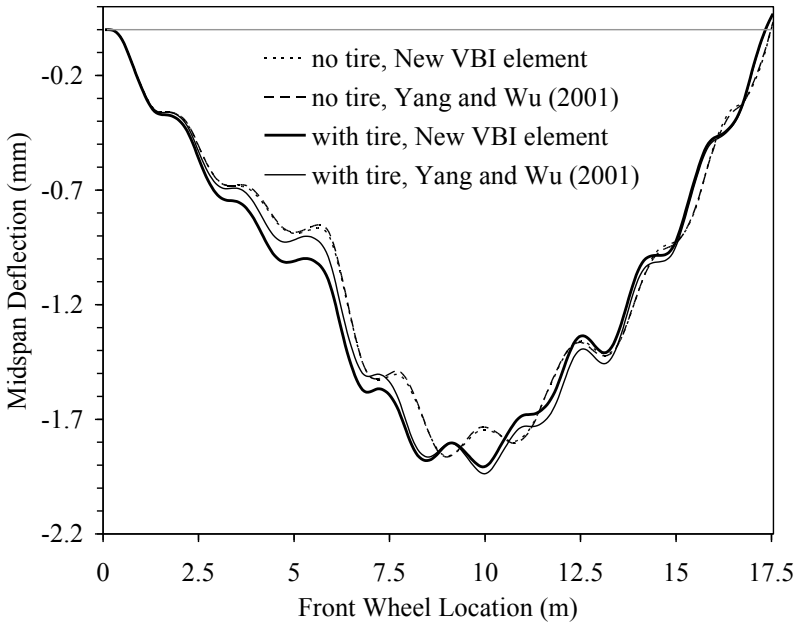

Fig. 5.36 Bridge midspan deflection of the truck model for μ=0.1

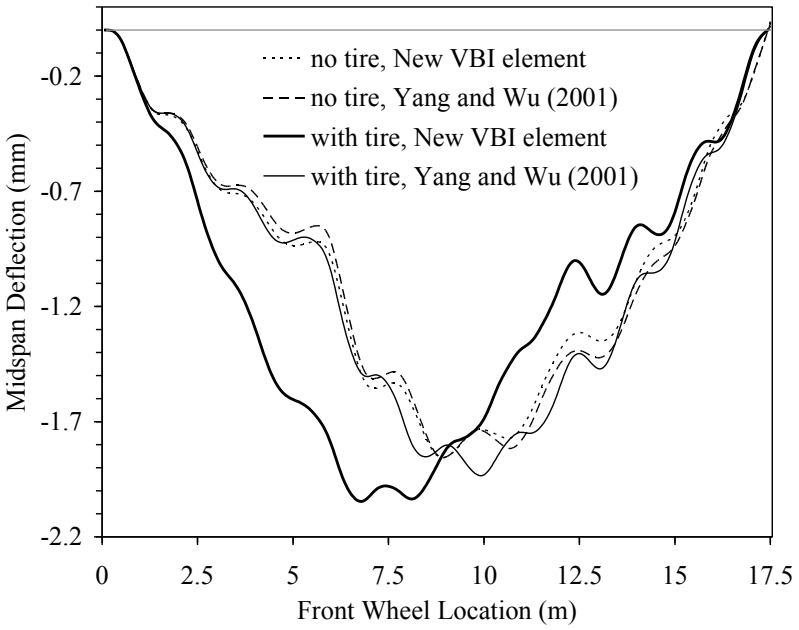

Fig. 5.37 Bridge midspan deflection of the truck model for μ=0.7

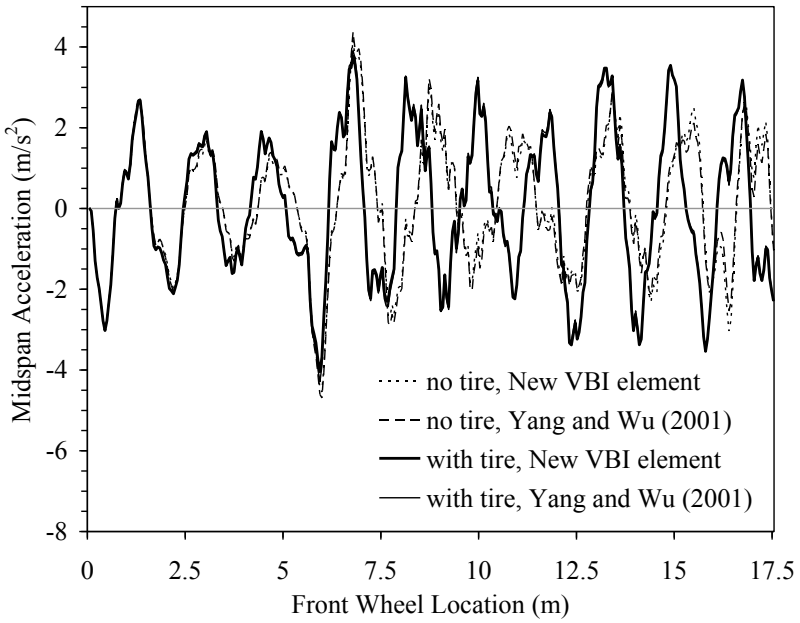

Fig. 5.38 Vehicle midspan acceleration of the truck model for μ=0.1

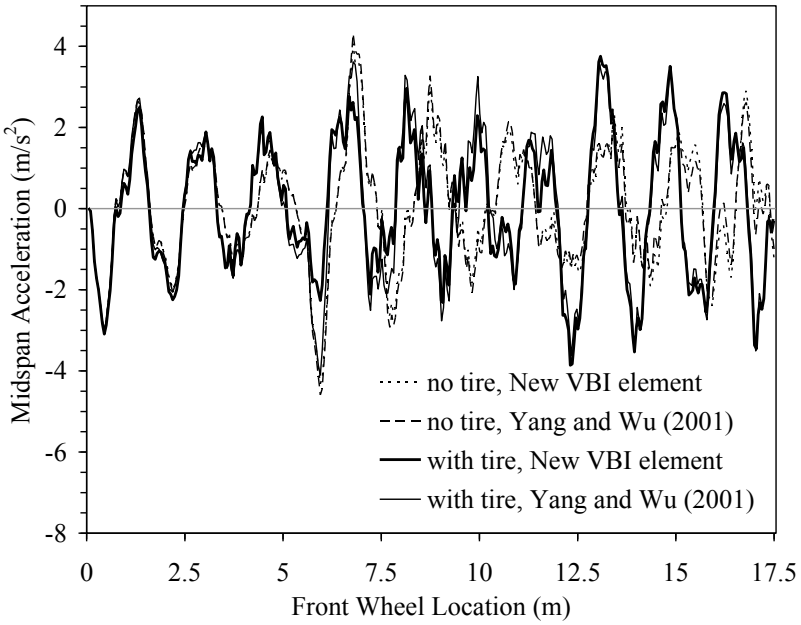

Fig. 5.39 Vehicle midspan acceleration of the truck model for μ=0.7

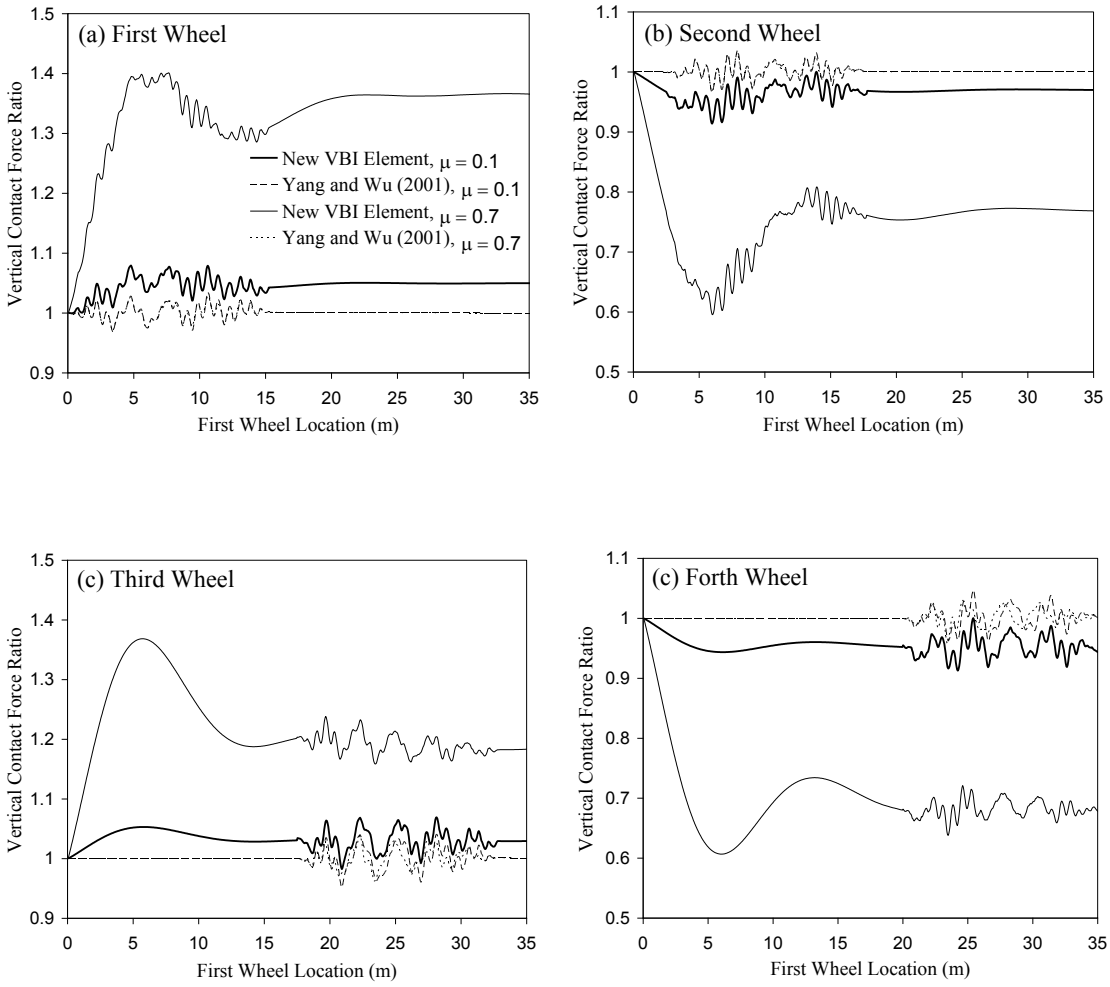

Fig. 5.40 Ratio of vertical contact forces over static contact forces of the train model, for initial vehicle speed of 50 m/s

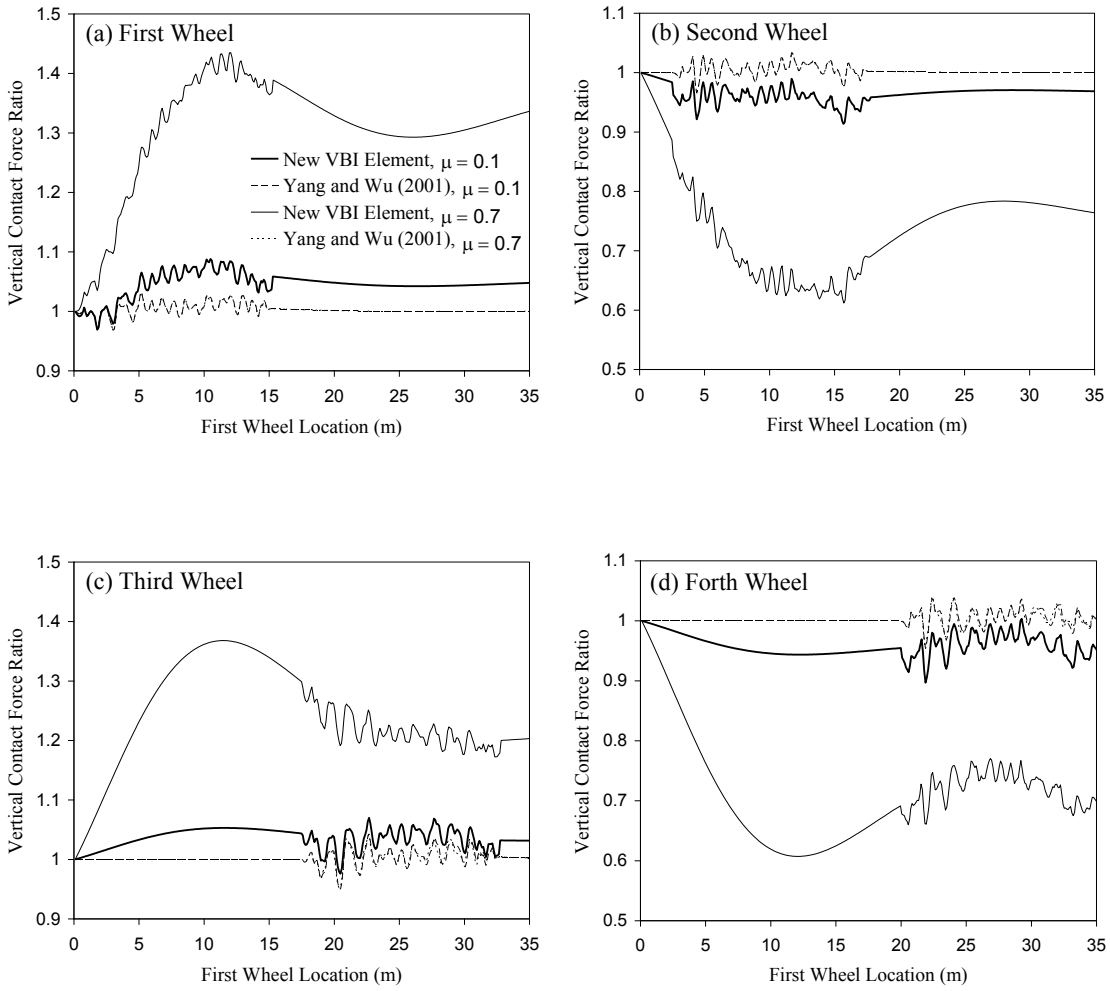

Fig. 5.41 Ratio of vertical contact forces over static contact forces of the train model, for initial vehicle speed of 100 m/s

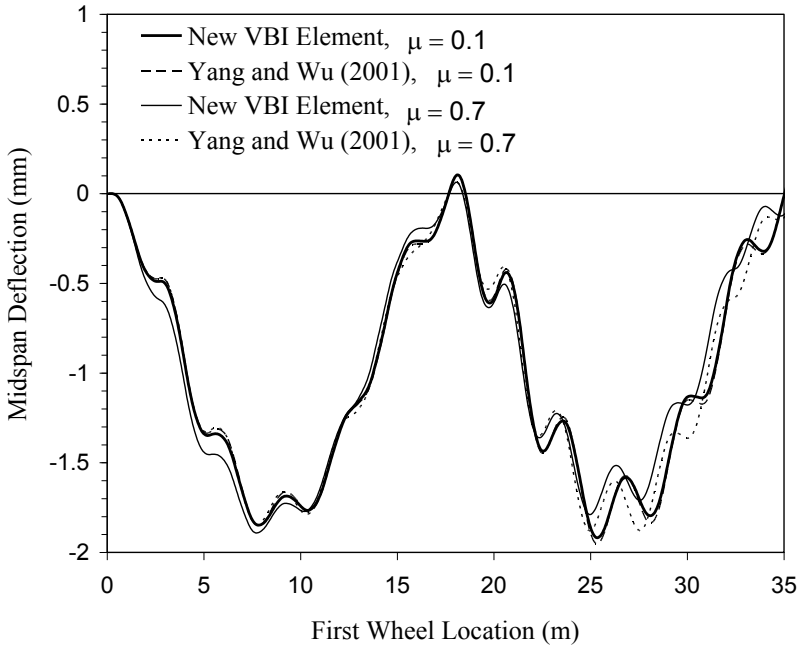

Fig. 5.42 Midspan deflection of the train model, for initial vehicle speed of 50 m/s

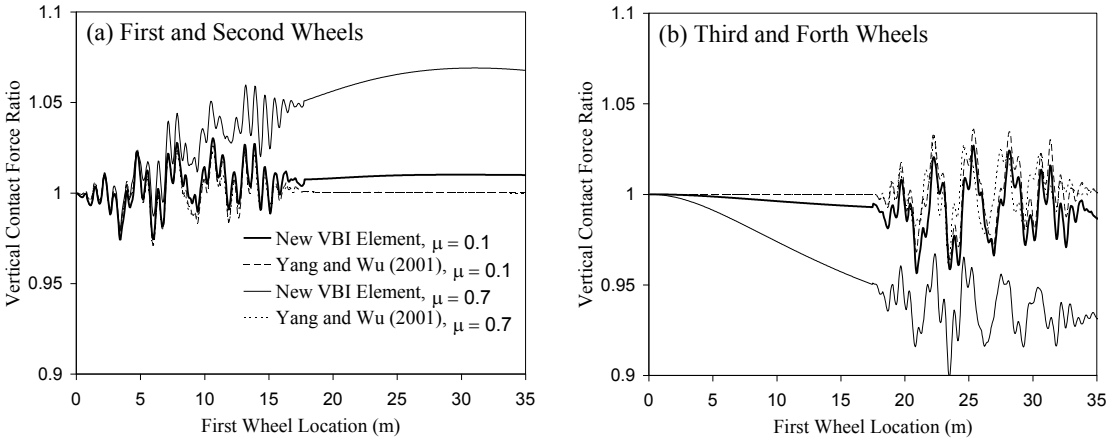

Fig. 5.43 Ratio of the summation of vertical contact forces under each bogie over corresponding total static contact forces of the train model, for initial vehicle speed of 50 m/s

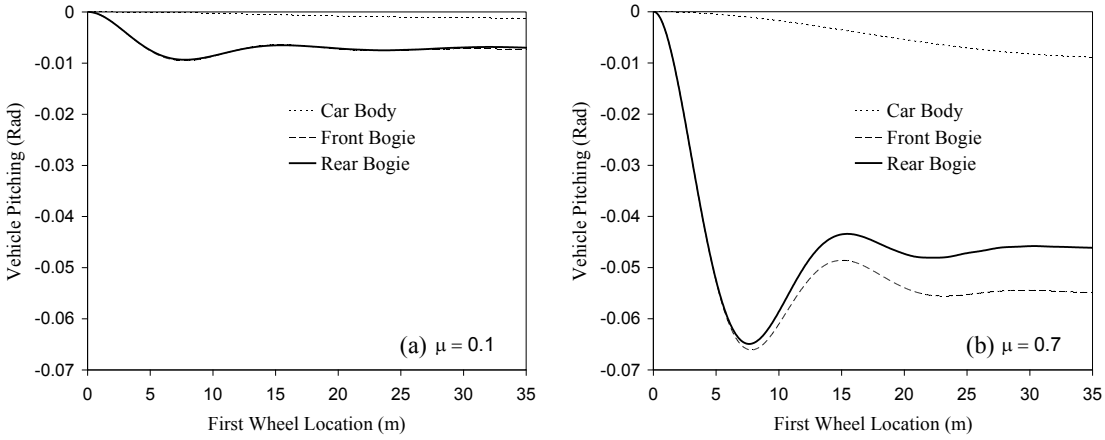

Fig. 5.44 Vehicle pitching of various parts of the train model, for initial vehicle speed of 50 m/s

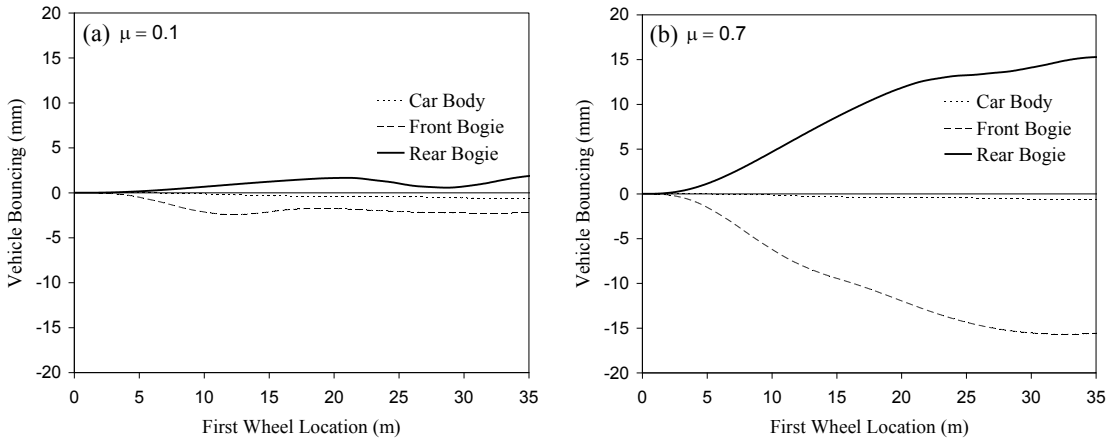

Fig. 5.45 Vehicle bouncing of various parts of the train model, for initial vehicle speed of 50 m/s

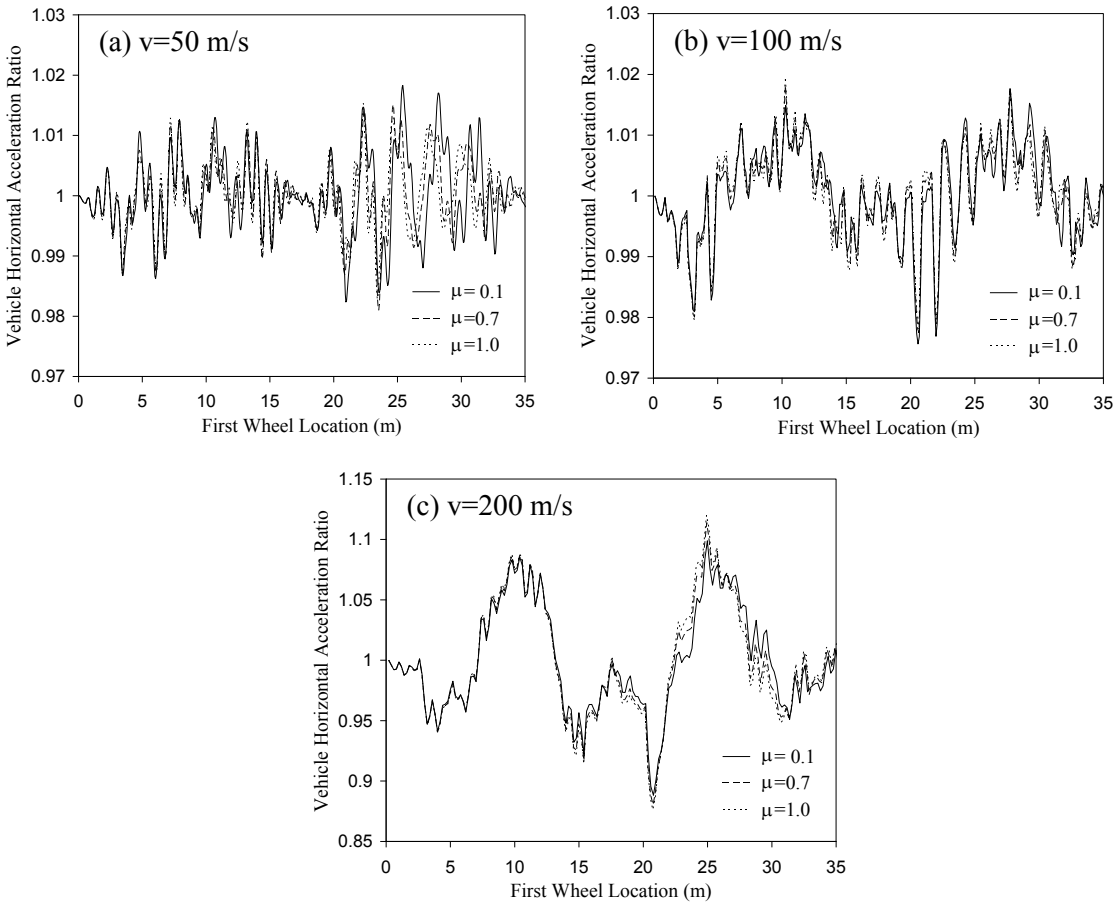

Fig. 5.46 Ratio of vehicle horizontal acceleration over initial acceleration of the train model for initial vehicle speeds of (a) 50 m/s, (b) 100 m/s, and (c) 200 m/s.

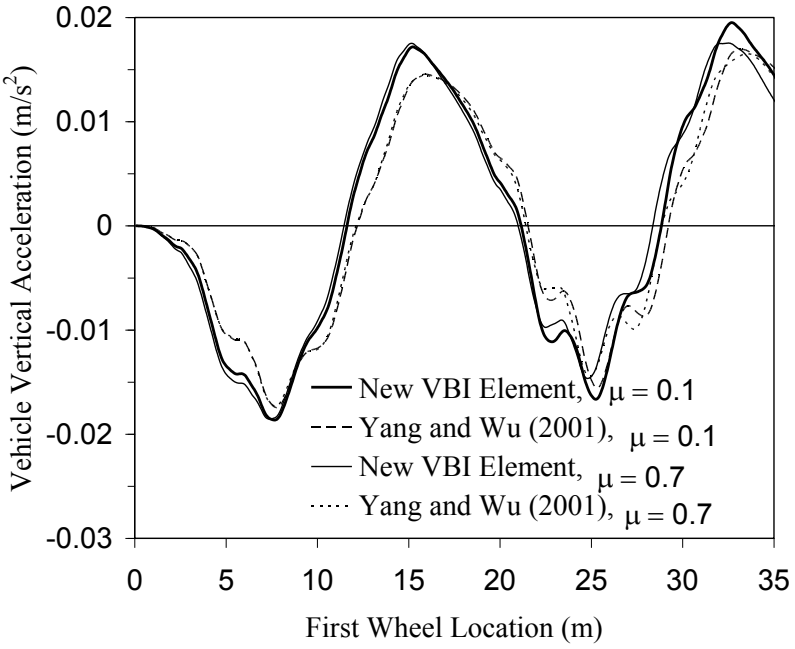

Fig. 5.47 Vertical acceleration of the car body of the train model, for initial vehicle speed of 50 m/s

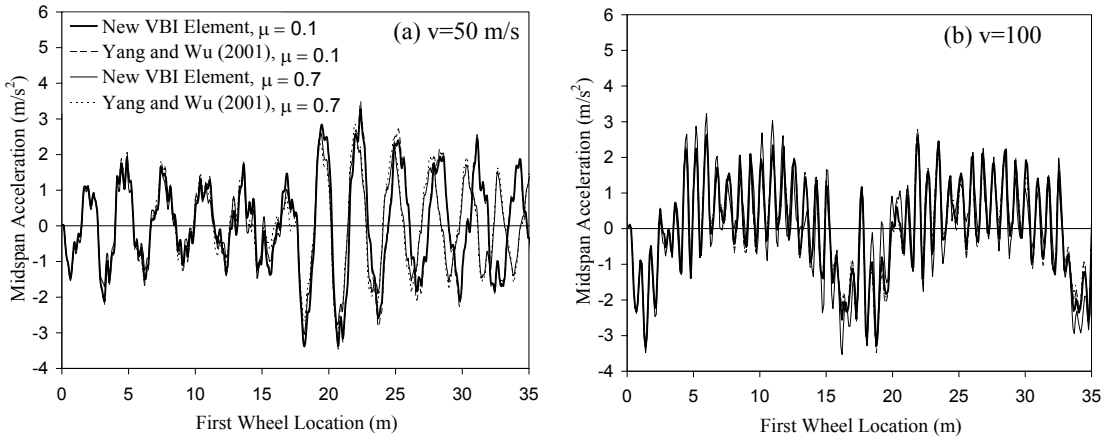

Fig. 5.48 Bridge midspan acceleration of the train model for initial vehicle speeds of (a) 50 m/s, and (b) 100 m/s

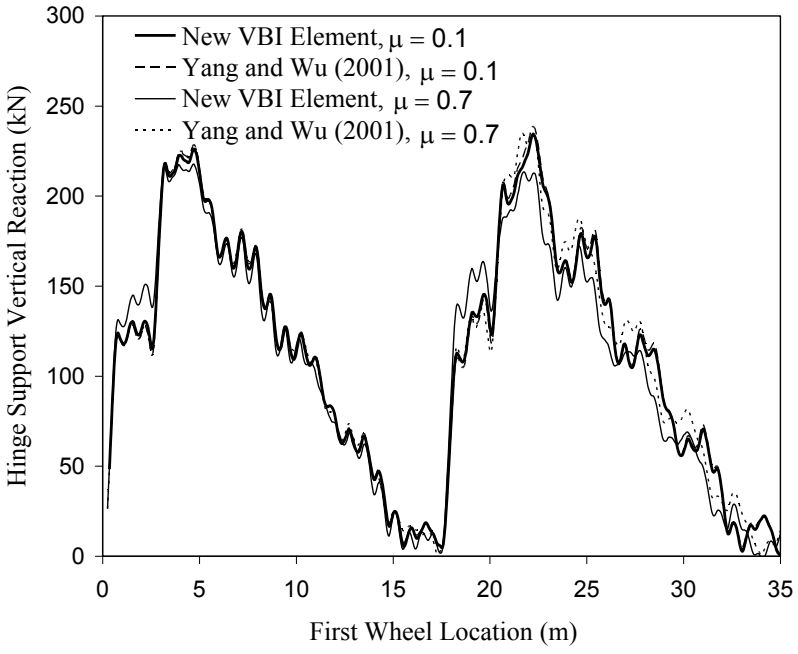

Fig. 5.49 Hinge support vertical reaction of the train model, for initial vehicle speed of 50 m/s.

CHAPTER 6

CONCLUSIONS AND RECOMMENDATIONS

6.1 SUMMARY

The principal objective of this study is to develop and evaluate numerical elements for the dynamic analysis of Vehicle-Bridge Interaction (VBI) problems where the response of the bridge and also the vehicle is required.

Two numerical VBI elements are developed; first one is for vehicles moving with constant velocity and the second one is for vehicles experiencing acceleration or deceleration. The first VBI element was used in the development of the second one. The general common notations are kept similar to the VBI element proposed by Yang and Wu (2001) for easier comparison between the two models. For vehicles experiencing acceleration or deceleration, the numerical formulation is written such that the effect of vehicle acceleration is included solely in one parameter called acceleration parameter.

A program was coded using MATLAB 7.6 (2008) programming language to perform the time-history analysis of vehicle-bridge interaction. Three numerical models were used to verify the developed numerical VBI elements and the coded MATLAB program.

The effects of shear deformations and consistent masses on the vehicle and bridge responses were also investigated. Eleven double plate-girder open-deck railway bridges with spans ranging from 4.0 m to 30.0 m were designed using AREMA Manual (2010). Timoshenko beam element was used to simulate the effect of shear deformations with

consistent masses including effect of rotary masses. Three types of bridge modeling were considered, regarding two types of stiffness and mass matrix.

A comprehensive parametric study was conducted to investigate the effect of the new VBI element for vehicles with constant velocity compared with the VBI elements available in literature. A new parameter was introduced in this study which is the ratio of the wheel mass to the vehicle body mass. The effect of the new VBI element for vehicles experiencing deceleration was studied for three types of vehicle models: symmetrical and unsymmetrical vehicles, and a train model.

6.2 CONTRIBUTIONS AND APPLICATIONS

There are two main contributions of the current research work:

1. A numerical VBI element was developed for vehicles with constant velocity. To develop this VBI element, contact forces are related to beam element nodal forces using Hermitian cubic interpolation functions. Suitable interpolation functions between the beam element displacement vector and those for contact points are considered. The velocity and the acceleration of the contact point are then obtained by the first and second derivation of the corresponding displacement vector. This result in the stiffness, mass, and damping properties of a new beam element, which is called VBI element as compared with the original beam element. Corresponding formulations are listed in Eqs. 3.15 to 3.18. The working procedure is explained in Section 3.2.5. The effect of rail irregularities (for railway bridges) or road roughness (for highway bridges) is also included in the VBI element.

2. Another numerical VBI element was developed for vehicles experiencing longitudinal acceleration or deceleration. Forces exerted by the vehicle longitudinal acceleration are formulated numerically based on vertical contact forces by defining suitable dimensionless matrices and vectors. Then, a new factor called acceleration parameter is defined to facilitate the formulation. This parameter can be calculated at the beginning of the analysis and is constant throughout the analysis, convenient for numerical programming. Consequently, this results in the modified VBI element including the effect of vehicle acceleration or deceleration. Corresponding formulations are listed in Eqs. 3.56 to 3.58. The working procedure is described in Section 3.3.6.

Despite the fact that the developed VBI elements are generalized and can be used in the analysis of the interaction of any moving object on an elastic support, there are two main practical applications in the field of structural engineering:

1. LRFD-based code development for design and evaluation of railway bridges is required to be carried out (Najjar 2006). In the development of new LRFD code for railway bridges, one major step is to obtain statistical characteristics of the dynamic load and impact on railway bridges through a numerical analysis. This has not been done yet for American railway bridges.

   The first step is to simulate in-service trains based on available data from daily traffic on railway bridges. The accuracy of the results and their reliability increases with the number of simulated trains. Various bridge types need to be considered with different conditions (e.g. track type and irregularities). The second step is to perform

a complete analysis of vehicle-bridge interaction for each simulated train, bridge type, and bridge condition. This leads to extensive number of required analyses.

Moreover, the development of numerical analytical procedures is required since modeling all sources of dynamic effects in the commercially available structural analysis software, such as SAP2000, is not feasible. For instance, the effect of track irregularities cannot be incorporated in these available software packages. On the other hand, the accuracy of the results is important since the dynamic interaction between railway bridges and trains are usually significant due to large loads being transported. In the current railway bridge design manual (AREMA 2011), dynamic effects can reach up to 40% of the live load depending on the bridge span; hence, appropriate calculation of dynamic effects can have a great influence on the final bridge design.

In summary, to obtain statistical characteristics of the dynamic load and impact on railway bridges, numerous detailed VBI analyses are required. An efficient and sufficiently accurate method of analysis, such as the analysis that could be performed using the developed VBI models, is essential and can save extensive amount of time and effort.

2. In the design of railway bridges for high-speed trains where the train response is important due to passenger comfort, sophisticated analytical methods are required to be used. Following the recent growth in the use of high speed trains in Japan, China, and Europe, much research was undertaken in these countries in the past two decades.

   Even though there is only one high-speed route currently in North America (Amtrak's Acela Express runs on the Northeast Corridor from Boston to Washington,

D.C), it was reported that there will be several high-speed constructions in USA as a part of the 2009 stimulus package (Billitteri, 2009). The construction is expected to begin as of September 2012 in Central Valley, California (Turner, 2010). For Canada, implementing new routes have been under discussion for a while in order to connect Edmonton to Calgary, and also another route from Windsor to Quebec City. Despite the possibility of future applications of high speed trains in North America, there is not much research in this area.

6.3 CONCLUSIONS

The following conclusions are obtained from results of the numerical analysis of the current research:

1. Accounting for the shear deformation in the VBI models formulation affects the mid-span deflection predictions by about 18% for 4.0m span bridge and around 8% for spans longer than 16.0m.
2. The effect of accounting of shear deformation becomes more imperative on the bridge dynamic responses, such as the peak mid-span acceleration; a significant difference of 70% in the response was obtained for a 6.0m bridge model with a speed parameter[1] S=0.6.
3. Consistent mass has no effect on the mid-span deflection and vehicle vertical acceleration for all vehicle speed ranges. However, there is a slight effect on the

[1] Speed parameter: $S = \frac{\pi v}{\omega L_B}$ where v is the vehicle speed, ω is the bridge fundamental frequency, and L_B is the bridge length.

mid-span acceleration of the very short bridges (span < 10 m) traversed by vehicles with speed parameter $S > 0.5$.

4. The new VBI elements have more effect on mid-span and vehicle vertical accelerations compared to DAF (Dynamic Amplification Factor) for all vehicle speed ranges. In addition, the effect of new elements on all of the bridge and vehicle responses increases when vehicle speed is augmented (for high-speed vehicles in particular). This is attributed to the effect of dynamic parameters (e.g. vehicle speed) presented in the formulations proposed for the new VBI elements.
5. DAF is not always increasing with vehicle velocity and can be even less than one for vehicles with average speeds. This region of decreasing DAF was observed for the bridge model of 15.5 m with speed parameter S=0.2. Despite this observation, it is still realistic to take DAF to be greater than 1 for practical engineering applications.
6. Parametric study demonstrated important influential parameters that affect the response are the vehicle mass parameter η and system mass parameter κ for any vehicle speed. Also, the response is sensitive to the frequency parameter γ in the case of high speed vehicles.
7. Results indicate that using fully loaded vehicles having less η will not always ensure upper bound responses for bridge and vehicle accelerations, particularly for high-speed vehicles. This should be considered in the pertinent design practices.
8. Considering 4-DOF and 6-DOF vehicle models, the vehicle longitudinal deceleration demonstrated significant influence on the vertical contact forces,

vehicle vertical acceleration, and also bridge mid-span deflection. The main reason is attributed to the alteration in the vertical contact forces captured by the new VBI element. However, the effect of the new VBI element is not prominent for bridge mid-span acceleration which is very much affected by the vehicle driving frequency (i.e. vehicle speed).

9. Studying a train model of 10-DOF, having two levels of medium and high braking situations, shows that the vertical contact forces may be significantly affected and they can be augmented by about ±50% for an extreme braking situation. This local effect could have implications on the design of the rail. On the other hand, such extreme braking situations have minor effect on the mid-span deflection and the vehicle vertical acceleration mainly due to the small arm between the two wheels under each bogie

Finally, it should be mentioned that the above conclusions are based on the limited number of numerical dynamic analyses done in this thesis. More analyses are needed if generalized conclusions are desired.

6.4 RECOMMENDATIONS FOR FUTURE RESEARCH

The following are suggested future research areas on the VBI analysis:

1. Extension of the developed VBI elements for 3D analysis of vehicle-bridge interaction, which would assist in performing research in the following areas:
    - Investigation of the individual track irregularities for each rail of railway bridges. This will provide a detailed modelling of track irregularities, and a better analysis of dynamic effects and impact factor.

- Analysis of torsional vibration of bridges due to the moving of vehicles off the center-line of the bridge.
- Analysis of lateral acceleration and bouncing of the vehicle.
- Studying the effect of vehicle rocking oscillation on the bridge response, which is an important parameter in the design of railway bridges. According to the AREMA manual (2011), vehicle contact loads are modified by ±20% on each rail due to the rocking effect.

2. Although this study covered several types of vehicles, it is suggested that more types of vehicles and also bridges be analyzed in order to be able to generalize the conclusions. For example, 6-axle locomotives can be investigated.
3. Bridge models used in this study were simply-supported girder bridges. A future investigation would study the response of continuous bridges with various structural systems.
4. A comprehensive study could be carried out on the effect of elastic bearing type and its influencing design parameters on the response of the bridge and also the vehicle.

REFERENCES

Akin, J.E., Mofid, M., 1989, Analytical Numerical Solution for Response of Beams with Moving Mass, Journal of Structural Engineering, ASCE, 115 (1), pp: 120-131.

Alvarez, L., Yi, J., Horowitz, R., Olmos, L., 2005, Dynamic friction model-based tire-road friction estimation and emergency braking control, Journal of Dynamic Systems, Measurements, and Control, ASME, 127(1), pp: 22–32.

Archer, J.S., 1963, Consistent Mass Matrix for Distributed Mass Systems, J. Structural Division, 89(1), pp: 161–178.

AREMA, American Railway Engineering and Maintenance-of-way Association, 2007, Manual of Recommended Practice, Chapter 15-Steel Structures, Washington, D.C.

Armstrong-Hélouvry, B., 1991, Control of Machines with Friction, Kluwer Academic Publishers, Dordrecht.

Biggs, J.M., 1964, Introduction to Structural Dynamics, McGraw-Hill, New York, N.Y., USA.

Billitteri, T.J., 1 May 2009, High-speed trains: Does the United States need supertrains?, *CQ Researcher*, *19*, pp: 397-420.
Retrieved from: http://library.cqpress.com/cqresearcher/

Biondi, B., Muscolino, G., Sofi, A., 2005, A substructure approach for the dynamic analysis of train–track–bridge system, Computers & Structures, 83, pp: 2271–2281.

Blejwas, T.E., Feng, C.C., Ayre, R.S., 1979, Dynamic interaction of moving vehicles and structures, Journal of Sound and Vibration, 67(4), pp: 513-521.

Brady, S.P., O'Brien, E.J., Znidaric, A., 2006, Effect of vehicle velocity on the dynamic amplification of a vehicle crossing a simply supported bridge, Journal of Bridge Engineering, ASCE, 11(2), pp: 241-249.

Butt H.J, Graf K., Kappl M., 2006, Physics and Chemistry of Interfaces, Wiley-VCH, Weinheim.

Calçada, R., Delgado, R., Matos, A.C., Goicolea, J.M., Gabaldon, F., 2009, Track-bridge interaction on high-speed railways, CRC Press, Taylor & Francis Group, London,UK.

Chang, D., and Lee, H., 1994, Impact factors for simple-span highway girder bridges, Journal of Structural Engineering, ASCE, 120(3), pp: 704-715.

Chen, Y.H., Li, C.Y., 2000, Dynamic response of elevated high-speed railway, J. bridge Eng., ASCE, 5(2), pp: 124-130.

Chopra, A.K., 2001, Dynamic of Structures: Theory and Applications to Earthquake Engineering, Prentice-Hall, Englewood Cliffs, New Jersey, USA.

Chu, K.H., Garg, V.K., and Dhar, C.L., 1979, Railway-bridge impact: simplified bridge and train model, J. Struct. Div., ASCE, 105(9), pp: 1823-1844.

Chu, K.H., Garg, V.K., and Wang, T.L., 1979, Impact in railway prestressed concrete bridges, Journal of Structural Engineering, ASCE, 112(5), pp: 1036-1051.

Cowper, G.R., 1966, The Shear Coefficient in Timoshenko's Beam Theory, ASME J. Appl. Mech., 33, pp: 335–340.

Dahl, P.R., 1976, Solid Friction Damping in Mechanical Vibrations, AIAA J., 14, pp: 1675- 1682.

Dahlquist, G., Bjorck, A., 2008, Numerical methods in scientific computing, SIAM, Philadelphia.

Delgado, R., Calçada, R., Goicolea, J.M., Gabaldon, F., 2009, Dynamics of high-speed railway bridges, CRC Press, Taylor & Francis Group, London,UK.

Dugush, Y.A., Eisenberger, M., 2002, Vibrations of non-uniform continuous beams under moving loads, Journal of Sound and Vibration, 254(5), pp: 911-926.

Dupont, P., Hayward, V., Armstrong-Hélouvry, B., Altpeter, F., 2002, Single State Elastoplastic Friction Models, IEEE Transactions on Automatic Control, 47(5), pp: 787-792.

Esmailzadeh, E., Jalili, N., 2003, Vehicle–passenger–structure interaction of uniform bridges traversed by moving vehicles, Journal of Sound and Vibration, 260(4), pp: 611-635.

Foutch, D.A., Tobias, D.H., Otter, D.E., Lopresti, J.A., Uppal, A.S., 1997, Experimental and Analytical Investigation of the Longitudinal Loads in an Open-Deck Plate Girder Railway Bridge, Association of American Railroads, Report No. R-905, Pueblo, CO, USA.

Frýba, L., 1967, The dynamic influence of wheel flats on railway bridges, Intl. Railway Congr. Assoc. Bullet., pp: 477–512.

Frýba, L., 1972, Vibration of solids and structures under moving loads. Noordhoff International Publishing, Groningen, Netherlands.

Frýba, L., 1996, Dynamics of railway bridges, Thomas Telford, London, UK.

Frýba, L., 1999, Vibration of solids and structures under moving loads, Thomas Telford, London, UK.

Frýba L., 2001, A rough assessment of railway bridges for high speed trains, Engineering Structures, 23(5), pp: 548-556.

Galdos, N.H., Schelling, D.R., Sahin, M.A., 1993, Methodology for impact factor of horizontally curved box girders, Journal of Structural Engineering, ASCE, 119(6), pp: 1917-1934.

Garg, V.K., Dukkipati, R.V., 1984, Dynamics of Railway Vehicle Systems, Academic Press, Toronto, Canada.

Gbadeyan, J.A., Oni, S.T., 1995, Dynamic behaviour of beams and rectangular plates under moving loads, Journal of Sound and Vibration, 182(5), pp: 677-695.

Genin, J., Chung, Y.I., 1979, Response of a continuous guideway on equally spaced supports traversed by moving vehicle, Journal of Sound and Vibration, 67, pp: 245-251.

Genin, J., Ginsberg, J.H., Ting, 1975, A complete formulation of inertial effects in the guideway-vehicle interaction problem, Journal of Sound and Vibration, 38(1), pp: 15-26.

Genin, J., Ting, E.C., Vafa, Z., 1982, Curved bridge response to moving vehicle. J. Sound and Vibration, 81(4), pp: 469–475.

Green, M.F., Cebon, D., 1994, Dynamic response of highway bridges to heavy vehicle loads: Theory and experimental validation, Journal of Sound and Vibration, 170(1), pp: 51-78.

Green, M.F., Cebon, D., 1997, Dynamic interaction between heavy vehicles and highway bridges, Computers & Structures, 62(2), pp: 253-264.

Humar, J.L., Kashif, A.M., 1993, Dynamic response of bridges under travelling loads, Can. J. Civ. Eng., 20, pp: 287-298.

Hwang, E.S., Nowak, A.S., 1991, Simulation of dynamic load for bridges, Journal of Structural Engineering, ASCE, 117(5), pp: 1413-1434.

Inbanathan, M.J., Weiland, M., 1987, Bridge vibrations due to vehicle moving over rough surface, Journal of Structural Engineering, ASCE, 113(9), pp: 1994-2008.

Iwnicki, S.E., 1999, The Manchester benchmarks for rail vehicle simulation, Swets & Zeitlinger, Lisse, The Netherlands.

Ju, S.H., Lin, H.T., 2007, A finite element model of vehicle–bridge interaction considering braking and acceleration, Journal of Sound and Vibration, 303 (1), pp: 46–57.

Kwark, J.W., Choi, E.S., Kim Y.J., Kim, S.I., 2004, Dynamic behavior of two-span continuous concrete bridge under moving high-speed train, Computers & Structures, 82(4-5), pp: 463-474.

Law, S.S., Zhu, X.Q., 2005, Bridge dynamic responses due to road surface roughness and braking of vehicle, Journal of Sound and Vibration, 282(3–5), pp:805-830.

Lee, C.H., Kawatani, M., Kim, C.W., Nishimura, N., Kobayashi, Y., 2006, Dynamic response of a monorail steel bridge under a moving train, Journal of Sound and Vibration, 294(3), pp: 562–79.

Lei, X., Noda, N.A., 2002, Analyses of dynamic response of vehicle and track coupling system with random irregularity of track vertical profile. Journal of Sound and Vibration, 258(1), pp: 147-165.

Levinson, M., 1981, A new rectangular beam theory, Journal of Sound and Vibration. 74, pp: 81-87.

Li, J., Su, M., Fan, L., 2003, Natural frequency of railway girder bridges under vehicle loads, Journal of Bridge Engineering, ASCE, 8(4), pp: 199–203.

Majka, M., Hartnett, M., 2008, Effects of speed, load and damping on the dynamic response of railway bridges and vehicles, Computers & Structures, 86(6), pp: 556–572.

Marcondes, J., Burgess, G.J., Harichandran, R., Snyder, M.B., 1991, Special analysis of highway pavement roughness, J. Transp. Eng., ASCE, 117(5), pp: 540-549.

MATLAB®, 2008, The Math Works Inc., Massachusetts.

McCalley, R.B., 1963, Rotatory inertia correction for mass matrices, General Electric Knolls Atomic Power Laboratory, Schenectady, N.Y., Report DIG/SA.

Najjar, W.S., 2006, A road map for developing LRFD specifications for railroad bridges, AREMA Annual Conference.

Nowak, A.S., 1999, Calibration of LRFD bridge design code, NCHRP Report 368, Washington (D.C.): Transportation Research Council.

Olofsson, U., Telliskivi, T., 2003, Wear, friction and plastic deformation of two rail steels — full scale test and laboratory study, Journal of Wear, 254, pp: 80-93.

Olsson, H., Åström, K.J., Canudas deWit, C., Gäfvert, M., Lischinsky, P., 1998, Friction Models and Friction Compensation, European Journal of Control, 4(3), pp: 176-195.

Pan, T.C., Li, J., 2002, Dynamic vehicle element method for transient response of coupled vehicle-structure systems, Journal of Structural Engineering, ASCE, 128(2), pp: 214-223.

Pesterev, A.V., yang, B., Bergman, L.A., Tan, C.A., 2001, Response of elastic continuum carrying multiple moving oscillators, J. Eng. Mech., ASCE, 127(3), pp: 260-265.

Pesterev, A.V., Bergman, L.A., Tan, C.A., Tsao, T.C., Yang, B., 2003, On asymptotics of the solution of the moving oscillator problem, Journal of sound and Vibration, 260, pp: 519-536.

Pfeiffer, F., Foerg, M., Ulbrich, H., 2006, Numerical aspects of non-smooth multibody dynamics, Comput. Methods Appl. Mech. Engrg., 195(50-51), pp: 6891-6908.

Pfeiffer, F., Glocker, C., 1996, Multibody Dynamics with Unilateral Contacts, John Wiley & Sons, New York, NY.

Przemieniecki, S., 1968, Theory of Matrix Structural Analysis, McGraw-Hill, New York, N.Y.

Przemieniecki, S., 1985, Theory of Matrix Structural Analysis, McGraw-Hill, New York, N.Y.

Rao, G.V., 2000, Linear dynamics of an elastic beam under moving loads, J. Vibr. & Acous., ASME, 122(7), pp: 281-289.

Reddy J.N., 1984, A simple higher-order theory for laminated composite plates, Journal of Applied Mechanics, 51, pp: 745-752.

Reddy J.N., 1997a, On Locking-free shear deformable beam finite elements, Computer Methods in Applied Mechanics and Engineering 149: 113-132.

Reddy J.N., 1997b, Mechanics of Laminated Composite Plates: Theory and Analysis, CRC Press, Boca Raton, FL.

Richardson, H.H., Wormley, D.N., 1974, Transportation vehicle/beam-elevated guideway dynamic interactions, a State-of-the-art-Review, J. Dynamic Systems Measurement and Control, 96, pp: 169–179.

Sadiku, S., Leipholz, H.H.E., 1987, On the dynamics of elastic systems with moving concentrated masses, Ingenieur-Archiv, 57, pp: 223-242.

Shurtz, M.L., Heydinger, G.J., Guenther, D.A., Zagorski, S.B., 2006, Effects of ABS controller parameters on heavy truck model braking performance, Commercial Vehicle Engineering Congress and Exhibition, Chicago, Ill. SAE International

Sridharan, N., Mallik, A.K., 1979, Numerical analysis of vibration of beams subjected to moving loads, Journal of Sound and Vibration, 65, pp: 147-150.

Stanišić, M.M., Hardin, J.C., 1969, on the response of beams to an arbitrary number of concentrated moving masses, J. Franklin Inst., 287, pp: 115-123.

Stanišić, M.M., 1985, On a new theory of the dynamic behavior of the structures carrying moving masses, Ingenieur-Archiv, 55, pp: 176-185.

Timoshenko, S.P., Young, D.H., 1955, Vibration problems in engineering, 3rd edn., D. Van Nostrand, New York, N.Y.

Ting, E.C., Genin, J., 1980, Dynamics of bridge structures, Struct. Mech. Archives, 5(3), pp: 217–252.

Ting, E.C., Genin, J., Ginsberg, J.H., 1974, A general algorithm for the moving mass problems, Journal of Sound and Vibration, 33(1), pp: 49-58.

Thomas, D.L., Wilson, J.M., Wilson, R.R., 1973, Timoshenko beam finite elements, Journal of Sound and Vibration, 31, pp: 315–330.

Turner, M., 24 November 2010, Plan submitted for state's first high-speed rail leg, Sacramento Business Journal, Retrieved 20 December 2010.

Urathaler Y., Reddy J.N., 2008, A mixed finite element for nonlinear bending analysis of laminated composite plates based on FSDT, Mechanics of Advanced Materials and structures, 15, pp: 335-354.

Uzzal, R.A., Ahmed, W., Rakheja, S., 2008, Dynamic analysis of railway vehicle-track interactions due to wheel flat with a pitch-plane vehicle model, Journal of Mechanical Engineering, 39(2), pp: 86-94.

Veletsos, A.S., Huang, T., 1970, Analysis of dynamic response of highway bridges, J. Eng. Mech. Div., Proc ASCE; 96(EM5), pp: 593– 620.

Wang, R.T., 1997, Vibration of multi-span Timoshenko beams to a moving force, Journal of Sound and Vibration, 207(5), pp: 731-742.

Weaver, W., Timoshenko, S.P., Young, D.H., 1990, Vibration problems in engineering, 5th edition, John Wiley & Sons, New York, N.Y.

Wu, J.S., Dai, C.W., 1987, Dynamic responses of multi-span non-uniform beam due to moving loads, Journal of Structural Engineering, ASCE, 113(3), pp: 458-474.

Wu, Y.S., Yang, Y.B., Yau, J.D., 2001, Three-dimensional analysis of train-rail-bridge interaction problems, Vehicle System Dynamics, 36(1), pp: 1-35.

Wu, Y.-S., Yang, Y.-B., 2003, Steady-state response and riding comfort of trains moving over a series of simply supported bridges, Engineering Structures, 25, pp: 251-265.

Xia, H., De Roeck, G., Zhang, H.R., Zhang, N., 2001, Dynamic analysis of train–bridge system and its application in steel girder reinforcement, Computers & Structures, 79(21–22), pp: 1851–1860.

Xia, H., Zhang, N., De Roeck, G., 2003, Dynamic analysis of high speed railway bridge under articulated trains, Computers & Structures, 81(26-27), pp: 2467-2478.

Yang, F., Fonder, G.A., 1996, An iterative solution method for dynamic response of bridge–vehicles systems. Earthquake Engineering & Structural Dynamics, 25(2), pp: 195–215.

Yang, Y.B., Chang, C.H., and Yau, J.D., 1999, An element for analyzing vehicle-bridge systems considering vehicle's pitching effect, Int. J. Num. Meth. Eng., 46, pp: 1031-1047.

Yang, Y.B., Lin, B.H., 1995, Vehicle-bridge interaction analysis by dynamic condensation method, Journal of Structural Engineering, ASCE, 121(11), pp: 1636-1643.

Yang, Y.B., Yau, J.D., 1997, Vehicle-bridge interaction element for dynamic analysis, Journal of Structural Engineering, ASCE, 123(11), pp: 1512-1518.

Yang, Y.B., Wu, Y. S., 2001, A versatile element for analyzing vehicle-bridge interaction response. Engineering Structures, 23(5), pp: 452-469.

Yang, Y.B., Yau, J.D., Wu, Y.S., 2004, Vehicle–bridge interaction dynamics with applications to high-speed railways, World Scientific Publishing Co., Singapore.

Zhang, Q.L., Vrouwenvelder, A., Wardenier, J., 2001, Numerical simulation of train–bridge interactive dynamics. Computers & Structures, 79(10), pp: 1059–1075.

Zheng, D.Y., Cheung, Y.K., Au, F.T.K., Cheng, Y.S., 1998, Vibration of multi-span non-uniform bridge under moving loads by using modified beam vibration functions, Journal of Sound and Vibration, 212, pp: 455-467.

Zhu, J.J., Ahmed, A.K.W., Rakheja, S., Khajepour, A., Hu, Y.S., 2009, Impact load due to railway wheels with multiple flats predicted using an adaptive contact model. Journal of Rail and Rapid Transit, 223(4), pp: 391-403.

Zhu, J.J., Ahmed, A.K.W., Rakheja, S., Khajepour, A., 2010, Development of a vehicle–track model assembly and numerical method for simulation of wheel–rail dynamic interaction due to unsupported sleepers, Vehicle System Dynamics, 48(12), pp: 1535-1552.

Zienkiewicz, O.C., Taylor, R.L., Zhu, J.Z., 2005, The finite element method: its basis and fundamentals, Six Edn. Elsevier.

APPENDIX A

VEHICLE-BRIDGE INTERACTION ELEMENT DEVELOPED BY YANG AND WU (2001)

A.1 Vehicle Equations and Contact Forces

Assume that a bridge is modeled by some beam elements which could be Euler-Bernoulli or other type of beam elements with nodal DOF's at both ends. Some of these elements will experience the vehicle wheels. The vehicle is decomposed into two parts: the upper or non-contact part (e.g. car body, bogie, and suspension system) and the contact part (i.e. wheels). Consider *n* wheelset can be represented each by one vertical DOF and let denote the corresponding displacement vector as $\{d_w\}$. Correspondingly, there are *n* contact points on the bridge which can be denoted by $\{d_c\}$. Similarly, the displacement vector for the upper part can be denoted as $\{d_u\}$.

Let $[m_v]$, $[c_v]$, and $[k_v]$ respectively denote the mass, damping, and stiffness matrix of the whole vehicle, and also $\{d_v\}$ the displacement vector of the vehicle. The equation of motion for the vehicle can be written as:

$$[m_v]\{\ddot{d}_v\}+[c_v]\{\dot{d}_v\}+[k_v]\{d_v\}=\{f_v\} \tag{A.1}$$

where $\{f_v\}$ is the force vector, and $\{d_v\}$ is the displacement vector for whole vehicle composed of $\{d_w\}$ and $\{d_u\}$, i.e. $\{d_v\}=\langle\langle d_u\rangle\langle d_w\rangle\rangle^T$. The vector $\{f_v\}$ can be decomposed into two parts:

$$\{f_v\}=\{f_e\}+[l]\{f_c\} \tag{A.2}$$

where $\{f_e\}$ denotes the external forces excluding the contact forces, $\{f_c\}$ denotes the contact forces acting on the bridge, and $[l]$ is the transformation matrix. The wheel displacement vector $\{d_w\}$ can be related to the contact displacement $\{d_c\}$ of the bridge by the constraint equation:

$$\{d_w\} = [\Gamma]\{d_c\} \tag{A.3}$$

where $[\Gamma]$ is the transformation matrix; if no jump is considered, $[\Gamma]$ is a unit matrix. This assumption was found to be satisfactory for the vehicle-bridge interaction especially for running trains.

Assuming that all kinematic information about the system is known in time *t*, it is required to determine the behaviour of the system for time $t+\Delta t$ while Δt is a small time increment. The equation of motion for the system in time $t+\Delta t$ can be written in terms of upper part and wheel part as following:

$$\begin{bmatrix} [m_{uu}] & [m_{uw}] \\ [m_{wu}] & [m_{ww}] \end{bmatrix} \begin{Bmatrix} \{\ddot{d}_u\} \\ \{\ddot{d}_w\} \end{Bmatrix}_{t+\Delta t} + \begin{bmatrix} [c_{uu}] & [c_{uw}] \\ [c_{wu}] & [c_{ww}] \end{bmatrix} \begin{Bmatrix} \{\dot{d}_u\} \\ \{\dot{d}_w\} \end{Bmatrix}_{t+\Delta t} + \begin{bmatrix} [k_{uu}] & [k_{uw}] \\ [k_{wu}] & [k_{ww}] \end{bmatrix} \begin{Bmatrix} \{d_u\} \\ \{d_w\} \end{Bmatrix}_{t+\Delta t} = \begin{Bmatrix} \{f_{ue}\} \\ \{f_{we}\} \end{Bmatrix}_{t+\Delta t} + \begin{bmatrix} [l_u] \\ [l_w] \end{bmatrix} \{f_c\}_{t+\Delta t} \tag{A.4}$$

Here, $\{f_{ue}\}$ and $\{f_{we}\}$ denote the external forces acting on the upper and wheel parts of the vehicle. The first row in Eq. (A.4) is regarding the equation of motion of the upper part and the second row is for the wheel part. Since the contact forces only act on the wheels, the submatrix $[l_u]$ has to be a zero matrix.

If one expands the first row of Eq. (4.4), it gives:

$$[m_{uu}]\{\ddot{d}_u\}_{t+\Delta t} + [c_{uu}]\{\dot{d}_u\}_{t+\Delta t} + [k_{uu}]\{d_u\}_{t+\Delta t} = \{f_{ue}\}_{t+\Delta t} - \{q_{uc}\}_{t+\Delta t} \tag{A.5}$$

where

$$\{q_{uc}\}_{t+\Delta t} = [m_{uw}]\{\ddot{d}_w\}_{t+\Delta t} + [c_{uw}]\{\dot{d}_w\}_{t+\Delta t} + [k_{uw}]\{d_w\}_{t+\Delta t} \tag{A.6}$$

Let $\{\Delta d_u\}$ denote the increment of the $\{d_u\}$ in the time step from t to $t+\Delta t$. Utilizing the Newmark-β procedure for this time increment, the vector $\{d_u\}$ and its derivatives can be related to those at time t which are known,

$$\{\ddot{d}_u\}_{t+\Delta t} = a_0\{\Delta d_u\} - a_1\{\dot{d}_u\}_t - a_2\{\ddot{d}_u\}_t \tag{A.7}$$

$$\{\dot{d}_u\}_{t+\Delta t} = \{\dot{d}_u\}_t + a_3\{\ddot{d}_u\}_t + a_4\{\ddot{d}_u\}_{t+\Delta t} \tag{A.8}$$

$$\{d_u\}_{t+\Delta t} = \{d_u\}_t + \{\Delta d_u\} \tag{A.9}$$

In the preceding formula, those with subscript t are regarding the initial values for the time increment, and all are known from the previous time increment. The coefficient of the formula denoted as a_i (i=0,…,4) depend on the β and γ of the Newmark method. These coefficients and three more that will be used later are as follows

$$\begin{aligned} &a_0 = \frac{1}{\beta\Delta t^2}; \quad a_1 = \frac{1}{\beta\Delta t}; \quad a_2 = \frac{1}{2\beta} - 1; \quad a_3 = (1-\gamma)\Delta t \\ &a_4 = \gamma\Delta t; \quad a_5 = \frac{\gamma}{\beta\Delta t}; \quad a_6 = \frac{\gamma}{\beta} - 1; \quad a_7 = \frac{\Delta t}{2}\left(\frac{\gamma}{\beta} - 2\right) \end{aligned} \tag{A.10}$$

If the values in Eq. A.7 to A.9 are substituted to Eq. A.5, then the following can be obtained and arranged accordingly

$$[\Psi_{uu}]\{\Delta d_u\} = \{f_{ue}\}_{t+\Delta t} - \{q_{uc}\}_{t+\Delta t} + \{q_u\}_t \tag{A.11}$$

where

$$[\Psi_{uu}] = a_0[m_{uu}] + a_5[c_{uu}] + [k_{uu}] \tag{A.12}$$

$$\{q_u\}_t = [m_{uu}]\left(a_1\{\dot{d}_u\}_t + a_2\{\ddot{d}_u\}_t\right) + [c_{uu}]\left(a_6\{\dot{d}_u\}_t + a_7\{\ddot{d}_u\}_t\right) - [k_{uu}]\{d_u\}_t \tag{A.13}$$

Using equation 4.11, the displacement increment can be obtained as

$$\{\Delta d_u\} = [\Psi_{uu}]^{-1}\left(\{f_{ue}\}_{t+\Delta t} - \{q_{uc}\}_{t+\Delta t} + \{q_u\}_t\right) \tag{A.14}$$

Having $\{\Delta d_u\}$, the displacement at the time $t+\Delta t$ and its derivative can be calculated from Eq. A.7 to A.9. It should be mentioned that the order of accuracy is the same as that for Newmark-β method and no more assumptions or any other sources of errors were made so far.

A.2 Solution of Contact Forces

If the displacement $\{d_u\}_{t+\Delta t}$ and its derivatives are substituted in the second row of Eq. A.4, then the contact forces $\{f_c\}_{t+\Delta t}$ is obtained,

$$\{f_c\}_{t+\Delta t} = [m_c]\{\ddot{d}_w\}_{t+\Delta t} + [c_c]\{\dot{d}_w\}_{t+\Delta t} + [k_c]\{d_w\}_{t+\Delta t} + \{p_c\}_{t+\Delta t} + \{q_c\}_t \tag{A.15}$$

where $[m_c]$, $[m_c]$, and $[m_c]$ are called the contact matrices which are:

$$[m_c] = [l_w]^{-1}\left([m_{ww}] - [\Psi_{wu}][\Psi_{uu}]^{-1}[m_{uw}]\right) \tag{A.16}$$

$$[c_c] = [l_w]^{-1}\left([c_{ww}] - [\Psi_{wu}][\Psi_{uu}]^{-1}[c_{uw}]\right) \tag{A.17}$$

$$[k_c] = [l_w]^{-1}\left([k_{ww}] - [\Psi_{wu}][\Psi_{uu}]^{-1}[k_{uw}]\right) \tag{A.18}$$

and the load vectors $\{p_c\}_{t+\Delta t}$ and $\{q_c\}_t$ are:

$$[p_c]_{t+\Delta t} = [l_w]^{-1}\left([\Psi_{wu}][\Psi_{uu}]^{-1}\{f_{ue}\}_{t+\Delta t} - \{f_{we}\}_{t+\Delta t}\right) \tag{A.19}$$

$$[q_c]_t = [l_w]^{-1}\left([\Psi_{wu}][\Psi_{uu}]^{-1}\{q_u\}_t - \{q_w\}_t\right) \tag{A.20}$$

where,

$$[\Psi_{wu}] = a_0[m_{wu}] + a_5[c_{wu}] + [k_{wu}] \tag{A.21}$$

$$\{q_w\}_t = [m_{wu}]\left(a_1\{\dot{d}_u\}_t + a_2\{\ddot{d}_u\}_t\right) + [c_{wu}]\left(a_6\{\dot{d}_u\}_t + a_7\{\ddot{d}_u\}_t\right) - [k_{wu}]\{d_u\}_t \tag{A.22}$$

Using the constraint equation presented in Eq. A.3, the contact forces $\{f_c\}_{t+\Delta t}$ can be reformulated in terms of contact displacement $\{d_c\}$ considering $[\Gamma]$ a unit matrix:

$$\{f_c\}_{t+\Delta t} = [m_c]\{\ddot{d}_c\}_{t+\Delta t} + [c_c]\{\dot{d}_c\}_{t+\Delta t} + [k_c]\{d_c\}_{t+\Delta t} + \{p_c\}_{t+\Delta t} + \{q_c\}_t \quad \text{(A.23)}$$

Then, i^{th} entry of the $\{f_c\}_{t+\Delta t}$ as the contact forces between i^{th} wheel and the bridge ($V_{i,t+\Delta t}$), can be calculated as:

$$V_{i,t+\Delta t} = p_{ci,t+\Delta t} + q_{ci,t} + \sum_{j=1}^{n}\left(m_{cij}\ddot{d}_{cj,t+\Delta t} + c_{cij}\dot{d}_{cj,t+\Delta t} + k_{cij}d_{cj,t+\Delta t}\right) \quad \text{(A.24)}$$

where m_{cij}, c_{cij}, and k_{cij} are respectively the entry in the i^{th} row and j^{th} column of the contact matrices $[m_c]$, $[c_c]$, and $[k_c]$. Similarly, the $p_{ci,t+\Delta t}$ and $q_{ci,t}$ are the entry located in the i^{th} row of the corresponding vectors, i.e. $\{p_c\}_{t+\Delta t}$ and $\{q_c\}_t$.

A.3 VBI Element Considering Vertical Contact Forces only

Consider that n wheels of the moving vehicle are acting on the n element k_1, k_2, …, k_n of the bridge elements. These elements are considered as VBI element since they are directly loaded with the vehicle. The rest of the bridge elements will be treated as the regular beam elements. For the k_ith beam element of the bridge, which is loaded by the contact force $V_{i,t+\Delta t}$, the equation of motion at time $t+\Delta t$ is:

$$[m_{bi}]\{\ddot{d}_{bi}\}_{t+\Delta t} + [c_{bi}]\{\dot{d}_{bi}\}_{t+\Delta t} + [k_{bi}]\{d_{bi}\}_{t+\Delta t} = \{f_{bi}\}_{t+\Delta t} - \{f_{bci}\}_{t+\Delta t} \quad \text{(A.25)}$$

where $[m_{bi}]$, $[c_{bi}]$, and $[k_{bi}]$ are the mass, damping and stiffness matrices of the k_ith beam element. $\{d_{bi}\}$ is the nodal displacement vector of this element and $\{f_{bi}\}$ is the vector of the nodal external forces. $\{f_{bci}\}_{t+\Delta t}$ is the vector of the equivalent nodal forces resulted

from $V_{i,t+\Delta t}$ contact force. One way to find these equivalent nodal forces is to use interpolation functions as applied in the finite element analysis. This is an assumption and introduces errors to the analysis. Let denote the interpolation function as $\{N_{ci}^v\}$, then:

$$\{f_{bci}\}_{t+\Delta t} = \{N_{ci}^v\} V_{i,t+\Delta t} \tag{A.26}$$

Since only vertical contact forces are considered here, then it will be a good assumption to only include entries associated with vertical DOF's in the interpolation vector $\{N_{ci}^v\}$ and the other entries being set to zero. If one consider Hermitian cubic polynomials as the interpolation functions, then $\{N_{ci}^v\}$ for a 6-DOF two dimensional beam element shown in Fig. 3.1 is:

$$\{N_{ci}^v\} = \langle 1 - 3\bar{x}^2 + 2\bar{x}^3, 0, 0, 3\bar{x}^2 - 2\bar{x}^3, 0, 0 \rangle^T \tag{A.27}$$

where $\bar{x}$ is the local coordinate of the i^{th} contact point on the k_ith element, i.e. $\bar{x} = x/L$. Now, using Eq. A.24 and A.26, bridge element equation of motion, Eq. A.25, can be arranged as follows,

$$\begin{aligned} &[m_{bi}]\{\ddot{d}_{bi}\}_{t+\Delta t} + [c_{bi}]\{\dot{d}_{bi}\}_{t+\Delta t} + [k_{bi}]\{d_{bi}\}_{t+\Delta t} \\ &= \{f_{bi}\}_{t+\Delta t} - \sum \left([m_{cij}^*]\{\ddot{d}_{bj}\} + [c_{cij}^*]\{\dot{d}_{bj}\} + [k_{cij}^*]\{d_{bj}\} \right) - \{p_{ci}^*\}_{t+\Delta t} - \{q_{ci}^*\}_t \end{aligned} \tag{A.28}$$

where the matrices with an asterisk are calculated using contact matrices and interpolation vectors as:

$$[m_{cij}^*] = \{N_{ci}^v\} m_{cij} \langle N_{ci}^v \rangle; \quad [c_{cij}^*] = \{N_{ci}^v\} c_{cij} \langle N_{ci}^v \rangle; \quad [k_{cij}^*] = \{N_{ci}^v\} k_{cij} \langle N_{ci}^v \rangle \tag{A.29}$$

and the equivalent nodal loads are:

$$\{p_{ci}^*\}_{t+\Delta t} = \{N_{ci}^v\} p_{ci,t+\Delta t}; \quad \{q_{ci}^*\}_t = \{N_{ci}^v\} q_{ci,t} \tag{A.30}$$

Eq. A.28 is regarded as the VBI element since the effect of the moving vehicle is considered explicitly with the asterisk matrices and vectors.

A.4 VBI Element Considering Vertical and Horizontal Contact Forces

The horizontal forces can be generated in the contact interface of the wheel and bridge by rolling, accelerating, or braking action of the wheel. The effect of the rolling is very small and is neglected here. Similar to the vertical loads, the horizontal contact loads, $H_{i,t+\Delta t}$, can be transferred to the nodal forces by introducing new interpolation function $\{N_{ci}^h\}$. Hence, the equivalent horizontal forces at the element nodes are calculated as $\{N_{ci}^h\}H_{i,t+\Delta t}$. Then, the total equivalent nodal forces due to vertical and horizontal contact forces are:

$$\{f_{bci}\}_{t+\Delta t} = \{N_{ci}^h\}H_{i,t+\Delta t} + \{N_{ci}^v\}V_{i,t+\Delta t} \tag{A.31}$$

$\{N_{ci}^h\}$ is the interpolation function where all entries are set to zero except those regarding horizontal DOF's. Using Lagrange's linear shape functions, $\{N_{ci}^h\}$ is determined as:

$$\{N_{ci}^v\} = \langle 0 \ , \ 1\text{-}\bar{x} \ , \ 0 \ , \ 0 \ , \ \bar{x} \ , \ 0 \rangle^T \tag{A.32}$$

one can find $H_{i,t+\Delta t}$ in terms of vertical contact force $V_{i,t+\Delta t}$ using the following formula,

$$H_{i,t+\Delta t} = \mu_i V_{i,t+\Delta t} \tag{A.33}$$

where μ_i is the friction coefficient between wheel and rail, which has different values for braking and acceleration. So, the contact force vector $\{f_{bci}\}_{t+\Delta t}$ is a function of vertical contact forces. By following the same procedure as described in Section A.3, the asterisk matrices can be found as follows

$$\begin{aligned}
\left[m_{cij}^{*}\right] &= \left\{N_{ci}^{h}\right\}\mu_i m_{cij}\left\langle N_{ci}^{v}\right\rangle + \left\{N_{ci}^{v}\right\}m_{cij}\left\langle N_{ci}^{v}\right\rangle \\
\left[c_{cij}^{*}\right] &= \left\{N_{ci}^{h}\right\}\mu_i c_{cij}\left\langle N_{ci}^{v}\right\rangle + \left\{N_{ci}^{v}\right\}c_{cij}\left\langle N_{ci}^{v}\right\rangle \\
\left[k_{cij}^{*}\right] &= \left\{N_{ci}^{h}\right\}\mu_i k_{cij}\left\langle N_{ci}^{v}\right\rangle + \left\{N_{ci}^{v}\right\}k_{cij}\left\langle N_{ci}^{v}\right\rangle
\end{aligned} \tag{A.34}$$

and also the asterisk force vectors are obtained as

$$\begin{aligned}
\left\{p_{ci}^{*}\right\}_{t+\Delta t} &= \left\{N_{ci}^{h}\right\}\mu_i p_{ci,t+\Delta t} + \left\{N_{ci}^{v}\right\}p_{ci,t+\Delta t} \\
\left\{q_{ci}^{*}\right\}_{t} &= \left\{N_{ci}^{h}\right\}\mu_i q_{ci,t} + \left\{N_{ci}^{v}\right\}q_{ci,t}
\end{aligned} \tag{A.35}$$

A.5 Bridge Equation of Motion

In the preceding sections, VBI elemente were introduced and the effect of vehicle load was incorporated in the asterisks matrices. The rest of bridge elements that are free of vehicle loads are treated as original beam elements. Versatility of the VBI element is such that it can be easily assembled into the whole bridge structural matrices, i.e. stiffness, damping and mass matrices. Consider the equation of motion for the entire bridge as following

$$\left[M\right]\left\{\ddot{D}\right\}_{t+\Delta t} + \left[C\right]\left\{\dot{D}\right\}_{t+\Delta t} + \left[K\right]\left\{D\right\}_{t+\Delta t} = \left\{F_b\right\}_{t+\Delta t} - \left\{P_c^{*}\right\}_{t+\Delta t} - \left\{Q_c^{*}\right\}_{t} \tag{A.36}$$

where $\{D\}$ represents the displacement matrix, $[M]$, $[C]$, and $[K]$ are the assembled structural matrices. $\{F_b\}$ is the vector of external forces, and $\{P_c^{*}\}$ and $\{Q_c^{*}\}$ are the equivalent contact forces in global coordinates. The assembled matrices can be obtained from

$$\begin{aligned}
\left[M\right] &= \left[M_b\right] + \left[M_c^{*}\right] = \sum\left[m_{bi}\right] + \sum\sum\left[m_{cij}^{*}\right] \\
\left[C\right] &= \left[C_b\right] + \left[C_c^{*}\right] = \sum\left[c_{bi}\right] + \sum\sum\left[c_{cij}^{*}\right] \\
\left[K\right] &= \left[K_b\right] + \left[K_c^{*}\right] = \sum\left[k_{bi}\right] + \sum\sum\left[k_{cij}^{*}\right]
\end{aligned} \tag{A.37}$$

where $[M_b]$, $[C_b]$, and $[K_b]$ are the structural matrices of the bridge which is free of any vehicle loads. Similarly, $[M_c^*]$, $[C_c^*]$, and $[K_c^*]$ are the contact matrices which includes the effect of the VBI elements in the global coordinate. In addition, vectors for global contact forces can be assembled as

$$\{P_c^*\}_{t+\Delta t} = \sum \{p_{ci}^*\}_{t+\Delta t}; \qquad \{Q_c^*\}_t = \sum \{q_{ci}^*\}_t \tag{A.38}$$

This concludes the formulation for dynamic analysis. This procedure is very well-suited for numerical programming and also flexible to add other effects, such as road irregularities.

APPENDIX B

REQUIRED VEHICLE MATRICES FOR DEVELOPED VBI ELEMENTS

In this section, vehicle matrices for all vehicle models used in this study required for dynamic analysis of Vehicle-Bridge Interaction (VBI) is listed. Letter *m* or *M* denote mass, *I* is for rotary mass, *k* for stiffness, *c* for damping, and *g* for ground acceleration.

B.1 Sprung Mass Model (Yang and Wu 2001)

Fig. 3.11 illustrates all parameters in the following matrices

$$[m_{uu}] = M_v \;\; ; \;\; [m_{ww}] = M_w \;\; ; \;\; [m_{uw}] = [m_{wu}] = 0 \tag{B.1}$$

$$[k_{uu}] = k_v \;\; ; \;\; [k_{ww}] = k_v \;\; ; \;\; [k_{uw}] = [k_{wu}] = -k_v \tag{B.2}$$

$$[c_{uu}] = c_v \;\; ; \;\; [c_{ww}] = c_v \;\; ; \;\; [c_{uw}] = [c_{wu}] = -c_v \tag{B.3}$$

$$\{f_{we}\}_{t+\Delta t} = -(M_v + M_w)g \tag{B.4}$$

B.2 Suspended Rigid Beam or 4 DOF Car Model (Yang and Wu, 2001)

Fig. 3.2 illustrates all parameters in the following matrices

$$[m_{uu}] = \begin{bmatrix} m_c & 0 \\ 0 & I_c \end{bmatrix} \tag{B.5a}$$

$$[m_{uw}] = [m_{wu}] = [0]_{2\times 2} \tag{B.5b}$$

$$[m_{ww}] = \begin{bmatrix} m_{w1} & 0 \\ 0 & m_{w2} \end{bmatrix} \tag{B.5c}$$

$$[k_{uu}] = \begin{bmatrix} k_{v1} + k_{v2} & k_{v2}d_2 - k_{v1}d_1 \\ k_{v2}d_2 - k_{v1}d_1 & k_{v1}d_1^2 + k_{v2}d_2^2 \end{bmatrix} \tag{B.6a}$$

$$[k_{uw}] = [k_{wu}]^T = \begin{bmatrix} -k_{v1} & -k_{v2} \\ k_{v1}d_1 & -k_{v2}d_2 \end{bmatrix} \tag{B.6b}$$

$$[k_{ww}] = \begin{bmatrix} k_{v1} & 0 \\ 0 & k_{v2} \end{bmatrix} \tag{B.6c}$$

$$[c_{uu}] = \begin{bmatrix} c_{v1} + c_{v2} & c_{v2}d_2 - c_{v1}d_1 \\ c_{v2}d_2 - c_{v1}d_1 & c_{v1}d_1^2 + c_{v2}d_2^2 \end{bmatrix} \tag{B.7a}$$

$$[c_{uw}] = [c_{wu}]^T = \begin{bmatrix} -c_{v1} & -c_{v2} \\ c_{v1}d_1 & -c_{v2}d_2 \end{bmatrix} \tag{B.7b}$$

$$[c_{ww}] = \begin{bmatrix} c_{v1} & 0 \\ 0 & c_{v2} \end{bmatrix} \tag{B.7c}$$

$$\{f_{we}\}_{t+\Delta t} = -g \begin{Bmatrix} \frac{d_2}{d_1 + d_2} m_c + m_{w1} \\ \frac{d_1}{d_1 + d_2} m_c + m_{w2} \end{Bmatrix} \tag{B.8}$$

B.3 Car Model Including the Effect of Tires with 6 DOFs

Fig. 3.5 illustrates all parameters in the following matrices

$$[m_{uu}] = \begin{bmatrix} m_c & 0 & 0 & 0 \\ & I_c & 0 & 0 \\ & & m_{w1} & 0 \\ Sym. & & & m_{w2} \end{bmatrix} \tag{B.9a}$$

$$[m_{wu}] = [m_{uw}]^T = [0]_{2\times 4} \tag{B.9b}$$

$$[m_{ww}] = \begin{bmatrix} m_{t1} & 0 \\ 0 & m_{t2} \end{bmatrix} \tag{B.9c}$$

$$[k_{uu}]=\begin{bmatrix} k_{v1}+k_{v2} & k_{v2}d_2-k_{v1}d_1 & -k_{v1} & -k_{v2} \\ k_{v2}d_2-k_{v1}d_1 & k_{v1}d_1^2+k_{v2}d_2^2 & k_{v1}d_1 & -k_{v2}d_2 \\ -k_{v1} & k_{v1}d_1 & k_{v1}+k_{t1} & 0 \\ -k_{v2} & -k_{v2}d_2 & 0 & k_{v2}+k_{t2} \end{bmatrix} \tag{B.10a}$$

$$[k_{wu}]=[k_{uw}]^T=\begin{bmatrix} 0 & 0 & -k_{t1} & 0 \\ 0 & 0 & 0 & -k_{t2} \end{bmatrix} \tag{B.10b}$$

$$[k_{ww}]=\begin{bmatrix} k_{t1} & 0 \\ 0 & k_{t2} \end{bmatrix} \tag{B.10c}$$

$$[c_{uu}]=\begin{bmatrix} c_{v1}+c_{v2} & c_{v2}d_2-c_{v1}d_1 & -c_{v1} & -c_{v2} \\ c_{v2}d_2-c_{v1}d_1 & c_{v1}d_1^2+c_{v2}d_2^2 & c_{v1}d_1 & -c_{v2}d_2 \\ -c_{v1} & c_{v1}d_1 & c_{v1}+c_{t1} & 0 \\ -c_{v2} & -c_{v2}d_2 & 0 & c_{v2}+c_{t2} \end{bmatrix} \tag{B.11a}$$

$$[c_{wu}]=[c_{uw}]^T=\begin{bmatrix} 0 & 0 & -c_{t1} & 0 \\ 0 & 0 & 0 & -c_{t2} \end{bmatrix} \tag{B.11b}$$

$$[c_{ww}]=\begin{bmatrix} c_{t1} & 0 \\ 0 & c_{t2} \end{bmatrix} \tag{B.11c}$$

$$\{f_{we}\}_{t+\Delta t}=-g\begin{Bmatrix} \dfrac{d_2}{d_1+d_2}m_c+m_{w1}+m_{t1} \\ \dfrac{d_1}{d_1+d_2}m_c+m_{w2}+m_{t2} \end{Bmatrix} \tag{B.12}$$

where usually $m_{t1}=m_{t2}=0$

B.4 Half-Car Planar Vehicle Model with 8 DOFs

Fig. 3.7 illustrates all parameters in the following matrices

$$[m_{uu}]=\begin{bmatrix} m_{p1} & 0 & 0 & 0 & 0 & 0 \\ 0 & m_{p2} & 0 & 0 & 0 & 0 \\ 0 & 0 & m_s & 0 & 0 & 0 \\ 0 & 0 & 0 & J & 0 & 0 \\ 0 & 0 & 0 & 0 & m_{t1} & 0 \\ 0 & 0 & 0 & 0 & 0 & m_{t2} \end{bmatrix} \tag{B.13a}$$

$$[m_{wu}]=[m_{uw}]^T=\begin{bmatrix} 0 & 0 & 0 & 0 & 0 & 0 \\ 0 & 0 & 0 & 0 & 0 & 0 \end{bmatrix} \tag{B.13b}$$

$$[m_{ww}]=\begin{bmatrix} 0 & 0 \\ 0 & 0 \end{bmatrix} \tag{B.13c}$$

$$[k_{uu}]=\begin{bmatrix} k_{p1} & 0 & -k_{p1} \\ 0 & k_{p2} & k_{p2} \\ -k_{p1} & -k_{p2} & k_{p1}+k_{p2}+k_1+k_2 \\ -k_{p1}d_1 & k_{p2}d_2 & k_{p1}d_1-k_{p2}d_2+k_1b_1-k_2b_2 \\ 0 & 0 & -k_1 \\ 0 & 0 & -k_2 \end{bmatrix} \quad \cdots$$

$$\begin{bmatrix} -k_{p1}d_1 & 0 & 0 \\ k_{p2}d_2 & 0 & 0 \\ \cdots \quad k_{p1}d_1-k_{p2}d_2+k_1b_1-k_2b_2 & -k_1 & -k_2 \\ k_{p1}d_1^2+k_{p2}d_2^2+k_1b_1^2+k_2b_2^2 & -k_1b_1 & k_2b_2 \\ -k_1b_1 & k_1+k_{t1} & 0 \\ k_2b_2 & 0 & k_2+k_{t2} \end{bmatrix} \tag{B.14a}$$

$$[k_{wu}]=[k_{uw}]^T=\begin{bmatrix} 0 & 0 & 0 & 0 & -k_{t1} & 0 \\ 0 & 0 & 0 & 0 & 0 & -k_{t2} \end{bmatrix} \tag{B.14b}$$

$$[k_{ww}]=\begin{bmatrix} k_{t1} & 0 \\ 0 & k_{t2} \end{bmatrix} \tag{B.14c}$$

$$\{f_{we}\}_{t+\Delta t}=-g\begin{Bmatrix} \dfrac{m_sb_2+m_{p1}(d_1+b_2)+m_{p2}(b_2-d_2)}{b_1+b_2}+m_{t1} \\ \dfrac{m_sb_1+m_{p2}(d_2+b_1)+m_{p1}(b_1-d_1)}{b_1+b_2}+m_{t2} \end{Bmatrix} \tag{B.15}$$

where usually $m_{t1} = m_{t2} = 0$. Damping matrices are constructed the same way that stiffness matrices are written in Eq. B.14.

B.5 Train Model with 10 DOFs

Fig. 3.9 illustrates all parameters in the following matrices

$$[m_{uu}] = \begin{bmatrix} m_c & 0 & 0 & 0 & 0 & 0 \\ & I_c & 0 & 0 & 0 & 0 \\ & & m_{b1} & 0 & 0 & 0 \\ & & & I_{b1} & 0 & 0 \\ & Sym. & & & m_{b2} & 0 \\ & & & & & I_{b2} \end{bmatrix} \tag{B.16a}$$

$$[m_{wu}] = [m_{uw}]^T = [0]_{4\times 6} \tag{B.16b}$$

$$[m_{ww}] = \begin{bmatrix} m_{w1} & 0 & 0 & 0 \\ & m_{w2} & 0 & 0 \\ & & m_{w3} & 0 \\ Sym. & & & m_{w4} \end{bmatrix} \tag{B.16c}$$

$$[k_{uu}] = \begin{bmatrix} k_{v1}+k_{v2} & k_{v2}l_2 - k_{v1}l_1 & -k_{v1} \\ k_{v2}l_2 - k_{v1}l_1 & k_{v1}l_1^2 + k_{v2}l_2^2 & k_{v1}l_1 \\ -k_{v1} & k_{v1}l_1 & k_{v1}+k_{w1}+k_{w2} \quad \dots \\ 0 & 0 & k_{w2}d_2 - k_{w1}d_1 \\ -k_{v2} & -k_{v2}l_2 & 0 \\ 0 & 0 & 0 \end{bmatrix}$$

$$\begin{bmatrix} 0 & -k_{v2} & 0 \\ 0 & -k_{v2}l_2 & 0 \\ \dots \quad k_{w2}d_2 - k_{w1}d_1 & 0 & 0 \\ k_{w1}d_1^2 + k_{w2}d_2^2 & 0 & 0 \\ 0 & k_{v2}+k_{w3}+k_{w4} & k_{w4}d_4 - k_{w3}d_3 \\ 0 & k_{w4}d_4 - k_{w3}d_3 & k_{w3}d_3^2 + k_{w4}d_4^2 \end{bmatrix} \tag{B.17a}$$

$$[k_{wu}] = [k_{uw}]^T = \begin{bmatrix} 0 & 0 & -k_{w1} & k_{w1}d_1 & 0 & 0 \\ 0 & 0 & -k_{w2} & -k_{w2}d_2 & 0 & 0 \\ 0 & 0 & 0 & 0 & -k_{w3} & k_{w3}d_3 \\ 0 & 0 & 0 & 0 & -k_{w4} & -k_{w4}d_4 \end{bmatrix} \tag{B.17b}$$

$$[k_{ww}] = \begin{bmatrix} k_{w1} & 0 & 0 & 0 \\ 0 & k_{w2} & 0 & 0 \\ 0 & 0 & k_{w3} & 0 \\ 0 & 0 & 0 & k_{w4} \end{bmatrix} \tag{B.17c}$$

$$\{f_{we}\}_{t+\Delta t} = -g \begin{Bmatrix} \left(m_{b1} + \dfrac{l_2}{l_1+l_2} m_c\right) \dfrac{d_2}{d_1+d_2} + m_{w1} \\ \left(m_{b1} + \dfrac{l_2}{l_1+l_2} m_c\right) \dfrac{d_1}{d_1+d_2} + m_{w2} \\ \left(m_{b2} + \dfrac{l_1}{l_1+l_2} m_c\right) \dfrac{d_4}{d_3+d_4} + m_{w3} \\ \left(m_{b2} + \dfrac{l_1}{l_1+l_2} m_c\right) \dfrac{d_3}{d_3+d_4} + m_{w4} \end{Bmatrix} \tag{B.18}$$

Similar to the half-car planar model, damping matrices are constructed the same way that stiffness matrices are written in Eq. B.17.

APPENDIX C

FRICTION MODELS AND COEFFICIENT OF FRICTION

Dry friction is a term describing the friction between two solids in contact. Dry friction is divided into static friction for non-moving surfaces, and kinetic friction for moving surfaces. The Coulomb friction is a model used commonly to model dry friction. Parameter μ_s is used for static friction and μ_k for kinetic friction. For vehicles moving by rolling of wheels, another type of friction called rolling friction exists. This is the friction that exists even when the vehicle is moving with constant velocity, for which the friction coefficient is usually very small (0.001) compared to kinetic friction which comes from sliding (Butt et al., 2006). In other words, any moving vehicle will gradually slow down due to rolling resistance. The factor used for rolling resistance is usually denoted by C_{rr} (Coefficient of Rolling Resistance).

The basics of rolling and the associated friction forces will assist to understand the phenomenon. Fig. C.1 shows a wheel of a moving vehicle having friction force F_f. By equating the torque applied about CG (center of gravity) of the wheel, we have

$$rF_f = T_E - J\ddot{\theta} \tag{C.1}$$

where r is the wheel radius, T_E is the torque applied by engine or brakes, J is the rotary inertia of wheel, and $\ddot{\theta}$ is the angular acceleration, shown in Fig. C.1. The input value is $T_{E,}$ while $\ddot{\theta}$ and also F_f are to be calculated. The force F_f depends on the frictional properties of the two surfaces and should be related to friction characteristics. In the braking or traction situations, depending on the level of the torque applied by the engine or brakes, the horizontal contact force or friction force (F_f) can vary. F_f obtained from μ_k

multiplied by the vertical contact force determines upper bound and lower bound of the contact force.

Several models have been developed to model the friction between two objects in various situations (Dahl, 1976; Armstrong-Hélouvry, 1991; Olsson, 1998; Dupont *et al.,* 2002), and still more to come. Due to the complex nature of the friction, the phenomenon is not yet completely understood. There is no exact solution for the friction forces by means of friction characteristics of the two surfaces (Pfeiffer and Glocker, 1996). All models available are based on some assumptions and simplifying approaches to obtain matching results with the experimental findings and to minimize computational problems. Two simplifying approaches that have been used frequently in dynamics of multi-body systems are *non-smooth approach* and *regularized approach* (or smooth approach).

The regularized approach tries to remove discontinuity from the friction problem. Discontinuity is a complex challenge in the numerical integration procedures. This approach assumes that the force F_f is a function of relative velocity between the contact point of the wheel and that of the support surface. This velocity is called *contact velocity*. The relationship is considered linear in the so-called *regularized approach*. However, non-linear relationship is also commonly considered using the *Smooth Non-Linear Friction Law,* in contrast with the Coulomb friction law, with a *tanh* mathematical function (Pfeiffer and Glocker, 1996),

$$F_f = \mu_k \tanh\left(\frac{v_r}{\gamma}\right) N \qquad \text{(C.2)}$$

where v_r is the contact velocity, γ is a characteristic value depending on the two surfaces in contact, and N is the normal force. Fig. C.2a shows the smooth non-linear friction law function, and Fig. C.2b shows the regularized approach, schematically.

There are two main drawbacks with this approach. The first shortcoming is due to the type of the functions used. These functions (linear or nonlinear) will cause the resulting ordinary differential equation (ODE) to become *stiff*; which is numerically problematic. The second drawback is regarding the zero contact velocity (Pfeiffer and Glocker, 1996). This method gives zero force when the contact velocity is zero which is not correct. Hence, the application of this method is limited and should be accompanied with attention for contact velocities close to zero.

The more advanced approach is *Non-smooth approach*. It includes the discontinuity in the contact force distinguishing between *stick* and *slip*. If the contact velocity is zero, *stick* condition happens otherwise *slip* occurs. For slip, $F_f = \pm \mu_k N$ and, for stick a constraint equation is added to ODE problem due to the same location of the contact point on the vehicle and the surface. This will cause an abrupt change in the numerical solution, as if an impact is introduced in the numerical integration. These complexities require special formulation of ODE with constraint equations (Pfeiffer et al., 2006).

Another representation of the simplified methods is to use an equivalent friction coefficient (μ_{eqv}). As mentioned above, the friction force F_f is bounded to $\left(F_f\right)_{max} = \pm \mu_k N$. Less values of F_f compared to $\left(F_f\right)_{max}$ happens when, for example, a medium braking (not a full braking) is applied by the driver. Therefore, one can simulate this situation with a percentage of the $\left(F_f\right)_{max}$ as:

$$F_f = \alpha \left(F_f\right)_{max} = \alpha\, \mu_k N \tag{C.3}$$

where α is between 1 and -1, and is selected depending on the severity of the braking or traction. Hence, one can define an equivalent virtual friction coefficient μ_{eqv} equals to $\alpha\, \mu_k$. This represents a point on the inclined line in Fig. C.2b, as if the regularized approach has been adopted. It should be mentioned that similar to all simplified methods, the application of μ_{eqv} includes approximation, while significantly reducing the complexity Using μ_{eqv}, one can have a quick and rough estimation of the vehicle and bridge responses.

The main objective of the current thesis is to develop a model useful for design purposes. In the design practices, the designer deals with extreme situations. For a vehicle experiencing acceleration or deceleration, these situations can be considered as extreme case for braking (so-called pure slipping) and for traction. For these cases, constant friction coefficient of μ_k can be used with Coulomb dry friction model and the results are of high accuracy. In less severe braking situations, μ_{eqv} can be used as an approximation. In the VBI analysis procedures available in the literature, simplified assumptions were adopted. Ju and Lin (2007) assumed constant vehicle acceleration, while Yang and Wu (2001) assumed constant friction coefficient. In the current thesis, the Yang and Wu (2001) assumption is adopted.

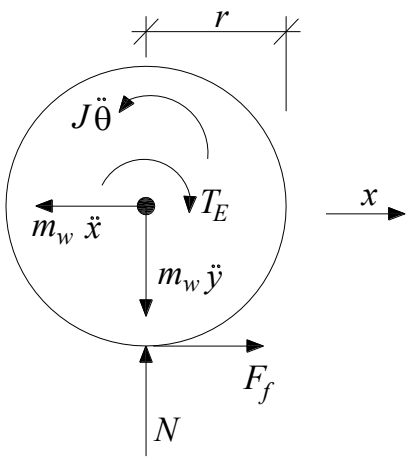

Fig. C.1 Free-body diagram of a wheel

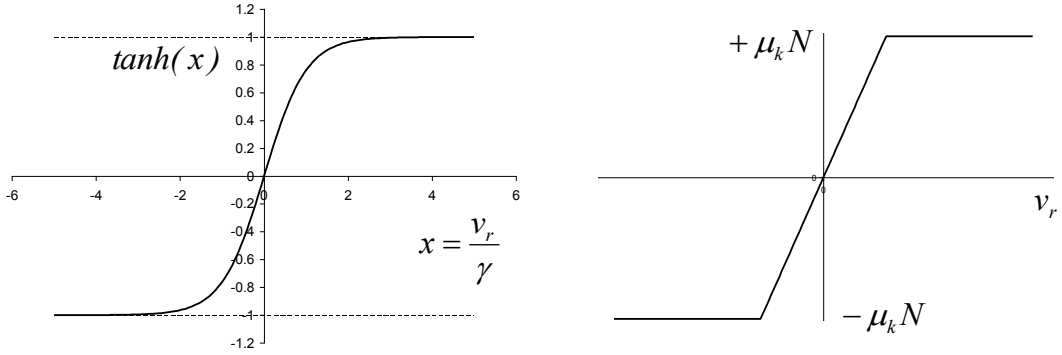

Fig. C.2 Simplified friction models, (a) smooth non-linear friction law, (b) regularized approach (Pfeiffer and Glocker, 1996)